1998

Zintl cluster chemistry in the alkali-metal-gallium systems

Robert William Henning
Iowa State University

INFORMATION TO USERS

This manuscript has been reproduced from the microfilm master. UMI films the text directly from the original or copy submitted. Thus, some thesis and dissertation copies are in typewriter face, while others may be from any type of computer printer.

The quality of this reproduction is dependent upon the quality of the copy submitted. Broken or indistinct print, colored or poor quality illustrations and photographs, print bleedthrough, substandard margins, and improper alignment can adversely affect reproduction.

In the unlikely event that the author did not send UMI a complete manuscript and there are missing pages, these will be noted. Also, if unauthorized copyright material had to be removed, a note will indicate the deletion.

Oversize materials (e.g., maps, drawings, charts) are reproduced by sectioning the original, beginning at the upper left-hand corner and continuing from left to right in equal sections with small overlaps. Each original is also photographed in one exposure and is included in reduced form at the back of the book.

Photographs included in the original manuscript have been reproduced xerographically in this copy. Higher quality 6" x 9" black and white photographic prints are available for any photographs or illustrations appearing in this copy for an additional charge. Contact UMI directly to order.

UMI

A Bell & Howell Information Company
300 North Zeeb Road, Ann Arbor MI 48106-1346 USA
313/761-4700 800/521-0600

Zintl cluster chemistry in the alkali-metal–gallium systems

by

Robert William Henning

A dissertation submitted to the graduate faculty

in partial fulfillment of the requirements for the degree of

DOCTOR OF PHILOSOPHY

Major: Inorganic Chemistry

Major Professor: John D. Corbett

Iowa State University

Ames, Iowa

1998

Graduate College

Iowa State University

This is to certify that the Doctoral dissertation of

Robert William Henning

has met the dissertation requirements of Iowa State University

Signature was redacted for privacy.

Major Professor

Signature was redacted for privacy.

For the Major Program

Signature was redacted for privacy.

For the Graduate College

TABLE OF CONTENTS

ABSTRACT[1]

Previous research into the alkali-metal–gallium systems has revealed a large variety of networked gallium deltahedra. The clusters are analogues to borane clusters and follow the same electronic requirements of 2n+2 skeletal electrons for closo-deltahedra. This work has focused on compounds that do not follow the typical electron counting rules.

The first isolated gallium cluster was found in Cs_8Ga_{11}. The geometry of the Ga_{11}^{7-} unit is not deltahedral but can be described as a penta-capped trigonal prism. The reduction of the charge from a closo-Ga_{11}^{13-} to Ga_{11}^{7-} is believed to be the driving force of the distortion. The compound is paramagnetic because of an extra electron but incorporation of a halide atom into the structure "captures" the unpaired electron and forms a diamagnetic compound. A second isolated cluster has been found in $Na_{10}Ga_{10}Ni$ where the tetra-capped trigonal prismatic gallium is centered by nickel. Stabilization of the cluster occurs through Ni-Ga bonding.

A simple two-dimensional network occurs in the binary K_2Ga_3. Octahedra are connected through four waist atoms to form a layered structure with the potassium atoms sitting between the layers. $Na_{30.5}Ga_{60-x}Ag_x$ is nonstoichiometric and needs only a small amount of silver to form ($x \sim 2$–6). The structure is composed of three different clusters which are interconnected to form a three-dimensional structure. The $RbGa_{3-x}Au_x$ system is also nonstoichiometric with a three-dimensional structure composed of Ga_8 dodecahedra and four-bonded gallium atoms. Unlike $Na_{30.5}Ga_{60-x}Ag_x$, the $RbGa_3$ binary is also stable. The binary is

---

[1]This work was performed at Ames Laboratory under Contract No. W-7405-Eng-82 with the U.S. Department of Energy. The United States government has assigned the DOE Report number IS-T 1840 to this thesis.

formally a Zintl phase but the ternary is not. Some chemistry in the alkali-metal–indium system also has been explored. A new potassium–indium binary is discussed but the structure has not been completely characterized.

INTRODUCTION

Exploration of the alkali-metal–gallium systems has revealed a vast array of new chemistry and interesting structure types. The structures and properties of these new materials have been studied in an attempt to understand the chemistry of this and other related systems. On first glance, these "alloys" display a dull metallic luster which would imply an intermetallic compound but further analysis typically reveals a closed electronic shell along with the corresponding semiconducting and diamagnetic properties. The properties are typically more consistent with valence (saltlike) compounds and therefore these materials can be viewed as a link between intermetallic and valence structures. These types of materials have become known as Zintl phases[1] and have traditionally been formed between the elements of type A, where A = alkali, alkaline-earth, or rare-earth metals, and of type B, where B = group 14, 15, or 16 elements. This work has not only expanded the range of known Zintl phases but has also contributed to our understanding of the structure/property relationships in the alkali-metal–gallium systems.

Until relatively recently, the range of main-group elements that formed Zintl phases was believed to stop at the "Zintl border."[2] This was an imaginary line between groups 13 and 14. Zintl phases were originally viewed as compounds that have discrete isolated anions or anionic frameworks and regular 2-center–2-electron bonding. The anions also followed regular octet rules and, with a modification by Klemm,[3] frequently formed pseudo elements from later groups. The elements of group 13 have only three valence electrons and were not considered good candidates for Zintl phases, one exception being NaTl[4] and related compounds which form a stuffed diamond framework.

The electron-poor valence configuration of the group 13 elements allows for the formation of new compounds with an abundance of orbitals but only a few electrons to fill them. The borane clusters were the first thoroughly explored group 13 compounds in which the resulting delocalized bonding was understood. This work lead to the development of Wade's rules[5] to correlate the observed electron counts with the various deltahedral geometries. This type of cluster chemistry was considered unique to the boranes $B_nH_n^{2-}$ (carboranes, etc.) because the poor bonding of the hydrogen atoms with the heavier triels precluded any chance of forming similar clusters. Clusters formed without any exo-bonds would require a formal electron pair on each vertex and an unreasonably high formal charge, e.g. Ga_{12}^{14-}.

Exploration of the alkali-metal–gallium binaries lead to the discovery of deltahedral clusters in the solid state.[6] The high formal charge on the clusters was usually alleviated by the formation of 2-center–2-electron bonds between clusters or via one, two, or three atom spacers. This produced structures with two-dimensional or three-dimensional anionic networks with the cations effectively filling the holes between the clusters and formally donating their valence electrons to the framework. The properties (magnetic and conduction) and electron counts were consistent with closed electronic shells and these materials were fittingly described as Zintl phases. This was in contrast to the earlier Zintl phases which had formal two-electron bonds throughout the structure and obeyed the octet rule. The combination of different cluster types, connectivity, and atom sizes allows for a large variety of structures to form even as binary phases.

This trend continues with the introduction of late transition metals into the gallium systems. Several new compounds have been reported, but many of the structures are quite complex owing to nonstoichiometry, condensed polyhedra, and partially occupied positions. Even with these considerations, the electron counts tend to be nearly closed shell, but only a few property measurements have been performed to confirm this. Another factor that makes these materials difficult to understand is when the third element substitutes for a gallium atom in the structure. This makes it difficult to completely characterize the compound and to perform electronic structure calculations which are frequently used to deduce structure/property relationships.

This research project has focused on finding new compounds in the alkali-metal–gallium systems with a goal of trying to understand the complex chemistry of this area of the periodic table. The discovery of the first isolated gallium clusters is an exciting result considering the tendency of gallium to form network structures. Even though the formation of network structures is the dominant method of reducing the high formal charge on the gallium clusters, other methods have been found. A distortion of the cluster away from the regular deltahedral geometry has been observed in A_8Tr_{11} and $A_8Tr_{11}X$ phases (A = K, Rb, and Cs; Tr = Ga, In, and Tl; X = Cl, Br, and I). The resulting isolated Tr_{11}^{7-} unit requires six fewer electrons than a closo-Tr_{11}^{13-} cluster. A second way that isolated gallium clusters can be stabilized is to insert an atom into the center of the cluster. This has been observed in $Na_{10}Ga_{10}Ni$. The centering atom contributes its valence electrons without adding additional orbitals.

In the search for new materials, several nonstoichiometric network structures have been identified in some ternary phases containing late transition metals. Since these materials are in between classical valence structures and intermetallic phases, it should not be surprising to find compounds that are open shell and have a more metallic character.

Experimental Techniques

Starting Materials

Most compounds were prepared from an appropriate mixture of the elements but a few situations required binaries such as CsCl. The elements were used as received from the manufacturer except for sodium which required the surface be cleaned with a scalpel. The sodium is in the form of a large block (5 x 5 x 10 cm) which is stored in an air-tight mason jar inside the dry box. The surface of the block is oxidized slightly so pieces that are removed need to have the oxidized part cut off. The other alkali-metals were obtained in small ampules which were used up before significant surface contamination occurred. The small ampules could also be stored inside mason jars which had excess alkali metal present to act as a getter. The manufacturer and purity levels for all starting materials are reported in each chapter where appropriate.

Inert Atmospheres

The air-sensitive nature of both the products and some of the starting materials required the use of several specialized procedures and modified sample holders. The first line

of defense was the use of either nitrogen or helium-filled dry boxes. Reactions were loaded in a nitrogen-filled dry-box from Vacuum Atmospheres Co., model PC-1. The products of the reactions were handled in either a Blickman nitrogen-filled dry box with a microscope attached or a Vacuum Atmospheres helium-filled dry box, model DLX-001-S-P. The environment was maintained in all three units by a Vacuum Atmospheres DRI-TRAIN regeneration system, model HE-493. Both moisture and oxygen were removed by the circulation of the inert gas through an activated Cu/molecular sieve catalyst. The moisture levels were continuously monitored to ensure a suitable working environment. All starting materials and products were handled in either glass petri dishes or in molybdenum weighing pans while inside the dry boxes.

Reaction Containers

The reactivity of the materials also required the use of 3/8" tantalum tubing as a reaction vessel. The tubing was cleaned beforehand in an acid mixture containing (by volume) 55% sulfuric (95% w), 25% nitric (70% w), and 20% hydrofluoric (49% w) and subsequently rinsed in distilled water. Lengths of 1.25" tubing (3/8") were first crimped on one end and sealed in an arc welder. The air-cooled welder was evacuated with a rough pump and back filled with an argon atmosphere before the tubes were welded.

Inside the glove box, the starting materials were placed into the clean tantalum tubing which had one end welded shut. The open end of the tube was then crimped and placed into a sealed glass jar for transportation out of the glove box and into the welder. The time outside the inert environment of the dry box was minimized (< 5 min.) to reduce the possibility of

contamination. The sample tubes were welded as before. To protect the tantalum tube from oxidation at the high reaction temperatures, the sample tubes were cleaned in a weak acid solution again and encapsulated into an evacuated silica jacket. A mercury diffusion pump was used to evacuate the silica tube. Before the silica jacket was removed from the vacuum line, the tube was heated with a natural gas/oxygen torch to remove any moisture from the silica and sealed off.

Furnaces

All reactions were carried out in simple tube furnaces (<800° C) or Marshall tube furnaces which could reach temperatures up to 1200° C. The temperatures were monitored by J-type thermocouples and adjusted by programable Eurotherm temperature controllers. A variety of temperatures and heating cycles were used to achieve the desired phases. Most reactions were heated above the highest melting point in the alkali-metal–gallium phase diagram and held at that temperature for 24 hours to ensure homogeneity. At this point the sample was allowed to slow cool (1–5° C/hr) to encourage crystal growth. If the phase melted incongruently, then the sample would first be quenched from the melt and then annealed at lower temperatures to achieve the desired product. To obtain a more complete reaction, the tube furnaces were tilted approximately 25° to collect all materials at one end of the tantalum tube.

Product Identification

Completed reactions were opened inside a nitrogen-filled dry box with a microscope attached. The tantalum tubing was opened by cutting off one or both of the welded ends with a tubing cutter. A spatula was used to remove as much material as possible from the tube walls and from the welded ends. At this point, visual observations were made. This included color, crystallinity, shape of crystals, brittleness, and whether the sample was sticky from excess alkali-metal being present. If crystals were present that appeared to be suitable for single crystal x-ray crystallography, they were sealed into 0.3 mm diameter capillary tubes and saved for further analysis. The remaining sample was then ground in a mortar and pestle and a small amount was mixed with NIST (NBS) standard silicon to be used for Guinier powder pattern analysis. The bulk part of the ground sample was saved in a pyrex tube with a stopcock attached and later sealed with a natural gas/oxygen torch after being evacuated.

Initial characterization of the reaction products was obtained through the use of Guinier X-ray powder diffraction patterns. The samples were fixed between two pieces of cellophane tape in order to protect the sample from the environment during transfer from the glove box to the camera. In addition to the cellophane, the samples were carried in a closed container. The sample chambers of the Enraf-Nonius cameras, model FR552, with monochromated Cu $K\alpha_1$ radiation (λ = 1.54056 Å), were under continuous rough pump evacuation (~150 mTorr). The powder patterns were recorded on photographic film.

Ideal Guinier powder patterns of known structures were obtained through the use of the program POWDERV8 on the VAX computer system. These were used for phase identification and yield estimates. Lattice parameters were obtained by first digitizing the

powder pattern on a LS20 Line Scanner, KEJ Instruments, Sweden. After identifying the diffraction lines of the internal silicon standard, the SCANPI8 program adjusted the data to account for film shrinkage, poor film cassette holder positioning, or any other factor that may have affected the diffraction lines. The least squares program LATT was used to obtain the final lattice parameters.

Single Crystal X-ray Analysis

Crystallites sealed into 0.3 mm capillaries were checked for singularity through Laue photographs on either a Weissenburg or precession camera with Cu $K\alpha_1$ radiation. Suitable crystals were then transferred to one of two single crystal x-ray diffractometers, a four circle Rigaku AFC6R with rotating anode or an Enraf-Nonius CAD4 instrument with a sealed tube. Each diffractometer used graphite-monochromated Mo $K\alpha$ radiation, $\lambda = 0.71069$ Å. Twenty-five reflections, obtained through a random search, were used to determine the cell type and lattice parameters. Additional information from previous work was also used to select the appropriate cell. Axial photographs obtained on the diffractometer were used to check axis lengths. All data sets were collected at room temperature with redundant information. After the data collection was complete, 3–6 psi-scans were measured to correct for absorption. The refinement and data manipulation was performed with the TEXSAN software package, Molecular Structures Corp., on a VAX workstation. In cases where the unit cell or space group information was difficult to determine, the single crystals were studied in greater detail through Weissenburg or precession film techniques.

Magnetic Susceptibility Measurements

Molar susceptibilities were measured with respect to temperature on a SQUID magnetometer from Quantum Design. The air-sensitive nature of the samples required the use of a special container. The powdered samples were held between two fused silica rods (3 mm o.d.) with a fused silica tube (3 mm i.d. and ~17 cm long) encapsulating the rods and the sample. All samples were loaded in a helium-filled dry box. The raw data obtained from the magnetometer was corrected for the sample holder and for the diamagnetic cores.

Electrical Resistivity Measurements

The electrical resistivities of powdered samples were determined with respect to temperature by the electrodeless Q-method. This technique relies on a change in the quality factor of a coil in response to the skin effect of the sample. Samples with a known grain size are required for this experiment so a sieve was used to obtain particles with diameters between 250 and 425 μm. Contact between particles had to be minimized so the samples were mixed with dry chromatographic Al_2O_3 to ensure isolation (total volume ~1 cm^3). The sample/Al_2O_3 mixture was sealed into an evacuated pyrex tube (10 mm o.d.) for the experiment. To measure the resistivity, the sample was placed inside a copper coil operating at 34 MHz and the quality factor (Q) of the coil was measured with a Hewlett-Packard model 4342A Q meter. The sample was then removed from the coil and the quality factor (Q_o) was measured again. The electrical resistivity (ρ) could be determined from the ΔQ by:

$$\rho = \frac{B(Va)}{\Delta(1/Q)}$$

where B is a constant for the coil and equals 4.84 x 10^5, V is the volume of the sample, *a* is the average radius of the particles, and $\Delta(1/Q)$ is equal to $1/Q-1/Q_o$. This procedure was repeated at several temperatures ranging from 100 K to room temperature.

Electronic Structure Calculations

Extended Hückel band calculations were performed using the EHMACC program running on a PC and with the program provided by Gordon Miller which is available on the Unix workstation at Iowa State University. This approach uses the tight-binding approximation to calculate the energy density of states (DOS) and crystal orbital overlap populations (COOP). The molecular orbital diagrams of networked clusters were determined by placing dummy atoms at all of the exo-bonding positions of the cluster. The dummy atoms were given a Slater type *s* orbitals with an energy equivalent to a gallium 4p orbital.

Dissertation Organization

The dissertation has been arranged in the form of papers suitable for publication. Each chapter, except for the introduction and conclusion, corresponds to one paper. The appendix discusses a research project which is not complete but still contains valuable results. The first paper has been published whereas the remaining papers are ready for submission.

References

(1) *Chemistry, Structure and Bonding of Zintl Phases and Ions*; Kauzlarich, S., Ed.; VCH Publishers: New York, 1996.

(2) Miller, G. in *Chemistry, Structure and Bonding of Zintl Phases and Ions*; Kauzlarich, S., Ed.; VCH Publishers: New York, 1996; Chapter 1.

(3) Klemm, W.; Busmann, E. Z. *anorg. allg. Chem.* **1963**, *319*, 297.

(4) Zintl, E.; Dullenkopf, W. *Z. Phys. Chem.* **1932**, *B16*, 195.

(5) Wade, K. Adv. *Inorg. Chem. Radiochem.* **1976**, *18*, 1.

(6) Belin, C.; Tillard-Charbonnel, M. *Prog. Solid St. Chem.* **1993**, *22*, 59.

Cs_8Ga_{11}, A NEW ISOLATED CLUSTER IN A BINARY GALLIUM COMPOUND. A FAMILY OF VALENCE ANALOGUES $A_8Tr_{11}X$: A = Cs, Rb; Tr = Ga, In, Tl; X = Cl, Br, I

A paper published in Inorganic Chemistry

Robert W. Henning and John D. Corbett*

Inorg. Chem. **1997**, *36*, 6039

Department of Chemistry and Ames Laboratory—DOE,[1]

Iowa State University, Ames IA 50011

Abstract

Fusion of the elements, and alkali-metal halide when appropriate, in stoichiometric amounts in Ta containers followed by slow cooling results in high yields of the title compounds. X-ray structures refined for rhombohedral Cs_8Ga_{11} ($R\bar{3}c$, $Z = 6$, $a = 9.9962(5)$ Å, $c = 50.839(6)$ Å) and $Cs_8Ga_{11}Cl$ ($R\bar{3}c$, $Z = 6$, $a = 10.0111(7)$ Å, $c = 50.504(6)$ Å) reveal isolated clusters of pentacapped, trigonal prismatic gallium anions, Ga_{11}^{7-}, the former compound being isostructural with K_8In_{11} and A_8Tl_{11} (A = K, Rb, Cs). The clusters are arranged in pseudo-ccp layers separated by double layers of cesium atoms. The halide in $Cs_8Ga_{11}Cl$ is bound in a preformed cavity within the cesium double layers where it is surrounded by eight cations. Of the nine examples reported for $A_8Tr_{11}X$, three chlorides occur in systems in which the binary A_8Tr_{11} do not form, Rb–Ga, Rb–In, Cs–In. These

halides are the first examples of Tr_{11}^{7-} compounds that are valence phases and do not contain an extra alkali-metal cation and electron. Magnetic susceptibility data indicate an apparently localized electron in paramagnetic Cs_8Ga_{11} and diamagnetism for $Cs_8Ga_{11}Cl$.

Introduction

The alkali-metal–gallium systems are rich in novel cluster chemistry, predominantly in interbonded network structures.[2] Many of the units are analogues of deltahedral clusters commonly found in borane chemistry, *closo*-Ga_8, -Ga_{11} and -Ga_{12} as well as their nido derivatives, for instance, and these can also be related via Wade's rules.[3,4] Larger species are also encountered, Ga_{15} and Ga_{17} for example. In the absence of exo bonded ligands (H, R, etc.), the higher charges ideally associated with these cluster anions have in practice always been reduced through extensive intercluster sigma bonding, sometimes via 1, 2, or 3 metal atom spacers. Even so, some of the resulting 2-D or, more often, 3-D gallium networks in fact appear to be closed-shell in electron count, or nearly so.[2] A discrete gallium cluster has been reported in a binary phase only as the tetrahedral units seen in $Ca_{11}Ga_7$.[5] In considerable contrast, the heavier congener indium forms several isolated, sometimes centered, clusters in alkali–metal systems, formally In_4^{8-},[6] In_{11}^{7-},[7] $In_{10}Zn^{8-}$,[8] and $In_{10}Ni^{10-}$,[9] for instance. A number of network structures also appear, most of which are different from those of gallium. The trend to discrete cluster species continues with thallium which forms many other isolated clusters (Tl_5^{7-}, Tl_9^{9-}, Tl_{13}^{11-}, etc.)[4,10,11] and very few networks. We have now reexamined the alkali-metal–gallium systems for isolated clusters, and herein report the first example in Cs_8Ga_{11}. This compound is isostructural with indium and thallium examples, which have been

formulated as $(A^+)_8Tr_{11}^{7-}e^-$ (Tr = In,[7] Tl[12]) on the basis of calculations and properties. Although these phases are electron-rich, the anions are significantly electron-poor (hypoelectronic) in cluster bonding electrons relative to Wade's rules. In addition, the halide derivatives of many A_8Tr_{11} phases have also been synthesized, affording the first examples of the valence-precise compounds $A_8Tr_{11}X$.

The Cs–Ga phase diagram reported in 1970 by Thümmel and Klemm[13] indicated the existence of three phases. The phases $CsGa_7$ and $CsGa_3$ were structurally characterized in 1985 by X-ray powder diffraction studies[14] but "Cs_5Ga_8" (analogous to "K_5In_8"[7]) has not been studied further. van Vucht reported a powder pattern for a new cesium–rich phase, but he was unable to determine the structure.[14] Both pertain to the Cs_8Ga_{11} compound reported here.

Experimental Section

Stoichiometric amounts of the elements and, where appropriate, cesium or rubidium halide were welded in Ta tubing using techniques described previously.[15] Cesium (99.9%, Johnson-Matthey), rubidium (99.9%, Alpha), gallium (99.99%, Johnson-Matthey), indium (99.999%, Cerac), and the alkali-metal halides (99.9%, Fisher) were used as received while the surface of thallium (99.998%, Johnson-Matthey) was cleaned with a scalpel. All materials were handled in a N_2-filled glovebox. All known A_8Tr_{11} ("A_5Tr_8") compounds appear to melt congruently, and "Cs_5Ga_8" has the highest melting point in its system, ~625 °C, so the mixtures were allowed to react at 700° C for 24 hours to ensure homogeneity and then cooled to room temperature at a rate of 3 °C/h. Single crystal refinements were obtained for Cs_8Ga_{11}

and $Cs_8Ga_{11}Cl$ while the remaining $A_8Tr_{11}X$ were identified by Guinier powder patterns. Analogous binary phases were not obtained with K or Rb.

Cs_8Ga_{11}. This very brittle product had a metallic luster and contained many crystals with smooth faces. The yield was substantially quantitative. Small crystals were selected, sealed in thin-walled capillaries and checked for singularity by Laue and oscillation film techniques. Most of the crystallites turned out to be multiple, but a suitable crystal was obtained from an otherwise unsuccessful reaction loaded as $Cs_8Ga_{10}Cu_2$. Lattice parameters for Cs_8Ga_{11} that were determined from Guinier powder data and least squares analysis for samples loaded both as Cs_8Ga_{11} and as $Cs_8Ga_{10}Cu_2$ were within 3σ (0.003 Å) of each other, so copper is not necessary for compound formation. A bar-like single crystal (0.25 x 0.28 x 0.40 mm) was selected for data collection on a Rigaku AFC6R single crystal diffractometer. Twenty-five reflections obtained from a random search were indexed with a rhombohedral unit cell. Four octants of data ($\pm h$, k, $\pm l$, hexagonal setting) were collected at room temperature with Mo Kα radiation up to 50° in 2θ and corrected for Lorentz and polarization effects. No violations of the R-centering condition were observed. The average of six ψ-scans collected at different 2θ angles were utilized for absorption correction. Systematic absences and Wilson plot statistics suggested space group *R*3*c* (no. 167). Application of direct methods[16] revealed two positions with separations appropriate for Cs-Cs contacts and three positions suitable for gallium. The routine refinement of the positional and anisotropic thermal parameters with the TEXSAN[17] package on a VAX station converged at an *R(F)* factor of 2.2%. The largest positive and negative peaks in the difference map were 0.77 $e^-/Å^{-3}$ (3.6 Å from Ga3) and -0.96 $e^-/Å^{-3}$.

$Cs_8Ga_{11}Cl$. As for the binary phase, this product was obtained phase pure, had metallic luster, and was brittle. Select crystals were sealed in thin-walled capillaries and checked for singularity as before. An irregular shaped crystal (0.14 x 0.20 x 0.25 mm) was selected for data collection on the same diffractometer. Twenty-five reflections obtained from a random search were indexed with a rhombohedral unit cell (hexagonal setting). Two octants of reflection data ($\pm h$, k, l) were collected at room temperature with Mo Kα radiation up to 50° in 2θ and corrected for Lorentz and polarization effects. No violations of the R-centering were observed. The average of three ψ-scans collected at different 2θ angles were used for absorption correction. Systematic absences and Wilson plot statistics suggested the same space group as for the binary compound, *R*3*c* (no. 167), and direct methods provided substantially the same cesium and gallium positions. Refinement of the positional and isotropic thermal parameters was followed by a difference Fourier analysis that revealed one peak appropriate for chlorine. Anisotropic refinement of all atoms reduced R(F) to 2.6%. The largest positive and negative peaks in the difference map were 0.72 $e^-/Å^3$ (2.9 Å from Ga2) and -1.56 $e^-/Å^3$.

Some crystal data for both studies are listed in Table 1, and atomic positions and isotropic-equivalent parameters are in Table 2. Additional data collection and refinement parameters and the anisotropic thermal parameters are given in the Supporting Information. These and the F_o/F_c data are also available from J.D.C.

Property measurements. Samples loaded as Cs_8Ga_{11} and $Cs_8Ga_{11}Cl$ were pure according to Guinier powder patterns but to ensure that cesium metal was not present, these were enclosed in two evacuated, sealed Pyrex tubes and heated at 100 °C for 24 hours. The

opposite end of the tubing that protruded outside of the furnace allowed a trace of excess cesium to accumulate, but none was found.

Magnetic susceptibility data were collected on a Quantum Design MPMS SQUID magnetometer. Powdered Cs_8Ga_{11} (40.9 mg) and $Cs_8Ga_{11}Cl$ (42.3 mg) in separate containers were held under helium between two silica rods, one which had already been sealed into a fused silica tube. The susceptibilities of each sample were measured in a field of 3 T over the temperature range of 6 – 300 K. Corrections were applied to the raw data to account for the sample holder, core diamagnetism, and Larmor precession of the cluster-based electrons.[18] The core correction factors for Cs_8Ga_{11} and $Cs_8Ga_{11}Cl$ were -3.36×10^{-4} emu/mol and -3.62×10^{-4} emu/mol, respectively, while the Larmor precession correction was -2.35×10^{-4} emu/mol for each. Field dependent measurements were also performed at 60 K and 110 K on the Cs_8Ga_{11} sample. The resistivity of Cs_8Ga_{11} was determined by the electrodeless "Q" method[19] over 100 – 293 K and 34 MHz. The 126.1 mg sample with an average grain size of ~200 μm was diluted with dry chromatographic Al_2O_3. ESR measurements were carried out on a Bruker ER-200D spectrometer (X-band, 95 GHz) at room temperature and under liquid-nitrogen-cooled conditions.

Results and Discussion

Structure descriptions. Cs_8Ga_{11} is isostructural with K_8In_{11},[7] Rb_8In_{11},[20] and A_8Tl_{11} (A = K, Rb, and Cs).[12] The predominant structural feature in Cs_8Ga_{11} is likewise the isolated, pentacapped trigonal-prismatic gallium cluster, Figure 1, where Ga3 atoms define the trigonal prism. The cluster has pseudo-D_{3h} symmetry, but a slight twist (2.7°) of the opposite ends of

the trigonal prism reduces the symmetry to D_3. The cluster is coordinated by 24 cesium atoms (18 Cs1 and 6 Cs2) in characteristically regular roles, as shown in Figure 2. The Cs1 atoms in double layers each cap Ga1–Ga2–Ga3 faces, bridge Ga2–Ga3 edges, and bond exo to Ga3 atoms on three different clusters. Likewise, six Cs2 atoms around the waist of each cluster cap Ga1–Ga3–Ga2–Ga3 faces, and each does so on three clusters. The closest contact between clusters is 5.763(1) Å (Ga1–Ga3). The clusters exhibit pseudo cubic-close-packing normal to the *c*-axis with double layers of the Cs1 atoms between the cluster layers, i.e., Figure 3 without the chlorine. The Cs1 atoms in the pair of cation layers have the same orientation as the nearest cluster layer. Since the closed shell anions in K_8In_{11} and A_8Tl_{11} are Tr_{11}^{7-}, an extra cation appears necessary for packing, and the compounds have accordingly always[7] been formulated as the metallic $(A)^+_8Tr_{11}^{7-}e^-$.

The cesium and gallium positions in $Cs_8Ga_{11}Cl$ are essentially the same as in the binary except for some minor distortions following the addition of the chlorine, which occupies a 3 void at the origin. The first coordination sphere around chlorine is a very compressed trigonal antiprism of Cs1 atoms at a distance of 3.4972(7) Å plus two Cs2 atoms at 3.764(1) Å along $\bar{c}$ that cap the trigonal faces, Figure 4. The dimensions of this cavity in Cs_8Ga_{11} are 3.513 Å to Cs1 and 3.950 Å to Cs2 (Table 3), so the contraction in the former on chlorine accommodation is quite small. The height of the trigonal antiprism increases by 0.04 Å in the process. The symmetry-equivalent Cs1–Cl contacts of 3.4972(7) Å are consistent with the sum of the six-coordinate crystal radii, 3.48 Å.[21] The most significant shift in atomic positions between the two structures occurs with Cs2. In Cs_8Ga_{11}, Cs2 sits in a relatively large cavity coordinated by 3 different clusters in the *a*-*b* plane with all Cs–Ga contacts greater than 3.9 Å

(vs ~3.72 Å about Cs1), consistent with its slightly larger thermal ellipsoid. Coulombic forces presumably are responsible for the 0.19 Å shift of Cs2 along the *c*-axis toward the intercalated chlorine, while all the other distances in the structure change by less than 0.07 Å. The Cs2 change also appears to affect the three closest Ga3 atoms and to reduce the amount of twist of the basal ends of the cluster to ~0°. The cluster in $Cs_8Ga_{11}Cl$ thus has an effective point symmetry of D_{3h}, but the structure does not contain the horizontal mirror plane. Bonding of chlorine in the structure also compresses the Cs1–Ga_{11}–Cs1 slab by 0.095 Å and reduces the overall *c* dimension by 0.33 Å.

Other Halide Examples. The discovery of $Cs_8Ga_{11}Cl$ prompted us to search for other pseudo-8:11 phases that are stabilized by halide. In these cases, we inferred ternary compound formation from the changes in lattice dimensions and volumes. These are generally rather telling since reproducibility of cell volumes is around ±2/4000 or less. Table 4 lists the lattice parameters for nine new $A_8Tr_{11}X$ phases together with those of their corresponding binaries where formed. All reactions were run under the same conditions as for Cs–Ga–Cl. The binary Cs_8Ga_{11} and the corresponding ternary halides (Cl, Br, and I) all form in 95–97% yields according to their Guinier powder patterns. The larger bromine and iodine mainly increase the *c* dimensions relative to the values with chlorine. The Rb-Ga system is interesting in that although we have been unable to synthesize Rb_8Ga_{11}, the corresponding $Rb_8Ga_{11}Cl$ is stable. This suggests that, in general, halide derivatives are more stable than the corresponding binaries; a volume contraction is often associated with the formation of derivatives with smaller interstitials. Reactions with the larger halides have not been attempted in the Rb-Ga system. Nothing new was found in the K–Ga–Cl system.

The Cs–In system is likewise interesting in that only the Cs_2In_3[22] binary is stable near this stoichiometry while $Cs_8In_{11}Cl$ forms in the presence of the chloride in similarly high yield. Reactions with the other halides have not been attempted in this system but the heavier $Cs_8In_{11}X$ compounds should form. The Rb–In system is also unusual in that both Rb_2In_3[22] and Rb_8In_{11}[20] have been reported in the literature, although they are very close in composition, 60.0 and 57.9 at.% In, respectively. However, we have been unable to reproduce the Rb_8In_{11} synthesis in either this or earlier work.[23] Slow cooling, annealing, or quenching from the melt have all produced only Rb_2In_3 and rubidium metal. However, when the reaction is loaded as $Rb_8In_{11}Cl$ and slowly cooled, the characteristic pattern of an 8–11 phase, appreciable Rb_2In_3 and, in contrast to other reactions, 5–10% RbCl are evident in the powder pattern. (The last two are in about the right proportion for the incomplete formation of $Rb_8In_{11}Cl$, although an equilibrium chlorine content <1 can probably not be ruled out.) Since Rb_8In_{11} does not form without RbCl, we presume the product must be $Rb_8In_{11}Cl$. The apparent lattice constant changes between those of the reported Rb_8In_{11} and $Rb_8In_{11}Cl$, Table 4, are irregular relative to those in the Cs–Ga–Cl and Cs–Tl–Cl systems. Reactions incorporating bromine or iodine in $Rb_8In_{11}X$ should probably work.

The $Cs_8Tl_{11}X$ results obtained after slow cooling follow the same trend as the Cs–Ga reactions but the halides could not be obtained in 100% yield. A known binary, $Cs_{15}Tl_{27}$,[24] is present in about 30% yield as well as the corresponding amount of cesium halide. Attempts to form pure $Cs_8Tl_{11}X$ phases by annealing quenched samples at 380 °C, above the peritectic melting point of $Cs_{15}Tl_{27}$ (~350° C), produced the same results. However, the lattice constant trends make it clear that the halides have formed. In the case of $Rb_8Tl_{11}Cl$, patterns of both

the Rb_8Tl_{11} and $Rb_{15}Tl_{27}$ types were observed as well as RbCl, as above, but the lattice constants of the possible chloride fell within 3σ of those of Rb_8Tl_{11}. Although it is thus doubtful that $Rb_8Tl_{11}Cl$ forms, reactions with the heavier halides may provide better information. A few reactions in the gallium and indium systems were loaded with RbF or KF, but only the known binaries formed. Apparently, fluorine is too small for proper coordination.

Binary Phase Formation. The stability of any particular phase is naturally also dependent on the stability of alternate phases. In the present A–Tr systems (Tr = Ga, In, Tℓ), the existence of either one or the other of the close-lying A_2Tr_3 and A_8Tr_{11} (60.0 and 57.9 at.% Tr, respectively), but not both provides a good correlation in seven systems. In the present Cs–Ga, modeling of the unknown Cs_2Ga_3 with the anion parameters of K_2Ga_3 results in Cs–Cs distances that are probably too short, about 3.6 Å. The one contradiction is reports of both Rb_2In_3 and Rb_8In_{11}, but we have described the basis for our serious doubts about the existence of the latter. The only other contrary result, in a negative sense, is the existence of neither Rb_2Ga_3 or Rb_8Ga_{11}, $RbGa_3$ being the alkali-metal-richest phase that evidently forms.

Properties of $Cs_8Ga_{11}(X)$. The molar susceptibilities as a function of temperature for pure Cs_8Ga_{11} shown in Figure 5 exhibit some unusual features. An apparent transition below 90 K (confirmed in a second sample of Cs_8Ga_{11}) is believed to reflect a structural change, which is accompanied, or followed, by a magnetic transition near 75 K. Such effects have not been observed with the other A_8Tr_{11} compounds or for $Cs_8Ga_{11}Cl$. It has not been possible to obtain any structural information on the low temperature phase. Field-dependence measurements of the susceptibilities at 60 K and 110 K over a range of 0–6 T show a linear M–T relationship with a positive slope, indicating paramagnetism at both temperatures. A

slight positive curvature of the 60 K data suggests that the low temperature phase is antiferromagnetic, but this is unconfirmed. Equally unusual, Cs_8Ga_{11} is paramagnetic and follows the linear Curie-Weiss law very well above 100 K to yield a magnetic moment of $1.43(1)\mu_B$ and a Weiss θ of –61.1 K. This too is in apparent contrast to the other A_8Tr_{11} phases which appear to be Pauli-paramagnetic and are customarily formulated as metallic, $(A^+)_8Tr_{11}^{7-}e^-$. The extra electron in Cs_8Ga_{11} is evidently localized within the solid. The resistivity in the 100-300 K range is high, >920 $\mu\Omega$-cm, the limitations of the Q method precluding a more precise measurement. Q measurements on the other 8:11 phases have shown metallic conductivity. No ESR signal could be detected for Cs_8Ga_{11} at room and liquid-nitrogen temperatures, the electron relaxation evidently being fast at the ESR timescale. Fortunately, the situation with the diamagnetic $Cs_8Ga_{11}Cl$ is clearer (Fig. 5) and consistent with the Zintl formulation $(Cs^+)_8Ga_{11}^{7-}Cl^-$.

The question naturally arises as to how and where the odd electron might be bound. Localization on the cluster is unlikely considering its closed-shell electronic structure. An extra cluster electron should also cause the cluster to distort, which is not evident. Localization on a single cesium does not seem physically reasonable, in contrast to the situation with $Cs^+(18\text{-crown-}6)_2e^-$,[25] but trapping of spin-free electrons within or "on" cesium polyhedral cavities seems plausible. The behavior of semiconducting Pr_2Br_5 and its relatives seems pertinent; the individual cations there all appear to be Pr^{3+} with the electrons in some sort of Mott insulating state. The site that becomes occupied by chloride is an attractive possibility here, its radius contracts therewith by only 0.01 Å. There is also a 12-fold

tetrahedral $(Cs1)_3Cs2$ cavity with a radius of 2.88 Å. ^{133}Cs NMR could be helpful in defining the interactions.

The occurrence of Ga_{11}^{7-} only with Cs^+ cations is an interesting result. For In_{11}^{7-}, the best cation seems to be K^+, and for Tl_{11}^{7-}, K^+, Rb^+, Cs^+, so the disparate ion sizes in the isostructural Cs_8Ga_{11} is unusual. One explanation may be that larger cavities are necessary to trap the odd electron, even though the cation field therein is less, while the metallic version is unstable. As a matter of fact, the properties of the indium and thallium A_8Tr_{11} analogues are a little "odd". The resistivities are moderately high, 230–630 μΩ•cm, with positive temperature coefficients of 0.18–0.32% K^{-1}, while all show a modestly temperature-independent "Pauli-like" paramagnetism in the range of (2–4.6) × 10^{-4} emu•mol^{-1}. Many cluster compounds of the heavier main-group-elements that otherwise appear to be Zintl phases exhibit metal-like conductivities, while the negative signs of their magnetic susceptibilities seem to be much more consistent with their apparent valence properties.[27]

Summary. The alkali-metal–gallium systems contain a wide variety of unusual clusters which, when combined with different methods of intercluster bonding, provide an interesting array of network structures. Cs_8Ga_{11} and the corresponding halides are unique in this system because they contain isolated clusters. The only other known isolated gallium clusters are $Ga_{10}Ni^{10-}$, Ga_6^{8-}, and Ga_4^{8-} in $Na_{10}Ga_{10}Ni$,[28] $Ba_5Ga_6H_2$,[29] and $Ca_{11}Ga_7$,[5] respectively. In the first, the high cluster charge is evidently stabilized by the central nickel atom and a small cation, while hydride is needed in the second to balance the electron count. The first two examples illustrate the significance of Zintl phase concepts in these types of systems while the third is an unstudied exception (but not a hydride, we have established). The clearly

stabilizing effect of halide in $A_8Tr_{11}X$ compounds is especially evident in the Rb–Ga, Rb–In and Cs–In systems where we have not been able to prepare the binary A_8Tr_{11} phases but do achieve the chlorides (Table 4). The preference of closed shell electronic states is evidently a strong driving force in the formation of these structures. This fact makes Cs_8Ga_{11} more interesting in that it does not completely conform to the traditional Zintl concept. Although, the extra electron would be expected to behave like those in the isostructural K_8In_{11} and A_8Tl_{11} (A = K, Rb, and Cs) compounds, the property measurements suggest otherwise. Further work is anticipated.

The overall existence not only of fourteen phases containing isolated Tr_{11}^{7-} ions but also of other homoatomic species such as Tr_6^{8-}, Tl_5^{7-}, Tl_{13}^{11-} bring to question the suitability of the descriptor "Zintl boundary" that was defined by Zintl and later so-named by Laves in a memorial article.[30] Zintl differentiated the triel from the tetrel and later elements (groups 13 vs group 14) in several ways. The latter in their formally most negative oxidation states yielded salt-like compounds with active metals, often with familiar structural types. These were likewise named Zintl phases by Laves, and the breadth of this classification was later greatly extended by Klemm.[31] These are now taken to be valence compounds that in classical cases follow octet rules. On the other hand, Zintl noted that analogous compounds of the triels and earlier elements were alloy-like in properties and structures, often with notable nonstoichiometries. Likewise, this distinction was supported by earlier studies of "Zintl ions"[32] that he identified in solution in liquid ammonia as alkali-metal salts of polyanionic species such as Tr_9^{4-} for Sn, Pb, and so forth. Naturally, modern chemistry has greatly extended our knowledge of Zintl phases and ions. In the present cases, we see that

considerable coulombic stabilization of many polyanionic compounds of the triel elements is achieved in their neat alkali-metal salts, in Cs_8Tr_{11} for example, preceding the Zintl boundary. "Modern" definitions of valence rules for Zintl phases now must also include the so-called electron-deficient, delocalized bonding found in many clusters, a feature which also applies to the Zintl anions of the tetrel elements.[27]

Acknowledgments. We are grateful to J. Ostenson for the magnetic measurements and D. Scott for the ESR data.

Supporting Information. Two tables listing more crystallographic data and the anisotropic displacement parameters are available (2 pages). Ordering information is given on any current masthead page.

References

(1) This research was supported by the Office of the Basic Energy Sciences, Materials Sciences Division, U.S. Department of Energy. The Ames Laboratory is operated by Iowa State University under Contract No. W-7405-Eng.82.

(2) Belin, C.; Tillard-Charbonnel, M. *Prog. Solid St. Chem.* **1993**, *22*, 59.

(3) Wade, K. Adv. *Inorg. Chem. Radiochem.* **1976**, *18*, 1.

(4) Corbett, J. D. *Structure and Bonding* **1997**, *87*, 157.

(5) Fornasini, M. L.; Merlo, F. *Z.Kristallogr.* **1989**, *187*, 111.

(6) Sevov, S. C.; Corbett, J. D. *J. Solid State Chem.* **1993**, *103*, 114.

(7) Sevov, S. C.; Corbett, J. D. *Inorg. Chem.* **1991**, *30*, 4875.

(8) Sevov, S. C.; Corbett, J. D. *Inorg. Chem.* **1993**, *32*, 1059.

(9) Sevov, S. C.; Corbett, J. D. *J. Am. Chem. Soc.* **1993**, *115*, 9089.

(10) Dong, Z.; Corbett, J. D. *J. Am. Chem. Soc.* **1994**, *116*, 3429.

(11) Dong, Z.; Corbett, J. D. *J. Am. Chem. Soc.* **1995**, *117*, 6447.

(12) Dong, Z. C.; Corbett, J. D. *J. Cluster Science*, **1995**, *6*, 187.

(13) Thümmel, R.; Klemm, W. *Z. Anorg. Allg. Chem.* **1970**, *376*, 44.

(14) van Vucht, J. H. N. *J. Less-Common Met.* **1985**, *108*, 163.

(15) Dong, Z. C.; Corbett, J. D. *J. Am. Chem. Soc.* **1994**, *116*, 3429.

(16) Sheldrick, G. M. SHELXS-86, Universität Göttingen, Germany, 1986.

(17) TEXSAN, version 6.0, Molecular Structure Corp., The Woodlands, Texas, 1990.

(18) Sevov, S. C.; Corbett, J. D. *Inorg. Chem.* **1992**, *31*, 1895.

(19) Shinar, J.; Dehner, B.; Beaudry, B. J.; Peterson, D. T. *Phys. Rev. B*, **1988**, *37*, 2066.

(20) Blase, W.; Cordier, G.; Müller, V.; Häußermann. U.; Nesper, R.; Some, M. *Z. Naturforsch. B*, **1994**, *48*, 754.

(21) Shannon, R. D. *Acta Cryst*, **1976**, *A32*, 751.

(22) Sevov, S. C.; Corbett, J. D. *Z. Anorg. Allg. Chem.* **1993**, *619*, 128.

(23) Sevov, S. C. Ph.D. Dissertation, Iowa State University, 1993.

(24) Dong, Z. C.; Corbett, J. D. *Inorg. Chem.* **1996**, *35*, 1444.

(25) Dye, J. L. *Science*, **1990**, *247*, 663.

(26) Meyer, G.; Meyer, H.-J. *Chem. Mat.* **1992**, *4*, 1157.

(27) Corbett, J. D. in *Chemistry, Structure and Bonding of Zintl Phases and Ions*; Kauzlarich, S., Ed.; VCH Publishers: New York, 1996; Chapter 3.

(28) Henning, R. W.; Corbett, J. D. to be submitted for publication.

(29) Henning, R. W.; Leon-Escamilla, E. A.; Zhao, J.-T.; Corbett, J. D. *Inorg. Chem.* **1997**, *36*, 1282.

(30) Laves, F. *Naturwiss.* **1941**, *17*, 244.

(32) Klemm, W.; Busmann, E. *Z. Anorg. Allg. Chem.* **1963**, *319*, 297.

(33) Adolphson, D. G; Corbett, J. D.; Merryman, D. J. *J. Am. Chem. Soc.* **1976**, 98, 7234.

(34) *Chemistry, Structure and Bonding of Zintl Phases and Ions*; Kauzlarich, S., Ed.; VCH Publishers: New York, 1996.

Table 1: Some Data Collection and Refinement Parameters

formula	Cs_8Ga_{11}	$Cs_8Ga_{11}Cl$
space group, Z	*R*3*c* (No. 167), 6	*R*3*c* (No. 167), 6
lattice params[a]		
a, Å	9.9962(5)	10.0111(7)
c, Å	50.839(6)	50.504(6)
V, Å^3	4399.4(9)	4383.5(8)
fw	1830.2	1865.6
d_{calc}, g/cm^3	4.144	4.240
temp, °C	23	23
residuals *R*, R_w,[b] %	2.2, 3.3	2.6, 2.2

[a]Guinier data with Si as an internal standard, λ = 1.540 562 Å, 23° C.
[b]$R = \Sigma||F_o|-|F_c||/\Sigma|F_o|$; $R_w = [\Sigma\omega(|F_o|-|F_c|)^2/\Sigma\omega(F_o)^2]^{1/2}$, $\omega = 1/\sigma_F^2$

Table 2: Positional and Thermal Parameters for Cs_8Ga_{11} and $Cs_8Ga_{11}Cl$[a]

Atom	Wyckoff	*x*	*y*	*z*	$B_{eq}(Å^2)$[b]
Ga1	18*e*	0.8137(1) 0.8128(2)	0	1/4	1.79(5) 1.54(8)
Ga2	12*c*	0	0	0.70594(2) 0.70565(3)	1.90(3) 1.72(5)
Ga3	36*f*	0.41093(8) 0.4142(1)	0.32969(8) 0.3323(2)	0.05623(1) 0.05623(2)	2.17(3) 1.97(4)
Cs1	36*f*	0.07460(5) 0.0761(1)	0.36485(6) 0.36176(9)	0.022718(9) 0.02251(1)	3.02(2) 2.45(3)
Cs2	12*c*	0	0	0.07780(2) 0.07453(2)	3.34(3) 2.95(3)
Cl	6*b*	0	0	0	2.7(2)

[a] Data for $Cs_8Ga_{11}Cl$ are listed second.

[b] $B_{eq} = (8\pi^2/3)\Sigma_i\Sigma_j U_{ij} a_i^* a_j^* \vec{a}_i \vec{a}_j$

Table 3: Selected Bond Distances in Cs_8Ga_{11} and $Cs_8Ga_{11}Cl$ (Å)

		Cs_8Ga_{11}	$Cs_8Ga_{11}Cl$			Cs_8Ga_{11}	$Cs_8Ga_{11}Cl$
Ga1–Ga3	2×	2.6421(7)	2.644(1)	Cs1–Cl			3.4972(7)
Ga1–Ga3	2×	2.6803(3)	2.655(1)	Cs1–Ga1		3.7159(7)	3.719(1)
Ga1–Ga2	2×	2.913(1)	2.920(2)	Cs1–Ga3		3.7210(8)	3.739(1)
Ga1–Cs1	2×	3.7159(7)	3.719(1)	Cs1–Ga3		3.9384(8)	3.930(1)
Ga1–Cs2	2×	4.2711(7)	4.285(1)	Cs1–Ga3		3.9770(9)	4.001(1)
				Cs1–Ga3		4.037(1)	4.008(1)
Ga2–Ga3	3×	2.6809(8)	2.669(1)	Cs1–Ga2	2×	4.0189(5)	4.0503(9)
Ga2–Ga1	3×	2.913(1)	2.920(2)	Cs1–Ga2		4.233(1)	4.211(1)
Ga2–Cs1	3×	4.0189(5)	4.0503(9)	Cs1–Cs1[a]	2×	4.0587(7)	4.0135(9)
Ga2–Cs1	3×	4.233(1)	4.211(1)	Cs1–Cs1		4.3566(8)	4.401(2)
				Cs1–Cs2		4.3928(9)	4.224(1)
Ga3–Ga1		2.6421(7)	2.644(1)	Cs1–Cs2		4.3928(9)	4.523(1)
Ga3–Ga1		2.6803(7)	2.655(1)				
Ga3–Ga2		2.6809(8)	2.669(1)				
Ga3–Ga3		2.756(2)	2.737(2)	Cs2–Cl		–	3.764(1)
Ga3–Cs1		3.7210(8)	3.739(1)	Cs2–Ga3	3×	3.9242(7)	3.914(1)
Ga3–Cs2		3.9242(7)	3.914(1)	Cs2–Ga3	3×	4.1609(8)	4.226(1)
Ga3–Cs1		3.9384(8)	3.930(1)	Cs2–Ga1	3×	4.2711(7)	4.285(1)
Ga3–Cs1		3.9770(9)	4.001(1)				
Ga3–Cs1		4.037(1)	4.008(1)	Cl–Cs1	6×		3.4972(7)
Ga3–Cs2		4.1609(8)	4.226(1)	Cl–Cs2	2×		3.764(1)

[a] d(Cs–Cs) < 4.8 Å.

Table 4: Lattice parameters[a] of the $A_8Tr_{11}X$ compounds

	a (Å)	*c* (Å)	V (Å^3)	Lines Indexed
$Rb_8Ga_{11}Cl$	9.7036(5)	49.079(4)	4002.2(5)	80
Cs_8Ga_{11}	9.9962(5)	50.839(6)	4399.4(9)	37
$Cs_8Ga_{11}Cl$	10.0111(7)	50.504(6)	4383.5(8)	84
$Cs_8Ga_{11}Br$	10.0587(5)	50.620(4)	4435.4(6)	73
$Cs_8Ga_{11}I$	10.1067(9)	50.820(8)	4495(1)	49
Rb_8In_{11}[b]	10.301(3)	52.367(7)	4812(2)	
$Rb_8In_{11}Cl$	10.250(2)	52.33(2)	4762(2)	21
$Cs_8In_{11}Cl$	10.5612(4)	53.820(4)	5198.8(6)	42
Cs_8Tl_{11}[c]	10.553(1)	53.771(9)	5186(2)	38
$Cs_8Tl_{11}Cl$	10.543(4)	53.23(5)	5124(6)	16
$Cs_8Tl_{11}Br$	10.595(4)	53.60(4)	5211(5)	25
$Cs_8Tl_{11}I$	10.603(1)	53.75(1)	5233(2)	47

[a] Guinier data with Si as an internal standard, λ = 1.540562 Å, 23° C.
[b] Ref. 20.
[c] Ref. 12.

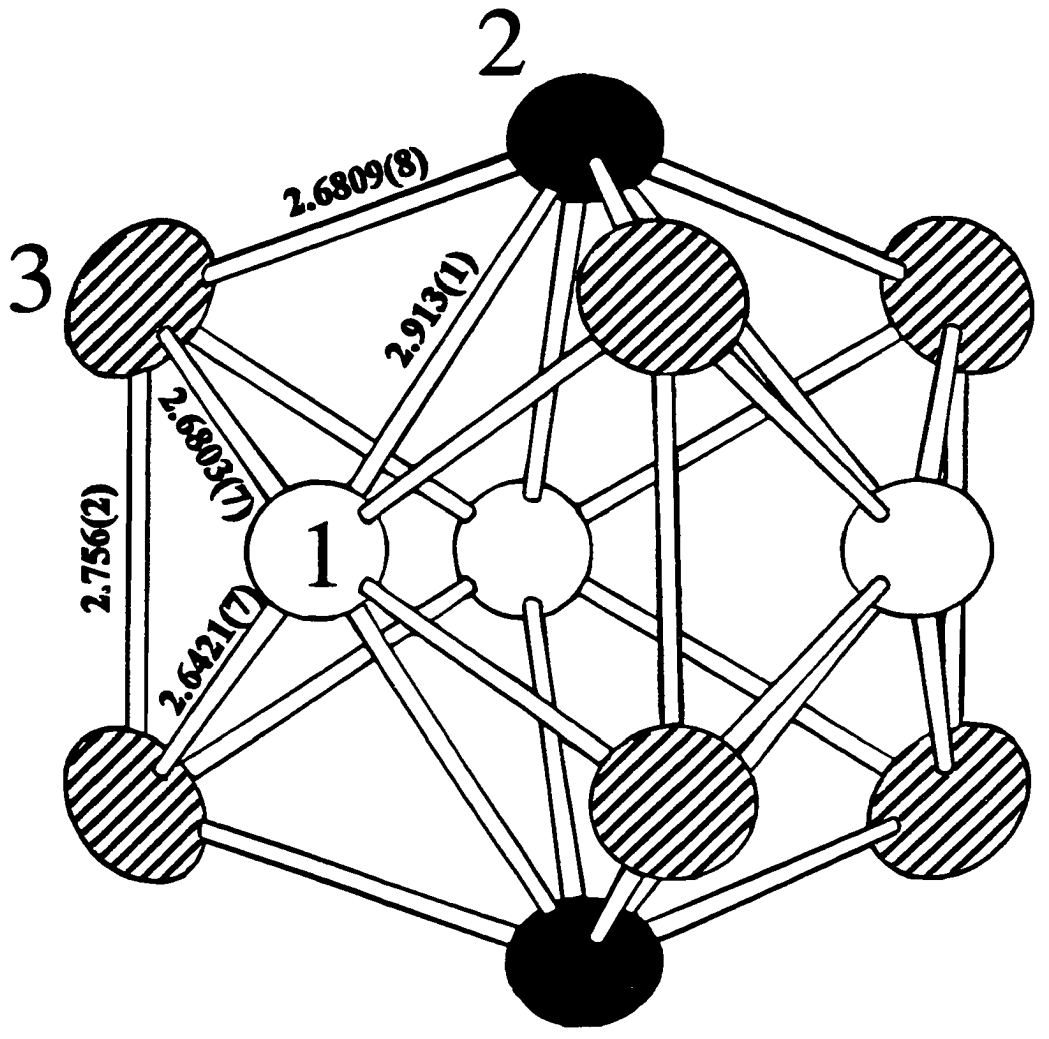

Figure 1. Isolated Ga_{11}^{7-} cluster in Cs_8Ga_{11} with the three-fold (*c*) axis vertical. Thermal ellipsoids are drawn at the 90% probability level.

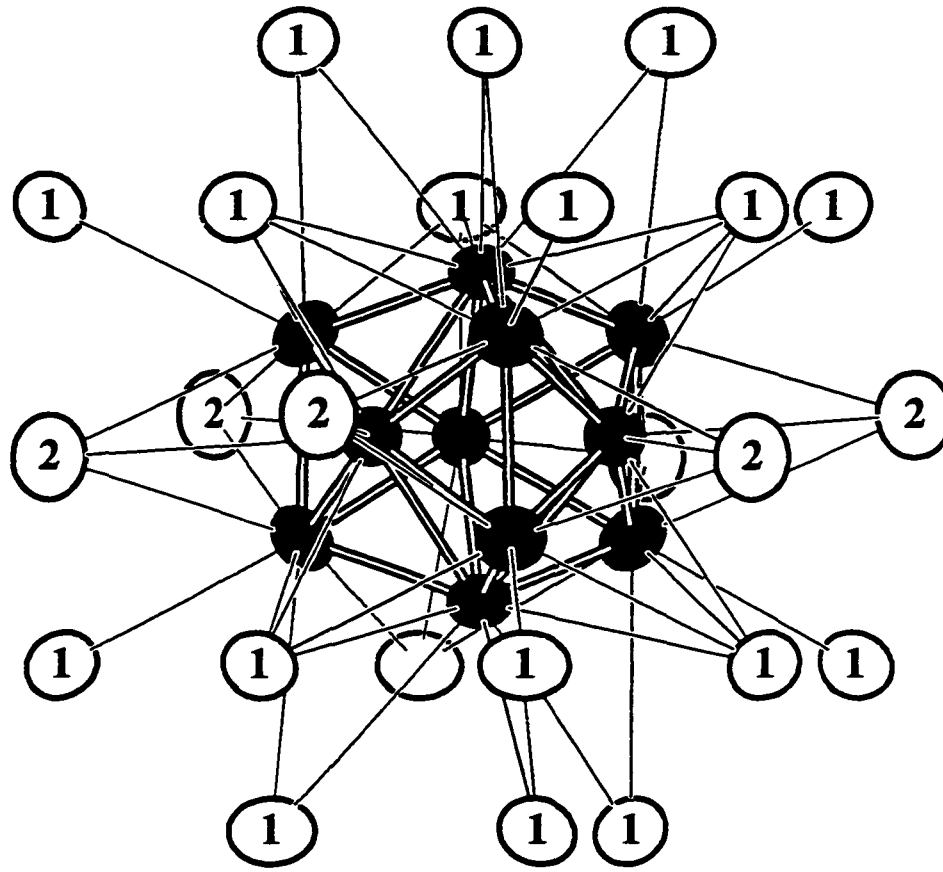

Figure 2. Cesium coordination environment around the Ga_{11}^{7-} cluster. Ellipsoids drawn at 90% probability.

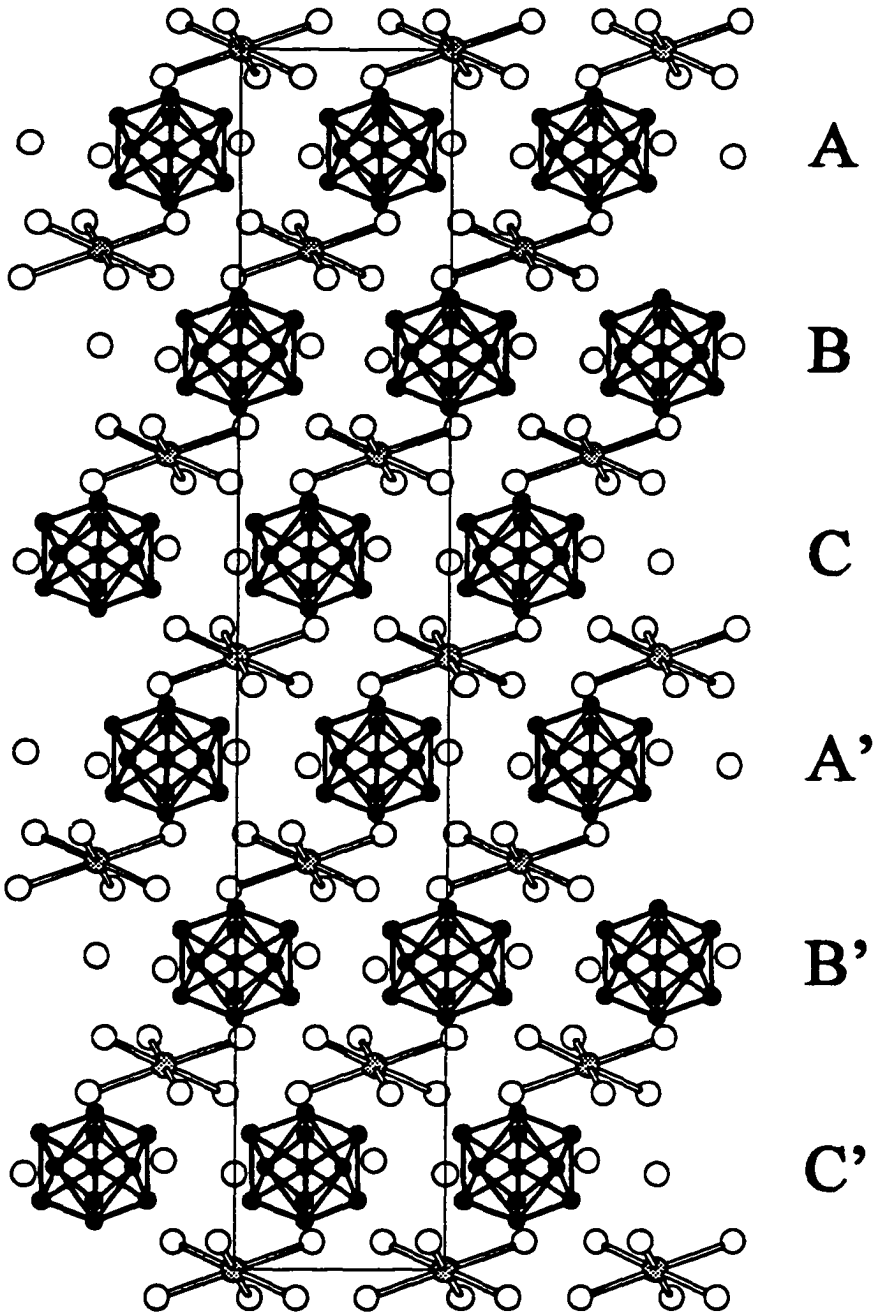

Figure 3. [100] view of $Cs_8Ga_{11}Cl$. The clusters are arranged in pseudo-ccp layers of clusters plus Cs2. These are interleaved with double layers of Cs1 atoms (open) with Cl in compressed, augmented trigonal antiprismatic cavities. Cs2 neighbors to one chlorine are dashed in.

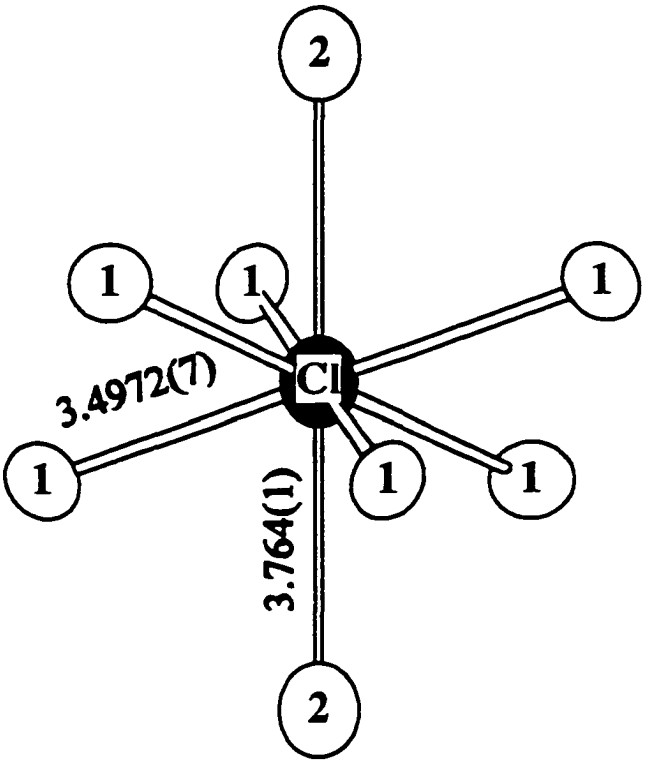

Figure 4. Environment around the Cl atom in $Cs_8Ga_{11}Cl$.

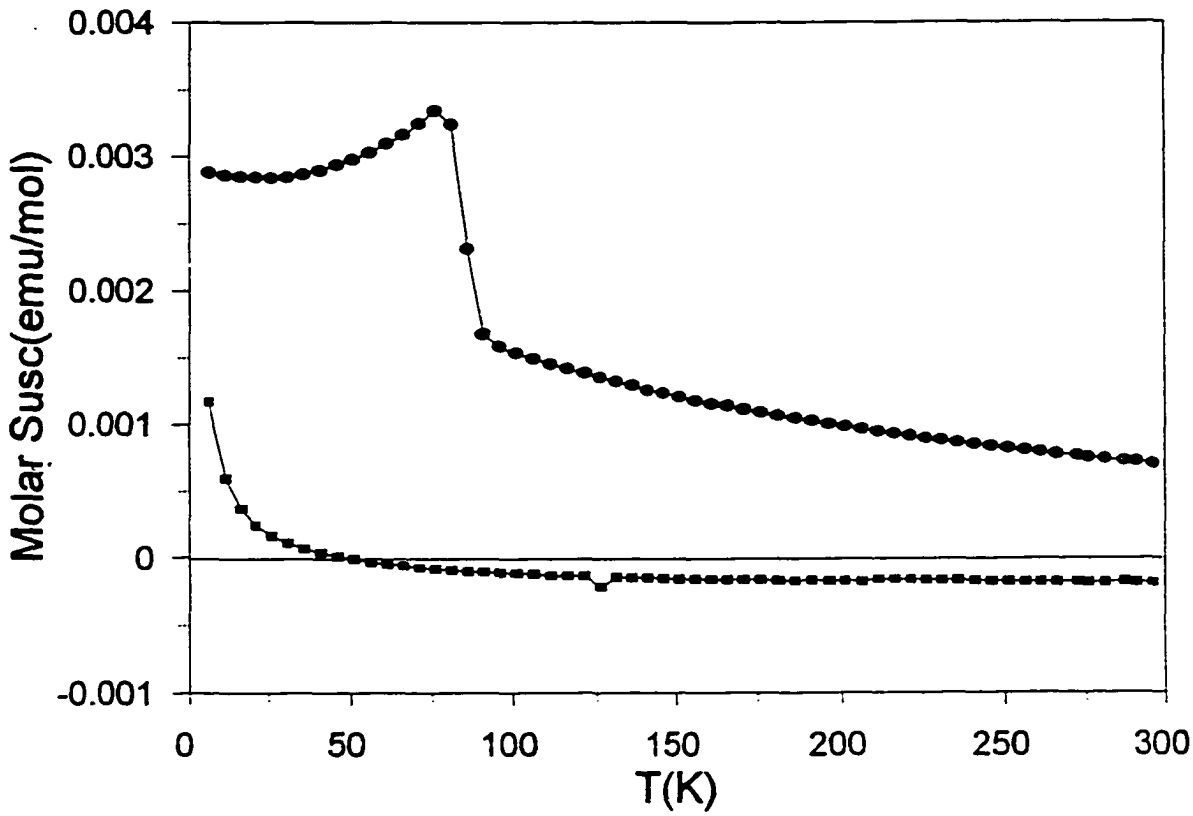

Figure 5. Temperature dependence of the magnetic susceptibilities of Cs_8Ga_{11} and $Cs_8Ga_{11}Cl$ at 3 T.

Supporting Information

Cs_8Ga_{11}, A New Isolated Cluster In a Binary Gallium Compound. A Family of Valence Analogues $A_8Tr_{11}X$: A = Cs, Rb; Tr = Ga, In, Tl; X = Cl, Br, I

Robert W. Henning and John D. Corbett*

Table S1: Data Collection and Refinement Parameters for Cs_8Ga_{11} and $Cs_8Ga_{11}Cl$

crystal size, mm	0.25 x 0.28 x 0.40	0.14 x 0.20 x 0.25
space group, Z	*R*3*c* (No. 167), 6	*R*3*c* (No. 167), 6
crystal size, mm	0.25 x 0.28 x 0.40	0.14 x 0.20 x 0.25
lattice params[a]		
a, Å	9.9962(5)	10.0111(7)
c, Å	50.839(6)	50.504(6)
V, Å^3	4399.4(9)	4383.5(8)
d_{calc}, g/cm^3	4.144	4.240
radiation; $2\theta_{max}$	Mo K_α; 50°	Mo K_α; 50°
octants measured	±h, +k, ±l	±h, +k, +l
scan method	ω	ω
temp, °C	23	23
transmission range	0.613-1.000	0.228-1.000
μ, cm^{-1} (Mo K_α)	196.2	197.8
number of reflections:		
measured	7927	2773
observed ($I \geq 3\sigma_I$)	4138	1032
unique observed ($I \geq 3\sigma_I$)	739	544
number of variables	31	32
R_{avg} ($I \geq 3\sigma_I$), %	9.1	6.0
residuals R, R_w[b] %	2.2, 3.3	2.6, 2.2
goodness of fit	1.20	1.04

[a]Guinier data with Si as an internal standard, λ = 1.540562 Å, 23° C.
[b]$R = \Sigma||F_o|-|F_c||/\Sigma|F_o|$; $R_w = [\Sigma\omega(|F_o|-|F_c|)^2/\Sigma\omega(F_o)^2]^{1/2}$, $\omega = 1/\sigma_F^2$.

Table S2: Anisotropic Thermal Parameters for Cs_8Ga_{11} and $Cs_8Ga_{11}Cl$[a]

Atom	U_{11}[b]	U_{22}	U_{33}	U_{12}	U_{13}	U_{23}
Ga1	0.0236(4)	0.0214(5)	0.0223(6)	0.0107	0.0002(2)	0.0004
	0.0188(7)	0.016(1)	0.0228(7)	0.0081	0.0005(3)	0.0011
Ga2	0.0266(4)	0.0266	0.0188(7)	0.0133	0	0
	0.0231(8)	0.0231	0.0192(8)	0.0116	0	0
Ga3	0.0239(4)	0.0312(4)	0.0280(5)	0.0143(3)	-0.0063(3)	0.0013(3)
	0.0203(7)	0.0274(8)	0.0275(4)	0.0121(6)	-0.0075(5)	0.0017(5)
Cs1	0.0370(3)	0.0525(3)	0.0319(3)	0.0274(2)	0.0034(2)	-0.0005(2)
	0.0314(5)	0.0348(5)	0.0316(3)	0.0202(4)	0.0028(3)	-0.0024(3)
Cs2	0.0371(3)	0.0371	0.0528(6)	0.0186	0	0
	0.0327(5)	0.0327	0.0468(6)	0.0164	0	0
Cl	0.030(3)	0.030	0.044(3)	0.015	0	0

[a] Listed second.

[b] $T = \exp[-2\pi^2(U_{11}h^2a^{*2} + U_{22}k^2b^{*2} + U_{33}l^2c^{*2} + 2U_{12}hka^*b^* + 2U_{13}hla^*c^* + 2U_{23}klb^*c^*)]$.

FORMATION OF ISOLATED NICKEL-CENTERED GALLIUM CLUSTERS IN $Na_{10}Ga_{10}Ni$ AND A 2-D NETWORK OF GALLIUM OCTAHEDRA IN K_2Ga_3

A paper to be submitted to Inorganic Chemistry

Robert W. Henning and John D. Corbett*

Department of Chemistry and Ames Laboratory—DOE,[1]

Iowa State University, Ames IA 50011

Abstract

Exploration of the sodium–gallium–nickel system has revealed a new compound containing an isolated gallium cluster, $Ga_{10}Ni^{10-}$. Single crystal x-ray diffraction of $Na_{10}Ga_{10}Ni$ (*Pnma*, Z = 12, a = 13.908(3) Å, b = 28.146(6) Å, c = 16.286(4) Å) indicates two similar types of "naked" clusters of ten gallium atoms which contain distorted, tetra-capped trigonal prismatic gallium centered by nickel. The sodium atoms serve to isolate the clusters from each other as well as to provide the cluster with a closed shell configuration of electrons. This is the first isolated gallium cluster in an alkali-metal system which is centered by a transition element. Molecular orbital calculations on the isolated cluster are also reported. The crystal structure of K_2Ga_3 (*I4/mmm*, Z = 4, a = 6.1382(3), c = 14.815(1)) has also been investigated. This compound is isostructural with A_2In_3 (A = Rb or Cs) and contains Ga_6^{4-} octahedra connected through the waist atoms to form a layered structure with the octahedra of adjacent

layers sitting in the depressions of the first. The potassium atoms have characteristically regular roles except for an unusually short K–K contact (d(K–K) = 3.242(4) Å). Magnetic measurements indicate that both phases are diamagnetic and consistent with the Zintl formalism, viz. $(Na^+)_{10}(Ga_{10}Ni)^{10-}$ and $(K^+)_4Ga_6^{4-}$.

Introduction

The alkali-metal–gallium systems are well known for the formation of cluster compounds.[2] Many of the clusters are related to the deltahedral clusters found in borane chemistry such as Ga_6 and Ga_{12} but others with unique geometries such as Ga_{15} and Ga_{17} also form. As in borohydride chemistry, the skeletal electron counts in the deltahedral clusters follow Wade's rules.[3] In addition, when the electrons from the cations are considered the compounds are electron precise or Zintl phases.[4] For closo-deltahedra, this means that for n atoms in the cluster, 2n + 2 electrons are needed for skeletal bonding. In addition, a lone pair is needed on each vertex atom. Since gallium only has three valence electrons, a high charge would occur on an isolated cluster, eg. Ga_{12}^{14-}. The high charge does not seem favorable for gallium or indium although several thallium examples have been reported. To reduce the high charge, the cluster may form exo-bonds (link) to an adjacent cluster or to gallium spacers between the clusters. This process forms layered or network structures which are commonly observed for gallium, e.g. AGa_3 (A = Rb[5] and Cs[6]) or in $Na_{22}Ga_{39}$.[7] Distortion of the clusters away from the ideal deltahedral symmetries also can reduce the number of skeletal electrons needed for cluster formation. This has been observed in the A_8Tr_{11} and $A_8Tr_{11}X$ structures (A = K, Rb, or Cs; Tr = Ga, In, or Tl; X = Cl, Br, or I).[8] Another way to reduce the charge on

the cluster is to introduce interstitial atoms inside the cluster without distortion. $Na_3K_8Tl_{13}$ forms thallium centered thallium icosahedra, Tl_{13}^{11-}, which are isolated from each other.[9] A combination of cluster distortion and centering is needed to stabilize $Na_{10}Ga_{10}Ni$. This type of stabilization is also seen in $K_8Tr_{10}Zn$ (Tr = In[10] and Tl[11]) and $K_{10}In_{10}Ni$[12] (isostructural with $Na_{10}Ga_{10}Ni$). The alkali-metal–gallium compounds are well known for forming network structures so the presence of isolated $Ga_{10}Ni0^{10-}$ clusters in $Na_{10}Ga_{10}Ni$ is quite novel.

K_2Ga_3 is an example of a Zintl phase in which gallium octahedra condense to form a two-dimensional layered compound.[13] This structure type has been reported for A_2In_3[14] (A = Rb or Cs) and observed by Guinier powder pattern for K_2Ga_3[13] but no structural information has been reported to date.

This paper reports the synthesis and characterization of both $Na_{10}Ga_{10}Ni$ and K_2Ga_3. The structures were elucidated by X-ray single crystal refinements and the properties of $Na_{10}Ga_{10}Ni$ by magnetic susceptibility data. Molecular orbital calculations were performed for the isolated $Ga_{10}Ni^{10-}$ cluster.

Experimental Section

Stoichiometric amounts of the elements for the title compounds were welded into tantalum tubing using techniques described previously.[15] Potassium (99.95%, Alfa), gallium (99.99%, Johnson-Matthey), and nickel (99.99%, Johnson-Matthey, 100 mesh) were used as received while the surface of the sodium metal (99.9%, Alpha) was cleaned with a scalpel before use. All materials were handled in a N_2-filled dry box. The reaction mixtures were

heated to 650 °C and held at that temperature for 24 hours to ensure homogeneity of the samples. This was followed by slow cooling (3 °C/h) to room temperature.

$Na_{10}Ga_{10}Ni$. A dull grey, microcrystalline product formed which was ~100% $Na_{10}Ga_{10}Ni$ according to Guinier powder patterns. Suitable crystals were sealed into thin-walled capillaries and checked for singularity by Laue photographs. Structural information was collected on a Rigaku AFC6R rotating anode X-ray diffractometer at room temperature with Mo Kα radiation. An orthorhombic unit cell was determined from 25 reflections which were obtained by a random search. Two octants of data (h, $\pm k$, l) were collected up to 50° in 2θ and corrected for Lorentz and polarization effects. Of the 14,801 reflections measured, 6902 were observed ($I \geq 3\sigma_I$) and 2,684 of these were unique. Three ψ-scans ($\mu = 135.2$ cm^{-1}) were applied to the data to correct for absorption. Systematic absences suggested the centrosymmetric space group *Pnma* (No. 62). One noncentrosymmetric space group was also possible, $Pna2_1$ (No. 33), but the N(Z) distribution gave strong indications that the structure is centrosymmetric.

Application of direct methods[16] revealed 19 heavy atom positions, two of which were assigned to nickel on the basis of atomic distances. The remaining peaks were assigned to gallium. Refinement of the positional parameters for nickel and gallium was followed by a difference Fourier analysis that revealed 17 peaks appropriate for sodium. Isotropic refinement of all atoms ($R(F) = 10.2\%$) was followed by DIFABS[17] which reduced the $R(F)$ to 9.6%. This also produced nearly spherical ellipsoids and smaller standard deviations in all parameters. Anisotropic refinement of all atoms reduced $R(F)$ to 6.2%. With 298 variables, the reflection parameter ratio is small at ~9:1. More data at higher angles would improve the

refinement but the combination of a weakly diffracting crystal with a large unit cell made this data collection unreasonable with current point-source techniques. The use of an area detector would be beneficial. The question arises if the sodium atoms should only be refined isotropically. This would reduce the number of variables to 204 and increase the corresponding reflection parameter ratio to ~13:1. Refining the structure in this manner did not change the $R(F)$ or any other factors appreciably. Even though Hamilton's test[18] suggests that refining the anisotropic thermal parameters of sodium is not statistical meaningful, the full refinement is still reported. The largest positive and negative peaks in the final difference map were 2.91 $e^-/Å^3$ (1.85 Å from Ga6A) and -1.77 $e^-/Å^3$. All refinements were carried out on a VAX workstation using the TEXSAN crystallographic package.[19]

Data collection parameters are listed in Table 1 and atomic positions and isotropic-equivalent parameters are in Table 2. Additional data collection and refinement parameters, a bond distance table, and the anisotropic thermal parameters are given in the Supporting Information. These and the F_o/F_c data are also available from J.D.C.

K_2Ga_3. This product also was obtained in high yield but it was more sensitive to moisture and air than most compounds in the alkali-metal–gallium systems. This made sharp Guinier powder patterns difficult to obtain. The crystals had a metallic luster and were very brittle. Single crystals were collected in the same manner as before, and data collection was performed on the same diffractometer. Twenty-five reflections obtained from a random search were indexed with a body-centered tetragonal unit cell. Four octants of reflection data (h, $\pm k$, $\pm l$) were collected at room temperature with Mo Kα up to 60° in 2θ and corrected for Lorentz and polarization effects. No violations of the body-centering were observed.

Absorption was corrected by applying six ψ-scans collected over a range of 2θ angles. Systematic absences and the N(Z) distribution suggested centrosymmetric space group *I*4/*mmm* (no. 139). Four other space groups were possible, I422, I4*mm*, I$\bar{4}$2*m*, and I$\bar{4}$*m*2, but they are noncentrosymmetric.

The structure solution obtained by direct methods contained four peaks. Two were assigned to gallium and two to potassium based on bond distances. The refinement proceeded smoothly with a final $R(F)$ of 1.8% without the use of DIFABS. The largest positive and negative peaks in the final difference map were 1.26 $e^-/Å^3$ (1.74 Å from K2) and -0.45 $e^-/Å^3$.

Data collection parameters, atomic positions and isotropic-equivalent parameters, and selected bond distances are in Tables 3, 4, and 5, respectively. Additional data collection and refinement parameters as well as the anisotropic thermal parameters are given in the Supporting Information. These and the F_o/F_c data are also available from J.D.C.

Property Measurements. Magnetic susceptibility measurements were collected on a Quantum Design MPMS SQUID magnetometer. The air sensitivity of $Na_{10}Ga_{10}Ni$ and K_2Ga_3 required the use of a special sample holder consisting of a 3 mm id. silica tube, ~17 cm long, and 2 silica rods (3 mm in diameter and ~8 cm long each) which fit snugly inside the larger tube. One rod was fused into one end of the tube. In a helium-filled glove box, powdered $Na_{10}Ga_{10}Ni$ (29.2 mg) or K_2Ga_3 (50.3 mg) was placed inside the tube and the second rod was inserted to fix the sample between the 2 rods. The second rod is then fused into the tube to seal the container. The susceptibility of each sample was measured in a field of 3 T over the temperature range of 6-300 K. The raw data were corrected for the sample holder and core

diamagnetism. The latter correction factors were -1.42 x 10^{-4} and -5.0 x 10^{-5} emu/mol for $Na_{10}Ga_{10}Ni$ and K_2Ga_3, respectively.

Electronic Calculations. Molecular orbital calculations were performed on the $Ga_{10}Ni^{10-}$ cluster using the EHMACC program on a PC. The H_{ii} parameters used for Ga[20] and Ni[21] were -14.58 and -6.75 eV for Ga 4s and Ga 4p, respectively, and -9.17, -5.15, and -13.49 eV for Ni 4s, Ni 4p, and Ni 3d, respectively.

Results and Discussion

$Na_{10}Ga_{10}Ni$. The most interesting structural features of $Na_{10}Ga_{10}Ni$ are the two isolated clusters of 10 gallium atoms centered by nickel, $Ga_{10}Ni^{10-}$. The gallium atoms on each cluster can be viewed as a strongly distorted trigonal prism with all three rectangular and one trigonal face capped by gallium (Figure 1). The trigonal face with the capping atom is expanded so that all Ga–Ni contacts are nearly equidistant (2.459(6)–2.529(4) Å, Supplementary Information). This is consistent with the Ga–Ni contacts in Ni_2Ga_3 which range from 2.38–2.61 Å and average 2.50 Å over eight distances.[22] Ga–Ga contacts on the clusters are typical for hypoelectronic clusters of this sort (2.6–2.9 Å). The two clusters (labeled A and B) have similar geometries except that B is located on a mirror plane while A is in a general position. More specifically, NiB, Ga2B, Ga4B, Ga5B, and Ga7B are on such special positions. Even though the basic geometry of the two clusters is the same, comparison of Ga–Ga bond distances show that some of the distances vary by as much as ~0.11 Å. This is mainly due to the lower symmetry cluster forming more consistent bond lengths between the gallium atoms. The clusters occur in the ratio of 2:1 (A:B) with each having a local

symmetry of ~C_{3v}. Each unit cell has twelve clusters with the closest contact between them at 4.88 Å (Figure 2). The thermal parameters for the nickel are slightly smaller than those for gallium but this is consistent with a 10-coordinate, tightly bound atom. The gallium atoms are not highly coordinated and have larger thermal ellipsoids but these are still quite spherical.

The clusters are arranged in close-packed layers in the *b*-*c* plane with hexagonal stacking of the layers along the *a*-axis (Figure 3). Since the clusters are roughly spherical, the close-packing leaves large trigonal antiprismatic voids between the layers. Many of the holes are appropriately sized for the sodium cations with Na–Ga and Na–Na contacts in the range of 3.0-3.3 and 3.35-3.6 Å, respectively. Some of the interlayer holes are a little large (radius ≥~3.2 Å) and the cations are poorly bound. These positions tend to have only two or three contacts that are reasonable and the rest are longer. This can be seen in the large thermal parameters (~6 $Å^2$) for several of the sodium atoms. Additional sodium atoms sit between the clusters within the layer. These positions tend to be more tightly bound to gallium and have slightly smaller ellipsoids (~3.5 $Å^2$). Attempts to substitute potassium into the structure always resulted in the formation of K_2Ga_3.

Although $Na_{10}Ga_{10}Ni$ can be prepared in ~100% yield from the melt by slow cooling, it was difficult to obtain single crystals that were large enough for single crystal X-ray diffraction. Extended annealing (≥ one month) at various temperatures resulted in decomposition of $Na_{10}Ga_{10}Ni$ into $Na_{22}Ga_{39}$, Ni_2Ga_3, and a small amount of sodium metal. Reactions loaded off stoichiometry either produced one of the known binaries or, in the case of excess sodium, did not completely react. Lattice constants for Guinier powder patterns from the reactions loaded off stoichiometry indicate that $Na_{10}Ga_{10}Ni$ is a line compound within

3σ. Attempts to incorporate the heavier palladium and platinum atoms into the cluster failed. Reactions with earlier transition metals (Co, Cr, Fe) also failed, presumably because of the lower electron count (discussed later).

This compound is isostructural with $K_{10}In_{10}Ni$.[12] The heavier analog has similar problems with large thermal ellipsoids for the cations but it appears to be more stable than $Na_{10}Ga_{10}Ni$. $K_{10}In_{10}Ni$ forms a well crystallized phase without any sign of side products. Several factors may affect the relative stability of these phases. Other isolated clusters are unusual for the alkali-metal–gallium systems with only the Cs_8Ga_{11}, $Cs_8Ga_{11}X$, and $Rb_8Ga_{11}X$ compounds known (X = Cl, Br, and I). Indium on the other hand is more tolerant of forming isolated clusters. This may be due to the greater stability of the lone pairs of s electrons on each vertex as you move down the column of the periodic table. This is especially true with the thallium system which contains an abundance of new isolated clusters. Another factor affecting the stability of $K_{10}In_{10}Ni$ is the lack of comparable decomposition products. Ni_2In_3 is known to exist but analogous $K_{22}In_{39}$ is not. All of these factors appear to contribute to the lower stability of $Na_{10}Ga_{10}Ni$ relative to $K_{10}In_{10}Ni$.

Electronic structure. Molecular orbital calculations were performed on the isolated $Ga_{10}Ni^{10-}$ cluster. Calculations were also performed on a gallium cluster without the centering atom to gain a better understanding of the nickel bonding within the cluster. Since the observed cluster is very close to the ideal C_{3v} point group symmetry such that the pseudo-degenerate energy levels are only split by approximately 0.06 eV, the calculations were performed on a slightly modified cluster with true C_{3v} symmetry. The lowest ten orbitals of the empty cluster calculation lie between -12 and -20 eV and are primarily composed of the

Ga 4s orbitals. These ten orbitals represent the delocalized equivalent of the lone pair electrons on each gallium vertex. The ten orbitals that lie just below the HOMO–LUMO gap (dotted line in Figure 4, ~1.0 eV) are the bonding cluster orbitals which are formed primarily of Ga 4p orbitals. Incorporation of nickel into the cluster does not have a significant effect on most of the molecular orbitals. Some mixing of the Ni 3d orbitals with the gallium cluster orbitals occurs around -14 eV. This lowers five of the cluster orbitals ~1 eV but also adds the five nickel orbitals to the system. The nickel d orbitals are fully occupied. Bonding between the centering atom and the rest of the cluster also occurs between the 4s orbital on nickel and the Ga 4p orbitals. The Ni 4s orbital interacts with the a_1 molecular orbital at -7 eV. This lowers the a_1 cage orbital ~1 eV primarily because of bonding interactions with the p_z orbital on the axial capping atom. The antibonding combination has strong interactions between the Ga p_z and Ni s orbitals and forces this level much higher (~10 eV) in energy. The net result is that nickel does not introduce any extra bonding orbitals but does stabilize a few cluster orbitals through Ni 4s–Ga 4p bonding. The Ni 4p orbitals are a little higher in energy and do not contribute significantly to most of the bonding orbitals.

This is analogous to the bonding within $In_{10}Ni^{10-}$ except that the energies of the gallium orbitals are lower. The main significance of this is that the Ni 4p orbitals are not as involved in the bonding orbitals while the Ni 3d occur at an energy suitable for mixing with some of the cluster orbitals.

Properties. The temperature dependent magnetic susceptibility measurements performed on $Na_{10}Ga_{10}Ni$ indicate the phase is diamagnetic (Figure 5). This is consistent with the closed shell nature of the material. Even though the susceptibility is within the range of a

diamagnetic material, a small temperature dependence is present which could indicate a paramagnetic impurity. Even though powder patterns indicate that this phase can be prepared single phase by slow cooling, some impurities could still be present especially considering the metastable nature of $Na_{10}Ga_{10}Ni$. The slope is also observed in the $K_{10}In_{10}Ni$ phase which may indicate some intrinsic properties of this compound but an impurity phase can not be ruled out.

K_2Ga_3. The main building blocks of K_2Ga_3 are gallium octahedra that are interconnected into a layered compound (Figure 6). The octahedra have local symmetry D_{4h} with Ga2 atoms in the waist of each octahedron and Ga1 on the other two vertices. Bonding between the clusters occurs through 2-center–2-electron bonds between pairs of Ga2 atoms on adjacent clusters. This forms a 4^4-layer of octahedra and a tetragonal structure. The octahedra of adjacent layers sit in the depressions of the first, creating a body-centered unit cell. This structure type has been observed in A_2In_3 (A = Rb or Cs) so it is not surprising to find it in the gallium system with an appropriately smaller cation.

The Ga–Ga bond distances within each cluster are consistent with those in related phases (Table 5). Ga1 forms four symmetry equivalent bonds to Ga2 (d(Ga1–Ga2) = 2.7393(8) Å) within the cluster but does not form an exo-bond. It is formally assigned a lone pair and is surrounded by four K1 cations at d(K1–Ga1) = 3.4829(4) Å and one K2 cation at d(K2–Ga1) = 3.729(2) Å. Each five bonded Ga2 atom is connected to two Ga1 apex atoms and to two other Ga2 atoms (d(Ga2–Ga2) = 2.5579(8) Å). Ga2 also forms an exo-bond to an adjacent cluster at d(Ga2–Ga2) = 2.521(1) Å. Contacts between potassium atoms are typical for these cations except for an unusually short K2–K2 distance of 3.242(4) Å.

A closer look at the cation arrangement in K_2Ga_3 reveals a framework that is similar to the gallium atoms in $NaGa_4$[23] (Figure 7). Gallium in this phase contains a layer of edge-sharing square pyramids with adjacent pyramids pointing in opposite directions. The apex of each pyramid connects with an apex atom in the adjacent layer. This is the same pattern that the potassium atoms exhibit in K_2Ga_3. The sodium atoms in $NaGa_4$ sit in the large holes generated by the gallium framework. This structure type has been observed in several other compounds such as $BaAl_4$. In the case of K_2Ga_3 (or K_4Ga_6), the gallium octahedra sit in the large hole which was formed by the potassium framework.

The octahedron is a classical example of a closo-deltahedral cluster which can be described by Wade's rules. The octahedron requires 14 skeletal electrons (2n + 2) and with only four exo-bonds would have a formal charge of Ga_6^{4-}, the four extra electrons acquired from the four cations per cluster. This makes K_2Ga_3 a closed shell compound and a Zintl phase. The closed shell nature of the compound has been confirmed through magnetic susceptibility measurements (Figure 5).

Conclusions

The alkali-metal–gallium binary systems are well known for forming network structures consisting of exo-bonded deltahedral clusters. The high formal charge on the clusters being alleviated by the interbonding of the clusters. K_2Ga_3 is a good a example of this type of connectivity. The only exception to this trend occurs with Cs_8Ga_{11} and related halide compounds which contain isolated Ga_{11}^{7-} units. Ternary phases with the late transition metals also produce framework materials but with other structure types, and these typically contain

anionic sites with mixed occupancy, e.g. $Na_{35}Cd_{24}Ga_{56}$[24] and $Na_{128}Au_{81}Ga_{275}$.[25] This strong tendency to form network materials makes the formation of isolated $Ga_{10}Ni^{10-}$ units in $Na_{10}Ga_{10}Ni$ a more interesting result. Moreover, this compound also conforms to the traditional Zintl concepts which have been well established in this area of the periodic table.

Acknowledgments

We are grateful to J. Ostenson for the magnetic measurements.

References

(1) This research was supported by the Office of the Basic Energy Sciences, Materials Sciences Division, U.S. Department of Energy. The Ames Laboratory is operated by Iowa State University under Contract No. W-7405-Eng.82.

(2) Belin, C.; Tillard-Charbonnel, M. *Prog. Solid St. Chem.* **1993**, *22*, 59.

(3) Wade, K. Adv. *Inorg. Chem. Radiochem.* **1976**, *18*, 1.

(4) Corbett, J. D. *Structure and Bonding* **1997**, *87*, 157.

(5) Ling, R. G.; Belin, C. Z. *Anorg Allg. Chem.* **1981**, *480*, 181.

(6) van Vucht, J. H. N. *J. Less–Common Met.* **1985**, *108*, 163.

(7) Ling, R. G.; Belin, C. *Acta. Cryst.* **1982**, *B38*, 1101.

(8) Henning, R.W.; Corbett, J.D. Inorg. Chem. in press (1997).

(9) Dong, Z.C.; Corbett, J. D. *J. Am. Chem. Soc.* **1995**, *117*, 6447.

(10) Sevov, S. C.; Corbett, J. D. *Inorg. Chem.* **1993**, *32*, 1059.

(11) Dong, Z.C.; Henning, R. W.; Corbett, J.D. *Inorg. Chem.* **1997**, *36*, 3559.

(12) Sevov, S. C.; Corbett, J. D. *J. Am. Chem. Soc.* **1993**, *115*, 9089.

(13) Tillard-Charbonnel, M.; Chouzibi, N.; Belin, C. *C. R. Acad. Sci. Série II*, **1990**, *311*, 69.

(14) Sevov, S. C.; Corbett, J. D. *Z. Anorg. Allg. Chem.* **1993**, *619*, 128.

(15) Dong, Z. C.; Corbett, J. D. *J. Am. Chem. Soc.* **1994**, *116*, 3429.

(16) Sheldrick, G. M. SHELXS-86, Universität Göttingen, Germany, 1986.

(17) Walker, N.; Stuart, D. *Acta. Cryst.* **1983**, *A39*, 158.

(18) Stout, G. H.; Jensen, L. H. "X-ray Structure Determination," Wiley, New York, 1989, 388.

(19) TEXSAN, version 6.0, Molecular Structure Corp., The Woodlands, Texas, 1990.

(20) Canadell, E.; Eisenstein, O.; Rubio, J. *Organometallics*, **1984**, *3*, 759.

(21) Lauher, J. W.; Elian, M.; Summerville, R. H.; Hoffmann, R. *J. Am. Chem. Soc.* **1976**, *98*, 3219.

(22) Hellner, E. *Z. Metal.* **1950**, *41*, 480.

(23) Bruzzone, G. *Acta. Cryst.* **1969**, *25B*, 1206.

(24) Tillard-Charbonnel, M.; Belin, C. *Mat. Res. Bull.* **1992**, *27*, 1277.

(25) Tillard-Charbonnel, M.; Belin, C. *Z. Krist.* **1993**, *206*, 310.

Table 1: Data Collection and Refinement Parameters for $Na_{10}Ga_{10}Ni$

Crystal size, mm	0.27 x 0.23 x 0.22
Space group, Z	*Pnma* (no. 62), 12
Lattice parameters,[a]	
a, Å	13.908(3)
b, Å	28.146(6)
c, Å	16.286(4)
V, Å^3	6375(4)
d_{calc}, g/cm^3	3.081
μ, cm^{-1} (Mo Kα)	134.76
$R_{avg.}$ ($I \geq 3\sigma_I$), %	5.6
Residuals R; R_w,[b] %	6.2; 6.3

[a]Guinier data with Si as an internal standard, λ = 1.540562 Å, 23° C.

[b]$R = \Sigma||F_o|-|F_c||/\Sigma|F_o|$; $R_w = [\Sigma\omega(|F_o|-|F_c|)^2/\Sigma\omega(F_o)^2]^{1/2}$, $\omega = 1/\sigma_F^2$

Table 2: Positional and Thermal Parameters for $Na_{10}Ga_{10}Ni$

Atom	Wyckoff	*x*	*y*	*z*	$B_{eq}(Å^2)^a$
Ga1A	8*d*	0.8644(2)	0.4257(1)	0.9737(2)	2.0(1)
Ga2A	8*d*	0.8690(2)	0.4764(1)	0.1256(2)	1.9(1)
Ga3A	8*d*	0.7236(2)	0.4934(1)	0.0097(2)	1.8(1)
Ga4A	8*d*	0.7574(2)	0.3367(1)	0.0247(2)	2.1(1)
Ga5A	8*d*	0.7701(2)	0.4093(1)	0.2344(2)	1.9(1)
Ga6A	8*d*	0.5692(2)	0.4270(1)	0.0776(2)	1.9(1)
Ga7A	8*d*	0.8935(2)	0.3725(1)	0.1216(2)	2.6(1)
Ga8A	8*d*	0.6740(2)	0.4830(1)	0.1712(2)	1.8(1)
Ga9A	8*d*	0.6707(2)	0.4067(1)	0.9459(2)	1.8(1)
Ga10A	8*d*	0.6510(2)	0.3538(1)	0.1572(2)	2.4(1)
NiA	8*d*	0.7448(2)	0.4167(1)	0.0855(2)	0.9(1)
Ga1B	8*d*	0.8440(2)	0.6970(1)	0.1481(2)	2.2(1)
Ga2B	4*c*	0.8673(3)	3/4	-0.0034(3)	2.3(2)
Ga3B	8*d*	0.6441(2)	0.6780(1)	0.1482(2)	2.2(1)
Ga4B	4*c*	0.6405(3)	3/4	0.9483(2)	2.5(2)
Ga5B	4*c*	0.7229(4)	3/4	0.2392(2)	2.5(2)
Ga6B	8*d*	0.7397(2)	0.6768(1)	0.0041(2)	2.1(1)
Ga7B	4*c*	0.5420(3)	3/4	0.0974(2)	1.9(2)
NiB	4*c*	0.7183(3)	3/4	0.0854(3)	1.3(2)
Na1	8*d*	0.6669(8)	0.5845(3)	0.9217(6)	2.9(5)
Na2	4*c*	0.691(1)	1/4	-0.085(1)	3.6(8)
Na3	8*d*	0.5054(8)	0.3353(4)	0.0044(6)	3.0(5)
Na4	8*d*	0.9254(8)	0.5431(4)	0.9651(7)	4.1(6)
Na5	8*d*	0.8095(9)	0.3506(4)	0.8282(7)	3.7(6)
Na6	8*d*	0.5672(9)	0.3433(5)	0.8049(7)	4.7(7)
Na7	8*d*	0.5110(8)	0.4250(4)	0.2554(6)	3.6(6)
Na8	8*d*	0.0082(8)	0.3420(4)	0.9680(7)	3.7(6)
Na9	4*c*	0.522(1)	3/4	0.302(1)	5(1)
Na10	8*d*	0.766(1)	0.5860(4)	0.1249(6)	3.9(6)
Na11	8*d*	0.710(1)	0.4851(4)	0.8177(6)	4.1(6)
Na12	8*d*	0.523(1)	0.5404(6)	0.0833(7)	6.4(8)
Na13	8*d*	0.537(1)	0.5433(5)	0.3160(7)	5.0(7)
Na14	8*d*	0.868(1)	0.6756(5)	0.8438(7)	5.3(7)
Na15	4*c*	0.895(1)	1/4	0.078(1)	6(1)
Na16	4*c*	0.634(2)	1/4	0.121(1)	5(1)
Na17	8*d*	0.607(1)	0.6808(4)	0.7982(8)	6.8(9)

$^aB_{eq} = (8\pi^2/3)\Sigma_i\Sigma_j U_{ij} a_i^* a_j^* \vec{a}_i \vec{a}_j$

Table 3: Data Collection and Refinement Parameters for K_2Ga_3

Crystal size, mm	0.09 x 0.12 x 0.25
Space group, Z	*I4/mmm* (No. 139), 4
Lattice parameters,[a]	
a, Å	6.1382(3)
c, Å	14.815(1)
V, Å^3	558.17(7)
d_{calc}, g/cm^3	3.419
μ, cm^{-1} (Mo Kα)	156.67
R_{avg} ($I \geq 3\sigma_I$), %	2.7
Residuals *R*; R_w,[b] %	1.8; 1.8

[a]Guinier data with Si as an internal standard, λ = 1.540562 Å, 23° C.

[b]$R = \Sigma||F_o|-|F_c||/\Sigma|F_o|$; $R_w = [\Sigma\omega(|F_o|-|F_c|)^2/\Sigma\omega(F_o)^2]^{1/2}$, $\omega = 1/\sigma_F^2$

Table 4: Positional and Thermal Parameters for K_2Ga_3

Atom	Wyckoff	x	y	z	$B_{eq}(Å^2)^a$
Ga1	4*e*	0	0	0.13886(6)	1.43(2)
Ga2	8*i*	0.2947(1)	0	0	1.20(2)
K1	4*d*	-0.5	0	0.25	2.33(5)
K2	4*e*	0	0	0.3906(1)	2.55(5)

$^aB_{eq} = (8\pi^2/3)\Sigma_i\Sigma_j U_{ij} a_i^* a_j^* \vec{a}_i \vec{a}_j$

Table 5: Selected Bond Distances in K_2Ga_3 (d < 5 Å)

Ga1	–Ga2	4×	2.7393(8)	K1	–Ga1		3.4829(4)
	–K1	4×	3.4829(4)		–K2	4×	3.709(1)
	–K2		3.729(2)		–K1	4×	4.3404(2)
Ga2	–Ga2		2.521(1)		–Ga2		3.9123(3)
	–Ga2	2×	2.5579(8)	K2	–K2		3.242(4)
	–Ga1	2×	2.7393(8)		–Ga2		3.6927(9)
	–K2	4×	3.6927(9)		–K1		3.709(1)
	–K1	2×	3.9123(3)		–Ga1		3.729(2)

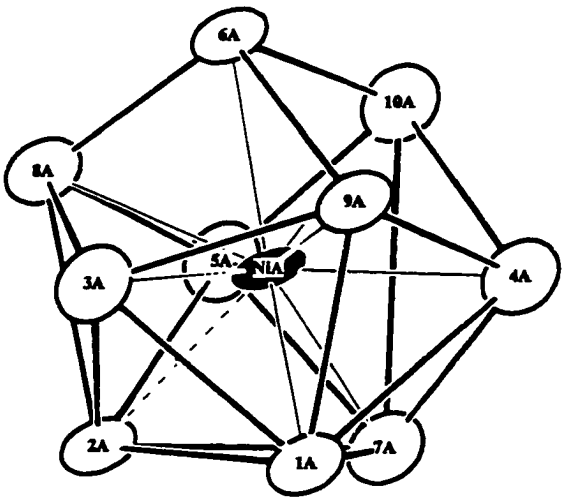

A

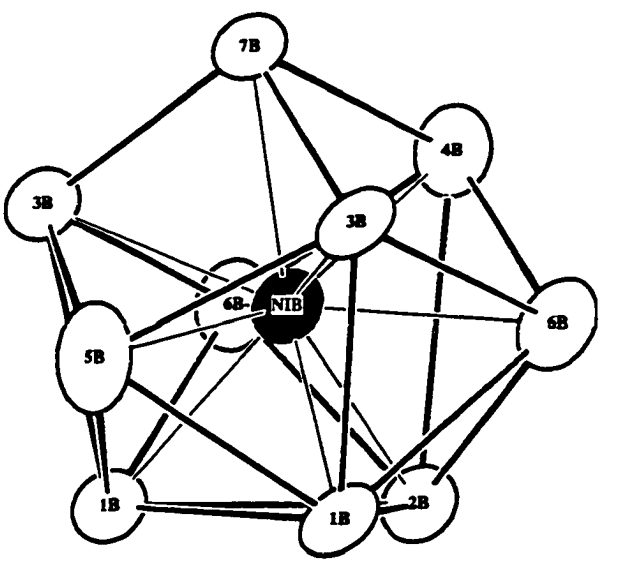

B

Figure 1. Isolated clusters in $Na_{10}Ga_{10}Ni$. Thermal ellipsoid probabilities drawn at 80%.

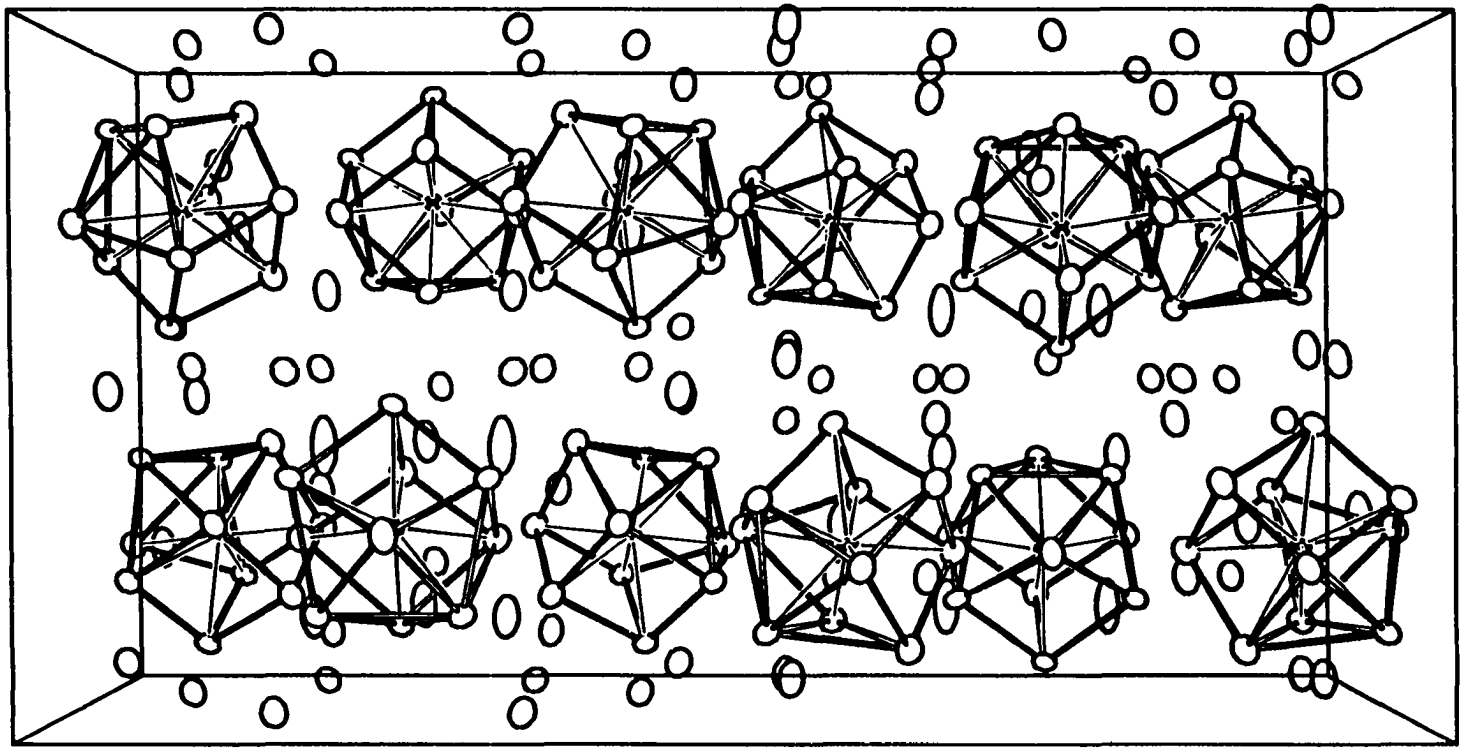

Figure 2. Unit cell of $Na_{10}Ga_{10}Ni$. View down the c-axis with mirror planes at y=1/4 and 3/4. Thermal ellipsoids drawn at 50% probability.

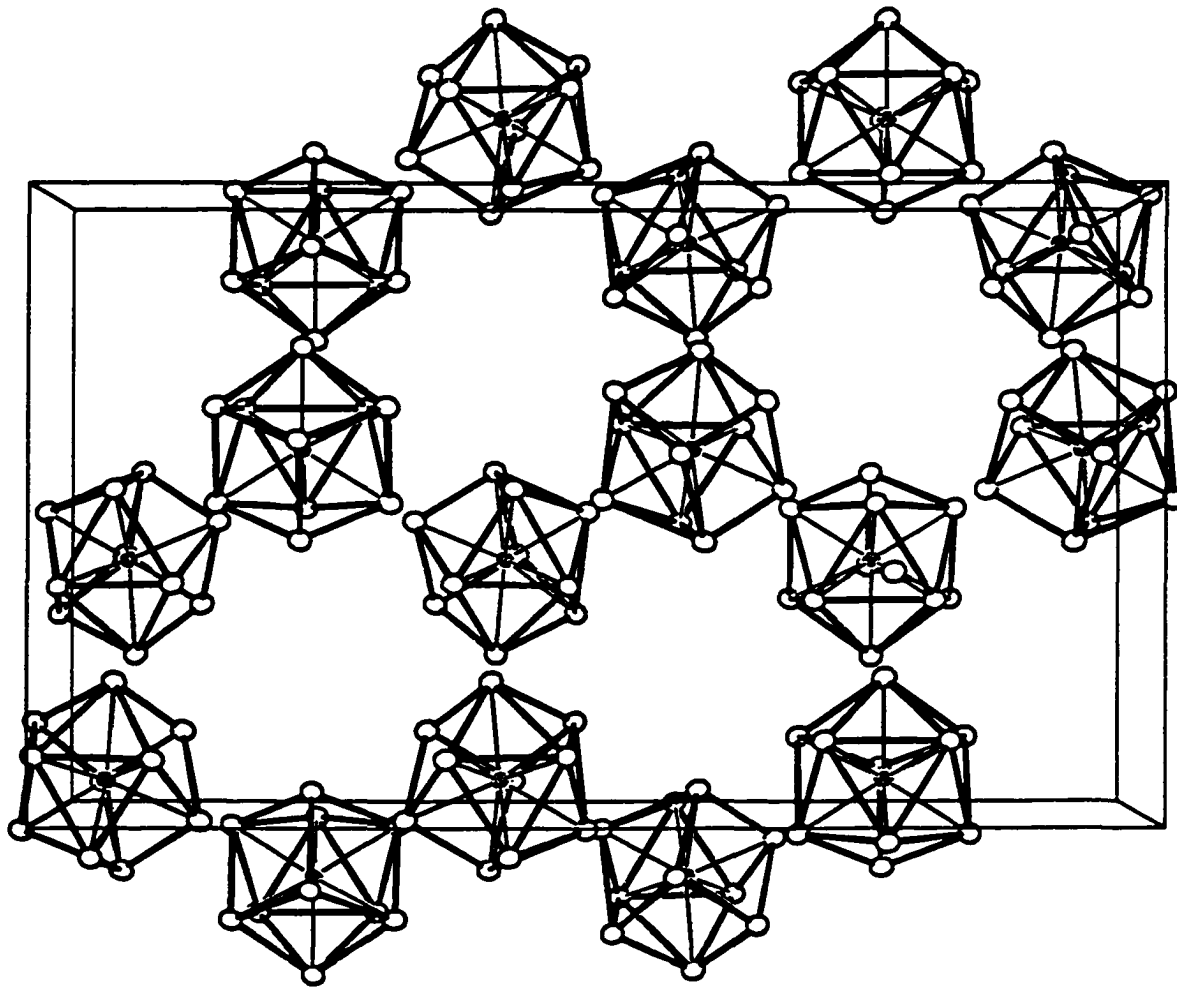

Figure 3. View down the c axis showing pseudo-hexagonal packing of two cluster layers. Thermal ellipsoids drawn at 50% probability.

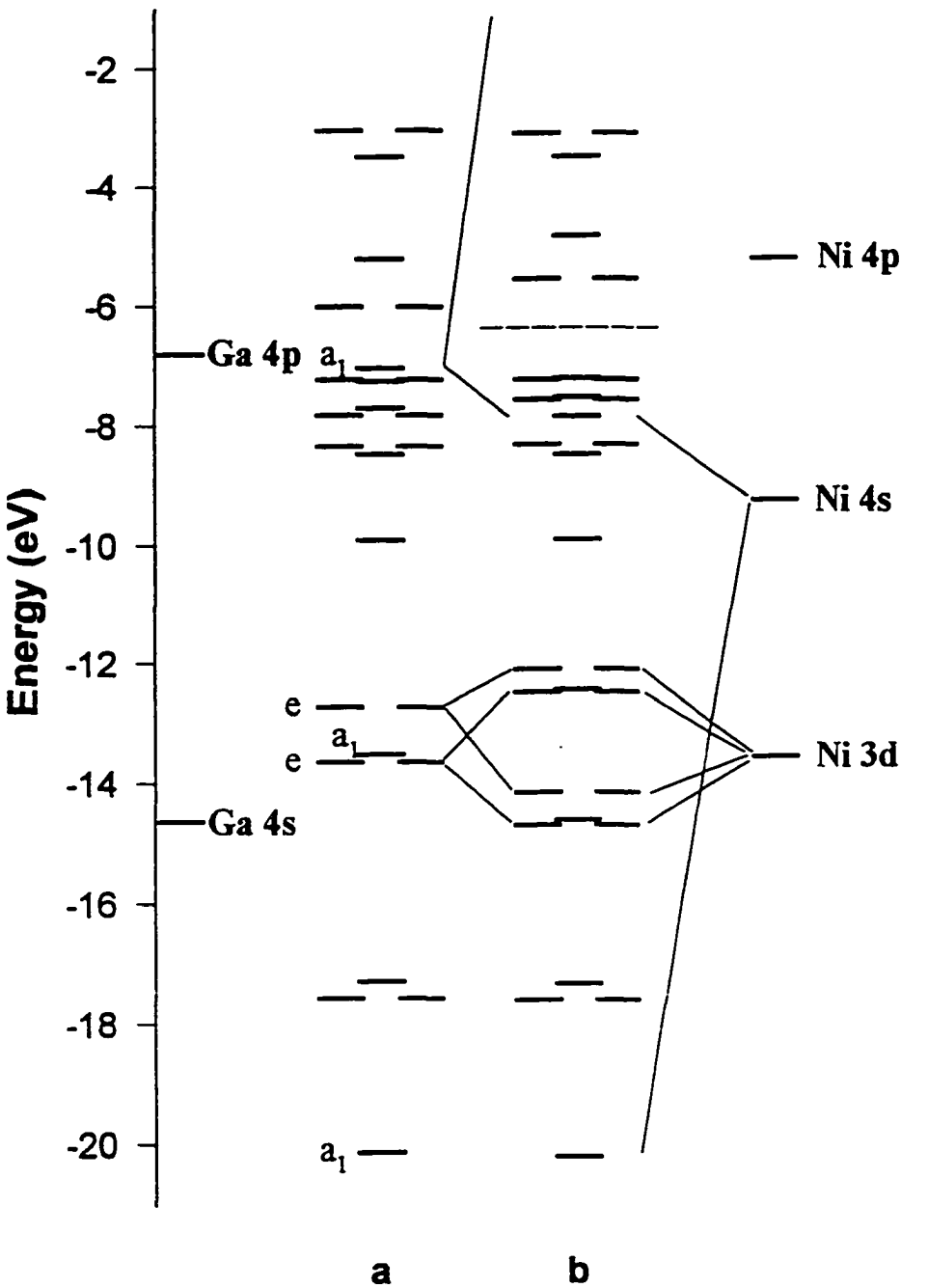

Figure 4. Molecular orbital diagram of empty Ga_{10} unit (a) and the observed $Ga_{10}Ni^{10-}$ cluster (b).

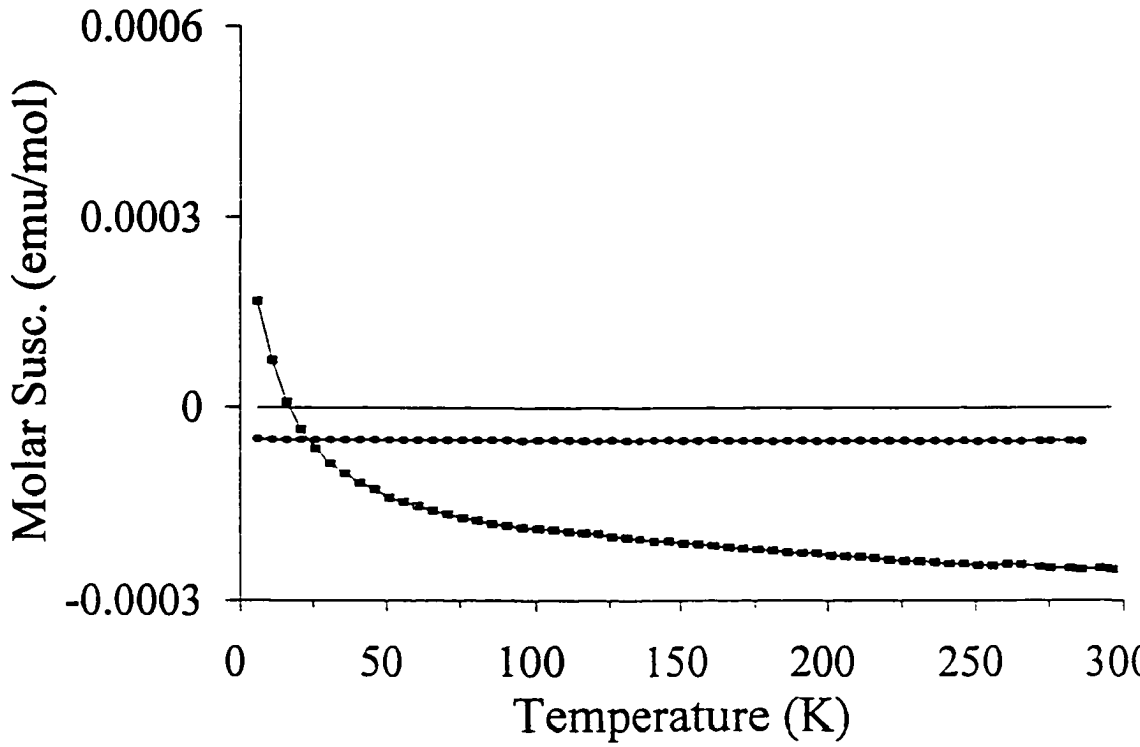

Figure 5. Magnetic susceptibility of $Na_{10}Ga_{10}Ni$ (■) and K_2Ga_3 (●) at 3 T.

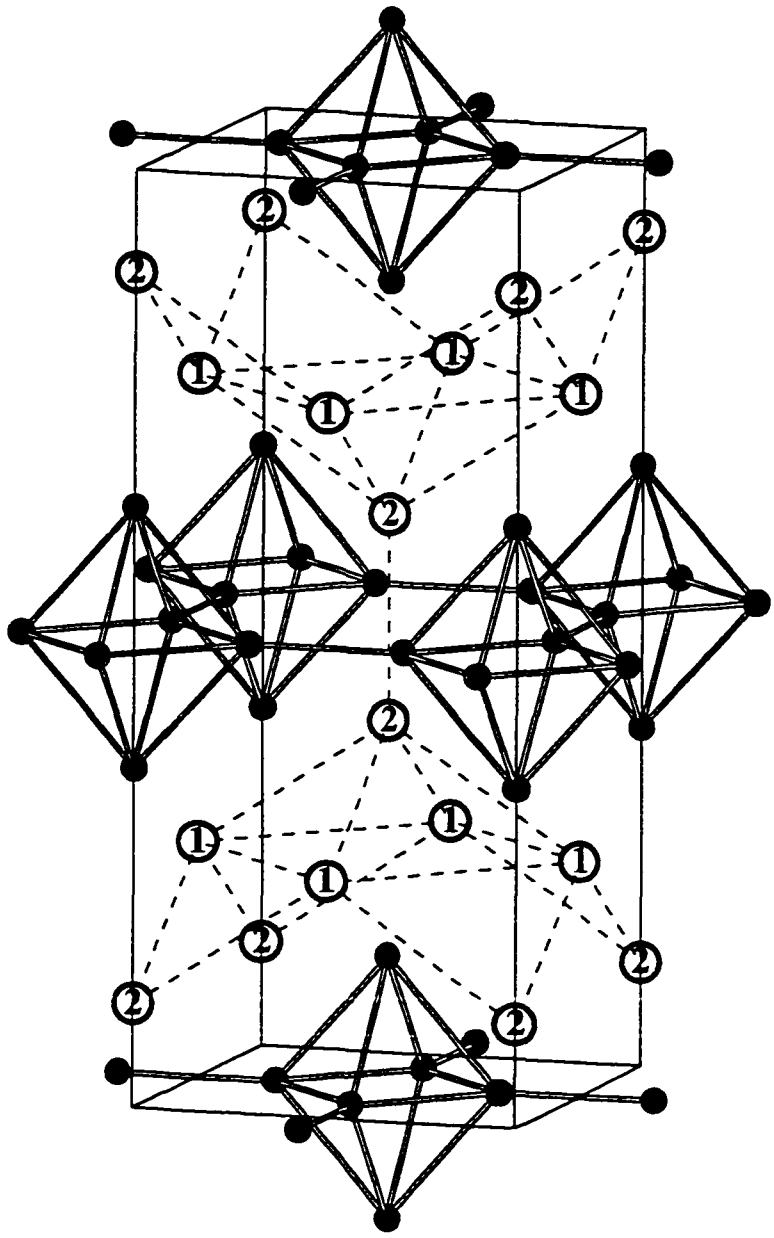

Figure 6. Unit cell of K_2Ga_3. Solid dark spheres represent gallium and the open spheres are potassium. Dotted lines between potassium atoms show structural similarity to inverse-KIn_4 structure.

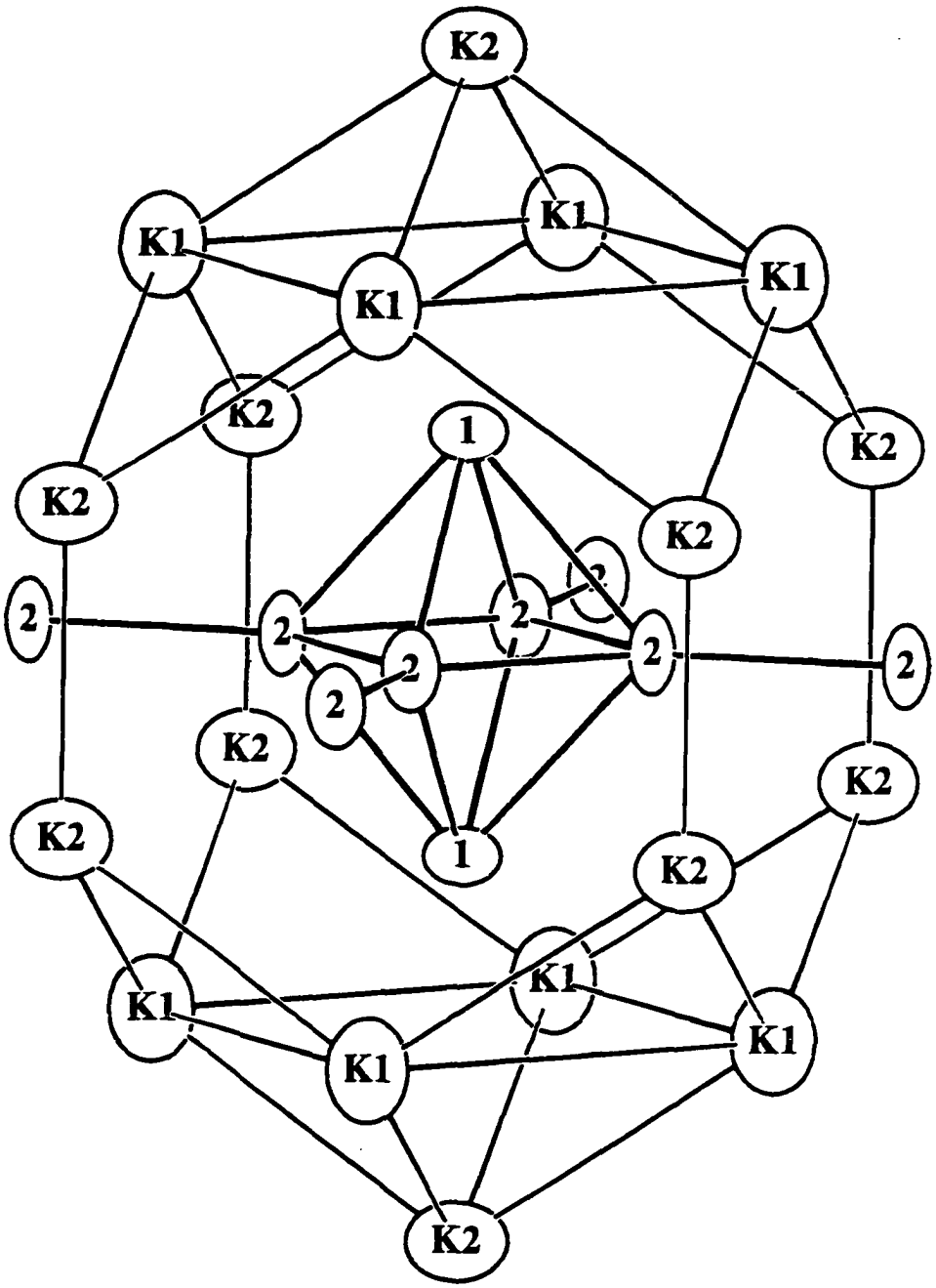

Figure 7. The cation coordination around the Ga_6 octahedra in K_2Ga_3. Thermal ellipsoids drawn at 90% probability. K1 atoms bridge each Ga1–Ga2 edge of the octahedron while K2 sits above a Ga2–Ga2 edge and is also exo-bonding a Ga1 atom on an adjacent cluster.

Supporting Information

Table S1: Data Collection and Refinement Parameters for $Na_{10}Ga_{10}Ni$

Crystal size, mm	0.27 x 0.23 x 0.22
Space group, Z	*Pnma* (no. 62), 12
Lattice parameters,[a]	
a, Å	13.908(3)
b, Å	28.146(6)
c, Å	16.286(4)
V, Å^3	6375(4)
d_{calc}, g/cm^3	3.081
Radiation; $2\theta_{max}$	Mo Kα; 50°
Octants measured	$h, \pm k, l$
Scan method	ω
Temperature, °C	23
Diffractometer	Rigaku AFC6R
Relative transmission coeff.	0.855-1.050
μ, cm^{-1} (Mo Kα)	134.76
Number of reflections:	
measured	14801
observed ($I \geq 3\sigma_I$)	6902
unique observed ($I \geq 3\sigma_I$)	2691
Number of variables	298
R_{avg} ($I \geq 3\sigma_I$), %	5.6
Residuals *R*; R_w,[b] %	6.2; 6.3
Goodness of fit	2.03

[a]Guinier data with Si as an internal standard, λ = 1.540562 Å, 23° C.
[b]$R = \Sigma||F_o|-|F_c||/\Sigma|F_o|$; $R_w = [\Sigma\omega(|F_o|-|F_c|)^2/\Sigma\omega(F_o)^2]^{1/2}$, $\omega = 1/\sigma_F^2$

Table S2: Thermal parameters for $Na_{10}Ga_{10}Ni$

Atom	U_{11}*	U_{22}	U_{33}	U_{12}	U_{13}	U_{23}
Ga(1A)	0.023(2)	0.029(2)	0.023(2)	0.004(1)	0.01(1)	0.002(1)
Ga(2A)	0.017(2)	0.025(2)	0.03(2)	-0.007(1)	-0.006(1)	-0.000(1)
Ga(3A)	0.035(2)	0.016(1)	0.017(1)	0.002(1)	-0.002(1)	0.002(1)
Ga(4A)	0.033(2)	0.019(1)	0.028(2)	0.000(1)	0.001(1)	-0.006(1)
Ga(5A)	0.035(2)	0.025(2)	0.013(1)	-0.001(1)	-.003(1)	-0.000(1)
Ga(6A)	0.018(2)	0.031(2)	0.024(2)	0.000(1)	-0.001(1)	-0.002(1)
Ga(7A)	0.031(2)	0.039(2)	0.028(2)	0.016(2)	-0.010(2)	-0.007(1)
Ga(8A)	0.025(2)	0.020(1)	0.024(1)	0.001(1)	0.004(1)	-0.003(1)
Ga(9A)	0.024(2)	0.030(2)	0.016(1)	-0.005(1)	-0.005(1)	0.003(1)
Ga(10A)	0.034(2)	0.028(2)	0.028(2)	-0.010(2)	0.004(1)	0.002(1)
Ni(A)	0.012(2)	0.011(1)	0.012(1)	0.000(1)	-0.002(1)	-0.001(1)
Ga(1B)	0.019(2)	0.035(2)	0.029(2)	0.007(1)	-0.004(1)	0.005(1)
Ga(2B)	0.023(2)	0.025(2)	0.041(3)	0	0.012(2)	0
Ga(3B)	0.019(2)	0.035(2)	0.029(2)	-0.005(1)	-0.004(1)	0.012(1)
Ga(4B)	0.036(3)	0.036(3)	0.024(2)	0	-0.010(2)	0
Ga(5B)	0.054(3)	0.028(2)	0.013(2)	0	0.000(2)	0
Ga(6B)	0.034(2)	0.019(1)	0.026(2)	0.001(1)	-0.001(1)	-0.010(1)
Ga(7B)	0.017(2)	0.022(2)	0.033(2)	0	-0.001(2)	0
Ni(B)	0.025(3)	0.014(2)	0.011(2)	0	-0.005(2)	0
Na(1)	0.059(8)	0.018(5)	0.033(6)	-0.009(6)	0.010(6)	0.001(5)
Na(2)	0.05(1)	0.04(1)	0.05(1)	0	0.01(1)	0
Na(3)	0.024(6)	0.047(7)	0.043(6)	-0.011(6)	-0.000(5)	-0.019(6)
Na(4)	0.028(7)	0.055(8)	0.072(8)	0.005(6)	0.006(6)	0.009(7)
Na(5)	0.054(8)	0.040(7)	0.048(7)	-0.007(6)	-0.003(7)	-0.016(6)
Na(6)	0.053(9)	0.08(1)	0.048(8)	-0.015(8)	0.011(7)	-0.000(7)
Na(7)	0.041(8)	0.052(7)	0.043(7)	-0.007(6)	0.022(6)	-0.003(6)
Na(8)	0.030(7)	0.044(7)	0.065(8)	0.025(6)	0.003(6)	-0.004(6)
Na(9)	0.05(1)	0.06(1)	0.07(1)	0	0.02(1)	0
Na(10)	0.09(1)	0.020(5)	0.042(7)	0.003(7)	-0.001(7)	-0.005(5)
Na(11)	0.08(1)	0.047(7)	0.026(6)	-0.027(7)	0.017(6)	0.007(6)
Na(12)	0.07(1)	0.13(1)	0.047(7)	0.07(1)	-0.003(7)	0.015(8)
Na(13)	0.06(1)	0.08(1)	0.052(7)	-0.035(8)	0.009(7)	-0.002(7)
Na(14)	0.09(1)	0.08(1)	0.039(7)	-0.013(9)	0.003(8)	-0.010(7)
Na(15)	0.07(1)	0.04(1)	0.11(2)	0	-0.05(1)	0
Na(16)	0.08(2)	0.03(1)	0.10(2)	0	0.02(1)	0
Na(17)	0.17(2)	0.039(8)	0.056(8)	0.02(1)	-0.01(1)	-0.017(7)

*$T = \exp[-2\pi^2(U_{11}h^2a^{*2} + U_{22}k^2b^{*2} + U_{33}l^2c^{*2} + 2U_{12}hka^*b^* + 2U_{13}hla^*c^* + 2U_{23}klb^*c^*)]$

Table S3: Bond distances in $Na_{10}Ga_{10}Ni$ (d_{Ga-Ga}<3.1, d_{Na-Ga}<3.7, and d_{Na-Na}<4.0 Å)

Ga1A	–NiA	2.479(4)	Ga6A	–NiA	2.464(4)	Ga1B	–NiB		2.515(5)
	–Ga9A	2.785(4)		–Ga9A	2.631(4)		–Ga5B		2.695(5)
	–Ga3A	2.794(4)		–Ga8A	2.633(4)		–Ga6B		2.815(4)
	–Ga2A	2.855(4)		–Ga10A	2.685(4)		–Ga3B		2.832(4)
	–Ga7A	2.866(4)		–Na3	2.98(1)		–Ga2B		2.901(5)
	–Ga4A	3.032(4)		–Na7	3.01(1)		–Ga1B		2.983(6)
	–Na13	3.04(1)		–Ga3A	3.056(4)		–Na8		3.00(1)
	–Na8	3.09(1)		–Na12	3.06(1)		–Na9		3.00(2)
	–Na4	3.21(1)		–Na12	3.26(2)		–Na6		3.06(1)
	–Na5	3.27(1)		–Na1	3.30(1)		–Na10		3.33(1)
	–Na4	3.41(1)							
			Ga7A	–NiA	2.484(4)	Ga2B	–NiB		2.528(6)
Ga2A	–NiA	2.496(4)		–Ga4A	2.663(4)		–Ga6B	2x	2.721(4)
	–Ga3A	2.808(4)		–Ga5A	2.719(4)		–Ga1B	2x	2.901(5)
	–Ga8A	2.818(4)		–Ga1A	2.866(4)		–Na8	2x	3.17(1)
	–Ga1A	2.855(4)		–Ga2A	2.943(4)		–Na14	2x	3.25(1)
	–Ga5A	2.933(4)		–Na7	2.98(1)		–Na15		3.52(2)
	–Ga7A	2.943(4)		–Na8	3.09(1)				
	–Na13	3.14(1)		–Na17	3.24(1)	Ga3B	–NiB		2.494(4)
	–Na7	3.12(1)		–Na15	3.521(5)		–Ga7B		2.610(4)
	–Na4	3.27(1)		–Na14	3.62(2)		–Ga6B		2.697(4)
	–Na4	3.31(1)					–Ga5B		2.741(4)
	–Na10	3.40(1)	Ga8A	–NiA	2.529(4)		–Ga1B		2.832(4)
	–Na11	3.49(1)		–Ga6A	2.633(4)		–Na6		3.09(1)
				–Ga5A	2.675(4)		–Na5		3.11(1)
Ga3A	–NiA	2.506(4)		–Ga3A	2.735(4)		–Na10		3.12(1)
	–Ga8A	2.735(4)		–Ga2A	2.818(4)		–Na3		3.26(1)
	–Ga9A	2.754(4)		–Na12	3.01(1)		–Na9		3.64(1)
	–Ga1A	2.794(4)		–Na11	3.02(1)				
	–Ga2A	2.808(4)		–Na7	3.11(1)	Ga4B	–NiB		2.481(6)
	–Na1	3.04(1)		–Na10	3.26(1)		–Ga6B	2x	2.640(4)
	–Ga6A	3.056(4)		–Na13	3.48(1)		–Ga7B		2.788(6)
	–Na11	3.14(1)					–Na17	2x	3.16(1)
	–Na4	3.22(1)	Ga9A	–NiA	2.513(4)		–Na3	2x	3.24(1)
	–Na10	3.27(1)		–Ga6A	2.631(4)				
	–Na12	3.31(1)		–Ga4A	2.643(4)	Ga5B	–NiB		2.506(6)
				–Ga3A	2.754(4)		–Ga1B	2x	2.695(5)
Ga4A	–NiA	2.467(4)		–Ga1A	2.785(4)		–Ga3B	2x	2.741(4)
	–Ga9A	2.643(4)		–Na11	3.09(1)		–Na9		2.97(2)
	–Ga10A	2.662(4)		–Na12	3.12(1)		–Na2		3.10(2)
	–Ga7A	2.663(4)		–Na5	3.15(1)		–Na5	2x	3.21(1)
	–Ga1A	3.032(4)		–Na3	3.20(1)				
	–Na2	3.16(1)		–Na6	3.24(1)	Ga6B	–NiB		2.466(4)
	–Na15	3.22(1)					–Ga4B		2.610(4)
	–Na5	3.30(1)	Ga10A	–NiA	2.490(4)		–Ga3B		2.697(4)
	–Na16	3.37(1)		–Ga5A	2.600(4)		–Ga2B		2.721(4)
	–Na3	3.52(1)		–Ga4A	2.662(4)		–Ga1B		2.815(4)
	–Na8	3.61(1)		–Ga6A	2.685(4)		–Na1		3.10(1)
				–Na16	2.990(5)		–Na14		3.16(1)
Ga5A	–NiA	2.460(4)		–Na3	3.25(1)		–Na10		3.25(1)
	–Ga10A	2.600(4)		–Na7	3.22(1)		–Na3		3.43(1)
	–Ga8A	2.675(4)		–Na14	3.16(1)		–Na8		3.58(1)
	–Ga7A	2.719(4)							
	–Ga2A	2.933(4)	NiA	–Ga5A	2.460(4)	Ga7B	–NiB		2.459(6)
	–Na1	3.18(1)		–Ga6A	2.464(4)		–Ga3B	2x	2.610(4)
	–Na17	3.23(1)		–Ga4A	2.467(4)		–Ga4B		2.788(6)
	–Na11	3.28(1)		–Ga1A	2.479(4)		–Na3	2x	2.99(1)
	–Na7	3.38(1)		–Ga7A	2.484(4)		–Na2		3.25(2)
	–Na14	3.55(1)		–Ga10A	2.490(4)		–Na6	2x	3.43(1)
	–Na7	3.65(1)		–Ga2A	2.496(4)		–Na9		3.34(2)
				–Ga3A	2.506(4)				
				–Ga9A	2.513(4)	NiB	–Ga7B		2.459(6)
				–Ga8A	2.529(4)		–Ga6B	2x	2.466(4)
							–Ga4B		2.481(6)
							–Ga3B	2x	2.494(4)
							–Ga5B		2.506(6)
							–Ga1B	2x	2.515(5)
							–Ga2B		2.528(6)

Na1	–Ga3A		3.04(1)	Na6	–Ga1B		3.06(1)	Na12	–Ga8A		3.01(1)
	–Ga6B		3.10(1)		–Ga3B		3.09(1)		–Ga6A		3.06(1)
	–Ga5A		3.18(1)		–Ga9A		3.24(1)		–Ga9A		3.12(1)
	–Ga6A		3.30(1)		–Na3		3.37(1)		–Ga6A		3.26(2)
	–Na11		3.33(2)		–Na9		3.39(2)		–Ga3A		3.31(1)
	–Na17		3.48(2)		–Na5		3.40(2)		–Na1		3.53(2)
	–Na3		3.51(2)		–Ga7B		3.43(1)		–Na12		3.60(3)
	–Na12		3.53(2)		–Na2		3.62(2)		–Na10		3.68(2)
	–Na10		3.59(1)		–Na12		3.95(2)		–Na11		3.70(2)
	–Na7		3.81(2)						–Na3		3.80(2)
	–Na4		3.85(2)	Na7	–Ga7A		2.98(1)		–Na13		3.80(2)
	–Na14		4.00(2)		–Ga6A		3.01(1)		–Ga3A		3.87(2)
					–Ga8A		3.11(1)		–Na6		3.95(2)
Na2	–Ga5B		3.10(2)		–Ga2A		3.12(1)				
	–Ga4A	2×	3.14(1)		–Ga10A		3.22(1)	Na13	–Ga1A		3.04(1)
	–Ga7B		3.25(2)		–Ga5A		3.38(1)		–Ga2A		3.14(1)
	–Na16		3.45(3)		–Na13		3.49(2)		–Ga8A		3.48(1)
	–Na5	2×	3.57(2)		–Na17		3.51(2)		–Na4		3.48(2)
	–Na6	2×	3.62(2)		–Na14		3.59(2)		–Na7		3.49(2)
	–Na3	2×	3.81(2)		–Na4		3.64(2)		–Na11		3.61(2)
	–Na15		3.88(2)		–Ga5A		3.65(1)		–Na5		3.68(2)
					–Na1		3.85(2)		–Na12		3.80(2)
Na3	–Ga6A		2.98(1)						–Na4		3.88(2)
	–Ga7B		2.99(1)	Na8	–Ga1B		3.00(1)				
	–Ga9A		3.20(1)		–Ga1A		3.09(1)	Na14	–Ga10A		3.16(1)
	–Ga4B		3.24(1)		–Ga7A		3.09(1)		–Ga6B		3.16(1)
	–Ga10A		3.25(1)		–Ga2B		3.17(1)		–Ga2B		3.25(1)
	–Ga3B		3.26(1)		–Na15		3.52(2)		–Ga5A		3.55(1)
	–Na6		3.37(1)		–Na4		3.54(2)		–Na8		3.55(2)
	–Ga6B		3.43(1)		–Na14		3.55(2)		–Na7		3.59(2)
	–Na1		3.51(2)		–Ga6B		3.58(1)		–Ga7A		3.62(2)
	–Ga4A		3.52(1)		–Na5		3.59(2)		–Na17		3.72(2)
	–Na16		3.55(2)		–Ga4A		3.61(1)		–Na1		4.00(2)
	–Na17		3.60(2)		–Na9		3.77(2)				
	–Na12		3.80(2)		–Na10		4.03(2)	Na15	–Ga4A	2×	3.22(1)
	–Na2		3.81(2)						–Ga7A	2×	3.521(5)
				Na9	–Ga5B		2.97(2)		–Ga2B		3.52(2)
Na4	–Ga1A		3.21(1)		–Ga1B	2×	3.00(2)		–Na8	2×	3.52(2)
	–Ga3A		3.22(1)		–Ga7B		3.34(2)		–Na16		3.70(3)
	–Ga2A		3.27(1)		–Na6	2×	3.39(2)		–Na2		3.88(2)
	–Ga2A		3.31(1)		–Ga3B	2×	3.64(1)				
	–Na4		3.39(2)		–Na5	2×	3.70(2)	Na16	–Ga10A	2×	2.990(4)
	–Ga1A		3.41(1)		–Na8	2×	3.77(2)		–Ga4A	2×	3.37(1)
	–Na13		3.48(2)						–Na2		3.45(3)
	–Na8		3.54(2)	Na10	–Ga3B		3.12(1)		–Na3	2×	3.55(2)
	–Na10		3.62(2)		–Ga6B		3.25(1)		–Na15		3.70(3)
	–Na7		3.64(2)		–Ga8A		3.26(1)		–Ga4B		3.98(2)
	–Na1		3.85(2)		–Ga3A		3.27(1)				
	–Na13		3.88(2)		–Ga1B		3.33(1)	Na17	–Ga4B		3.16(1)
					–Ga2A		3.40(1)		–Ga5A		3.23(1)
Na5	–Ga3B		3.11(1)		–Na1		3.59(1)		–Ga7A		3.24(1)
	–Ga9A		3.15(1)		–Na4		3.62(2)		–Na1		3.48(2)
	–Ga5B		3.21(1)		–Na12		3.68(2)		–Na7		3.51(2)
	–Ga1A		3.27(1)		–Na11		3.74(2)		–Na3		3.69(2)
	–Ga4A		3.30(1)		–Na5		3.91(2)		–Na14		3.72(2)
	–Na6		3.40(2)						–Na17		3.89(2)
	–Na2		3.57(2)	Na11	–Ga8A		3.02(1)				
	–Na8		3.59(2)		–Ga9A		3.09(1)				
	–Na13		3.68(2)		–Ga3A		3.14(1)				
	–Na9		3.70(2)		–Ga5A		3.28(1)				
	–Ga1B		3.87(1)		–Na1		3.33(2)				
	–Na10		3.91(2)		–Ga2A		3.49(1)				
					–Na13		3.61(2)				
					–Na12		3.70(2)				
					–Na10		3.74(2)				

Table S4: Data Collection and Refinement Parameters for K_2Ga_3

Crystal size, mm	0.09 x 0.12 x 0.25
Space group, Z	*I*4/*mmm* (No. 139), 4
Lattice parameters,[a]	
a, Å	6.1382(3)
c, Å	14.815(1)
V, Å^3	558.17(7)
d_{calc}, g/cm^3	3.429
Diffractometer	Rigaku AFC6R
Radiation; $2\theta_{max}$	Mo Kα; 60°
Octants measured	h, $\pm k$, $\pm l$
Scan method	ω
Temperature, °C	23
Transmission range	0.756-1.0
μ, cm^{-1} (Mo Kα)	156.67
Number of reflections:	
measured	3568
observed ($I \geq 3\sigma_I$)	1245
unique observed ($I \geq 3\sigma_I$)	218
Number of variables	13
$R_{avg.}$ ($I \geq 3\sigma_I$), %	2.7
Residuals R; R_w,[b] %	1.8; 1.8
Goodness of fit	1.71

[a]Guinier data with Si as an internal standard, λ = 1.540562 Å, 23° C.
[b]$R = \Sigma||F_o|-|F_c||/\Sigma|F_o|$; $R_w = [\Sigma\omega(|F_o|-|F_c|)^2/\Sigma\omega(F_o)^2]^{1/2}$, $\omega = 1/\sigma_F^2$

Table S5: Thermal Parameters for K_2Ga_3

Atom	U_{11}*	U_{22}	U_{33}	U_{12}	U_{13}	U_{23}
Ga1	0.0210(3)	0.0210	0.0124(4)	0	0	0
Ga2	0.0072(3)	0.0124(3)	0.0257(3)	0	0	0
K1	0.0240(6)	0.0240	0.040(1)	0	0	0
K2	0.0366(8)	0.0366	0.023(1)	0	0	0

*$T = \exp[-2\pi^2(U_{11}h^2a^{*2} + U_{22}k^2b^{*2} + U_{33}l^2c^{*2} + 2U_{12}hka^*b^* + 2U_{13}hla^*c^* + 2U_{23}klb^*c^*)]$

Table S6: Bond angles (deg.) between the gallium atoms in K_2Ga_3

Atom	Atom	Atom	Angle
Ga2	Ga1	Ga2	55.67(2)
Ga2	Ga1	Ga2	82.64(3)
Ga1	Ga2	Ga1	97.36(3)
Ga1	Ga2	Ga2	62.167(9)
Ga1	Ga2	Ga2	131.32(1)

$Na_{30.5}GA_{60-X}AG_X$: A THREE-DIMENSIONAL NETWORK COMPOSED OF GA_3, GA_{12}, AND GA_{18} CLUSTERS

A paper to be submitted to the Journal of Solid State Chemistry

Robert W. Henning and John D. Corbett

Department of Chemistry and Ames Laboratory—DOE,[1]

Iowa State University, Ames IA 50011

Abstract

Single crystal x-ray structural determinations of $Na_{30.5}Ga_{57.4(2)}Ag_{2.6(2)}$ and $Na_{30.5}Ga_{53.6(2)}Ag_{6.4(2)}$ (*P6/mmm*, Z = 1) reveal Ga_3 triangles, Ga_{12} icosahedra, and Ga_{18} ·xacapped, hexagonal prisms that are interconnected to form three-dimensional network structures. Silver substitutes on one of the outer gallium sites of the Ga_{18} unit and presumably reduces the overall electron count by two electrons per silver atom. The amount of silver in the compound varies with the initial composition. Extended Hückel band calculations were performed in order to gain a better understanding of the nonstoichiometry of this compound. Stacking of the Ga_{18}-"drums" along the c-axis creates a channel in which some of the sodium atoms reside. The sodium positions within this channel change with the amount of silver in the structure. The other sodium cations in the structure lie between the clusters and coordinate the gallium atoms in typical roles.

Introduction

Previous work in binary alkali-metal–gallium systems has shown that gallium typically forms regular deltahedra that are linked together to form three-dimensional network structures with the cations residing between the clusters.[2] The clusters are reminiscent of the borane anions ($B_nH_n^{2-}$) and therefore can be considered an extension of the borohydride-like chemistry into the solid state. Although deltahedral clusters dominate these systems, other types of clusters, or spacers, exist. They range from simple one, two, or three atoms units to more complex features such as the -Ga_{15} units in Na_7Ga_{13}[3] and $Na_{22}Ga_{39}$.[4] One driving force for the creation of these extensive networks is to achieve structures with closed electronic shell configurations. Zintl concepts[5] and Wade's rules[6] have been found to be invaluable tools in attempts to understand the range of structural diversity of alkali-metal–group 13 compounds.

Introduction of late transition elements into these systems has produced an even greater range of structure types, some with cluster sizes exceeding the regular 12-atom deltahedron in the form of closo-Ga_{15} and -Ga_{16} clusters. It has been noted that only a small change in the electron count can have a dramatic affect on the structure. This can be seen in $Na_{36}Ga_{73}Ag_7$[7] where only a small amount of the third element is needed to stabilize a new compound. Many of the structures that contain late transition elements have mixtures of gallium and the third element on the same site. This is the case for $Na_{36}Ga_{73}Ag_7$ where the silver substitutes some of the gallium atoms in the Ga_{16} cluster. Although a majority of the structures can be described by simple electron counting rules, several clusters have been found which do not follow Wade's rules or even the more elaborate electron counting schemes

developed by Burdett[8] and Teo[9]. Extended Hückel calculations can help one to understand the bonding in these diverse systems.

This paper reports a new structure in the alkali-metal–gallium silver system. $Na_{30.5}Ga_{57.4(2)}Ag_{2.6(2)}$ and $Na_{30.5}Ga_{53.6(2)}Ag_{6.4(2)}$ form isostructural networks which are related to $Na_8K_{23}In_{48}Cd_{12}$ but have mixed silver and gallium on the cadmium site. The amount of silver is variable and is dependent on the loaded composition. Guinier powder patterns confirm that a range of compositions are present. The $(Ga,Ag)_{18}$ "drum," a new cluster type for gallium systems, has been explored in more detail through molecular orbital and band calculations. The synthesis, structure, and electronic calculations will be presented and discussed.

Experimental Section

The handling of all materials was carried out in an N_2-filled glovebox. Gallium (99.99%, Johnson-Matthey) and silver (99.99%, powder, Fisher) were used as received while the surface of sodium (99.9%, Alpha) was cleaned with a scalpel. Fusion of the elements at a composition of $Na_{30}Ga_{60-x}Ag_x$ (x = ~6) in welded tantalum tubing at 650 °C was followed by slow cooling (3 °C/hr) to produce $Na_{30.5}Ga_{60-x}Ag_x$ as the major phase (~95%) and a small amount of Ag_3Ga[10] (~5%). Reactions loaded with fewer than six silver atoms per formula unit still produced the desired phase but in lower yield. A reaction loaded as $Na_{30}Ga_{56}Ag_4$, for example, produced $Na_{30.5}Ga_{60-x}Ag_x$ (70%), Na_7Ga_{13}[3] (25%), and Ag_3Ga (5%). If more than six silver atoms were loaded, $Na_{30}Ga_{52}Ag_8$, then greater amounts of Ag_3Ga would form (5-10%) but no Na_7Ga_{13}. Larger amounts of silver produced more Ag_3Ga. The formation of Ag_3Ga in the silver-poorer samples ($x < 6$) suggests that the reactions are not at equilibrium.

Attempts to anneal the silver-poorer samples ($Na_{30}Ga_{56}Ag_4$) for ~1 month below the estimated melting point of $Na_{30.5}Ga_{60-x}Ag_x$ (~525 °C) at 400, 450, and 500 °C did not change the yields according to Guinier powder patterns even when the sample was pressed into a pellet. A sample that was loaded as $Na_{30}Ga_{54}Ag_6$ and annealed at 500 °C for one week (without initial fusion at higher temperatures) produced $Na_{30.5}Ga_{60-x}Ag_x$ (90%), Na_7Ga_{13} (5%), and Ag_3Ga (5%). It is not clear why Ag_3Ga always forms in this system. A closer look at the Ag–Ga phase diagram[11] indicates that "Ag_3Ga" has a phase width between 22 and 35 % gallium and that it under goes a phase transformation at ~425 °C to form another phase (labeled ζ) that has not been completely characterized. Na_7Ga_{13} is stoichiometric according to indexed Guinier powder patterns. Annealing the samples at slightly higher temperatures (~520 °C) for much longer periods of time (several months) may improve the yield.

Reactions loaded with a composition of $Na_{30}Ga_{50}Ag_{10}$ produced silver-saturated products with lattice parameters of a = 15.192(1) Å, c = 9.299(2) Å, and V = 1858.9(5) Å^3 plus ~10% Ag_3Ga. Greater amounts of silver produced the same set of lattice parameters but a greater excess of Ag_3Ga was observed in the powder patterns. Reactions that were loaded with six silver atoms per formula unit produced the same structure but with a smaller unit cell. The smallest lattice parameters obtained from $Na_{30}Ga_{54}Ag_6$ were a = 15.1394(5) Å, c = 9.2694(6) Å, and V = 1839.9(2) Å^3 plus ~5% Ag_3Ga. Lattice parameters have been obtained in between these extremes so the composition appears to be continuously variable and not just two different stoichiometries. Reactions with fewer than six silver atoms produced greater amounts of Na_7Ga_{13} (and ~5% Ag_3Ga) but the unit cell parameters did not decrease any further. The lattice parameters were unaffected by the initial sodium concentration. Slowly

cooling a sample (3 °C/h) from 650 °C with excess sodium, $Na_{60}Ga_{54}Ag_6$, produced elemental sodium in the final product (plus ~5% Ag_3Ga) while smaller amounts of sodium, $Na_{15}Ga_{54}Ag_6$, produced 50% $Na_{30.5}Ga_{60-x}Ag_x$, 45% $Na_{34}Ga_{105-x}Ag_x$ ($x \sim 14$),[12] and 5% Ag_3Ga, The exact composition range of the silver was difficult to determine because the Ag_3Ga binary consumed a large portion of the silver and altered the stoichiometry. The highest yields were obtained from reactions loaded with a range from six to ten silver atoms but the actual amount is lower because the binary affects the stoichiometry. All unit cell parameters were determined through Guinier powder patterns with silicon used as an internal standard (NIST).

The products of the high yield reactions had a metallic appearance and were very brittle. Crystals were obtained from two separate samples that were loaded with different silver content and that had Guinier powder patterns that indexed to two different sized unit cells. The silver-rich crystal was obtained from a reaction loaded with a large excess of silver, $Na_{30}Ga_{33}Ag_{27}$ (yield $Na_{30}Ga_{53.6(2)}Ag_{6.4(2)}$ (50%) and Ag_3Ga (50%)) while the second crystal was obtained from $Na_{30}Ga_{54}Ag_7$ ($Na_{30}Ga_{57.4(2)}Ag_{2.6(2)}$ (90%) and Ag_3Ga (10%)) . Several irregularly shaped crystals were sealed into 0.3 mm thin-walled capillaries and checked for singularity by Laue and oscillation film techniques. A Rigaku AFC6R single crystal diffractometer was used to collect a data set for the silver-rich crystal and an Enraf-Nonius CAD4 instrument was used for the other data collection. A random search yielded 25 reflections which were indexed to a primitive hexagonal cell. The 6-fold axis of the silver-rich phase was later confirmed by precession photographs. Four octants of data were collected at room temperature with Mo Kα radiation up to 50° in 2θ for $Na_{30.5}Ga_{53.6(2)}Ag_{6.4(2)}$ and to 60°

for $Na_{30.5}Ga_{57.4(2)}Ag_{2.6(2)}$ and each corrected for Lorentz and polarization effects. The data sets were corrected for absorption by applying three ψ-scans.

Systematic absences and the N(Z) distribution clearly suggested the centrosymmetric space group P6/*mmm* (no. 191) for both crystals but four acentric space groups were possible, P622 (no. 177), P6*mm* (no. 183), P$\bar{6}$2*m* (no. 189), and P$\bar{6}$*m*2 (no. 187). The initial structure solutions for space group P6/*mmm* were obtained by the application of direct methods.[13] Six peaks were appropriate for gallium and were included in the model. Refinement of the gallium positions was followed by a difference Fourier analysis. This produced six peaks that were appropriate for sodium. Refinement of all atomic positions and isotropic thermal parameters reduced the R_f to ~8.2% for each structure and revealed that the Ga5 position had a smaller thermal ellipsoid than the other gallium atoms. Since the mixing of silver and gallium on the same site occurs in other compounds (Ag_3Ga[10] and $Na_{36}Ga_{73}Ag_7$[7]), the ratio of gallium/silver was allowed to refine on the Ga5 position with the total occupancy fixed to 100%. The isotropic thermal parameter for Ga5 also was allowed to refine and converged at ~2.0. The R_f dropped to ~6.9% for each structure. To check whether silver was mixing on any other gallium position, the occupancy and isotropic thermal parameter for the gallium atoms were allowed to refine simultaneously while the sodium atoms were held at full occupancy. All other gallium positions refined to within 3σ (within 4%) of full occupancy. R_{avg} ($I \geq 3\sigma_I$) for $Na_{30.5}Ga_{53.6(2)}Ag_{6.4(2)}$ and $Na_{30.5}Ga_{57.4(2)}Ag_{2.6(2)}$ was 4.9 and 6.2%, respectively, and reduced the R_f to 3.3 and 3.4%.

A second problem occurred with the sodium atoms in a channel along 0, 0, z formed by the drums. Disorder and poor coordination along the *c*-axis makes it difficult to model

these atom positions accurately. A Fourier electron density map (F_{obs}) of this region is shown in Figure 1 for $Na_{30.5}Ga_{53.6(2)}Ag_{6.4(2)}$. The plot was generated when the refinement had an R_f of 6.0% and without any of the positions in the channel included in the model. This is a [110] section through the center of the $(Ga,Ag)_{18}$-drum with the *c*-axis vertical. Each contour line represents one electron. This plane also intercepts the origin of the unit cell (Na6) and the Ga6 and Na3 atoms. The main peak occurs inside the drum and refines as a fully occupied sodium atom. This position has been labeled Na5. One problem with the position of this peak is that it has a symmetry equivalent position ~2.9 Å away in the other half of the drum. This is too short for a Na–Na contact which are usually greater than 3.3 Å . Refining the structure in lower symmetry space groups (P6) to remove the symmetry element between these positions did not change the Fourier map. A smaller peak (~7 e-/Å^3) that is adjacent to Na5 (0.75 Å away along the channel) may indicate that some disorder is present along the *c*-axis but the total electron density of this peak and Na5 is greater than 100 %. If the peak adjacent to Na5 is included in the refinement, strong coupling between this peak and the Na5 position occurs. Since the smaller peak is physically unreasonable and is strongly coupled to Na5, it was not included in the model. Even though the Na5 position has a short contact, it has been fixed at full occupancy. The second largest peak in the channel occurs at the origin of the unit cell and has been labeled Na6. From the Fourier map it is obvious that it is not fully occupied so the occupancy was determined by fixing the isotropic thermal parameter to 2.0 which is similar to the well refined positions in the structure. The refined occupancy was 54(5)% so in the final model it was fixed at 50% occupancy and the isotropic thermal parameter was allowed to refine. Anisotropic refinement of all atoms yielded nearly spherical thermal ellipsoids except

for Na5 and Na6. Both atoms formed long "cigar"-shaped thermal ellipsoids down the length of the channel. The U11 and U22 thermal parameters on Na5 refined to negative values while U33 on Na6 continued to grow and would not converge. Since the electron density map does not confirm the elongated thermal ellipsoids and no significant coupling is observed in the refinement with these two positions, these poorly defined peaks were refined isotropically in the final model. Attempts to refine the structure in lower symmetry space groups did not improve the refinement.

Similar problems were encountered in the crystal refined as $Na_{30.5}Ga_{57.4(2)}Ag_{2.6(2)}$ except the positions of the main sodium peaks were shifted along the channel. The Na5 peak is closer to the origin so it does not have any problems with a short contact with its symmetry equivalent position but now it is 2.84(4) Å away from Na6. The Na5 and Na6 positions are not fully occupied and refine to 56(5)% and 43(4)%, respectively, (with B_{iso} refining) so the short contact could be reasonable. Another difference between the crystal structure refinements is that Na6 is in a different position. It has shifted away from the origin 0.4 Å along the *c*-axis. Both of these positions were fixed at 50% occupancy, and the isotropic thermal parameters were allowed to refine. As in the first crystal, a smaller peak is 0.63 Å away from Na5 in the channel. This peak corresponds to roughly 3 $e^-/Å^3$ (24(8)% of Na) and has been refined isotropically as Na7 but the large amount of error makes this peak questionable. Another peak (~3 e^-) occurs at 0, 0, 0.5 which is in the center of the drum but strong coupling occurred with the other atoms in the channel so this peak was not included in the final model. As before, anisotropic refinement of these positions produces large thermal ellipsoids in the U33 direction so they were all modeled isotropically. The refined amount of

sodium in each structure corresponds to 30.5 atoms per unit cell but considering the large amount of error associated with the sodium atoms in the channel, this value could range from 30 to 31 electrons per unit cell. Besides the residual electron density in the channel, no other significant peaks (<1.5 $e^-/Å^3$) were observed in the rest of the structure.

Some data collection parameters, atomic positions, anisotropic thermal parameters, and selected bond distances are listed in Tables 1, 2, 3, and 4, respectively. The F_o/F_c data are available from J.D.C.

Results and Discussion

Structure description

$Na_{30.5}Ga_{57.4(2)}Ag_{2.6(2)}$ and $Na_{30.5}Ga_{53.6(2)}Ag_{6.4(2)}$ have the same structure but differ in the amounts of silver mixed on the Ga5 positions. The three-dimensional structure is formed by three different clusters: Ga_3 triangles, Ga_{12} icosahedra, and $(Ga,Ag)_{18}$ "drums" (Figures 2 and 3). The Ga_3 triangles are formed by Ga1 (Figure 4a) with each Ga1 atom having two bonds within the triangle and two exo-bonds to Ga4 on two different icosahedra. So each Ga_3 unit is connected to six icosahedra. The gallium icosahedron (Figure 4b) formed by Ga2, Ga3, and Ga4 is a regular deltahedron with a point group symmetry of D_{2h}. All 12 gallium atoms form exo-bonds to adjacent clusters: four bonds (Ga4–Ga1) to Ga3 triangles, four bonds (Ga2–Ga2) to other icosahedra, and four bonds (Ga3–Ga5) to hexacapped-hexagonal prisms ("drums"). The "drums" cans be viewed as hexagonal prisms (D_{6h}) of Ga5/Ag with Ga6 atoms sitting slightly outside of the rectangular faces (Figure 5). Each Ga5/Ag atom forms two links to the Ga6 atoms at ~2.62 Å, one exo-bond to an icosahedron at ~2.6 Å, and two

Ga5–Ga5 contacts at ~3.0 Å. The Ga6 atoms are bonded to four Ga5 atoms and to two Ga6 atoms around the waist of the cluster. Comparison of the Ga–Ag contacts to those observed in Ag_3Ga[10] (2.68 Å) indicates that the bonds are slightly shorter (~0.04 Å) in the title compound. The mixing of gallium and silver on the same site would give an average distance which is smaller than a typical Ga–Ag contact.

The inside of the drum has a diameter of ~5.75 Å at the waist that increases to about 6.1 Å on the end hexagons, but both of these are dependent on the amount of silver in the structure. The large opening is sufficient for two sodium atoms to reside inside the drum. The drums are aligned along the c-axis with ~5.0 Å between them which creates a channel for the sodium atoms.

The first four sodium atoms in both structures are well behaved and coordinate the gallium framework in characteristic roles (Figure 6). Typical coordination includes capping triangular faces on the icosahedra and on the drum and edge bridging the triangular Ga_3 unit (Figure 6). The Na5 and Na6 positions (and Na7 in $Na_{30.5}Ga_{57.4(2)}Ag_{2.6(2)}$) do not refine very well and several attempts to model these positions have failed to generate reasonable results. These positions occur in the 0, 0, z channel formed by the drums. In $Na_{30.5}Ga_{57.4(2)}Ag_{2.6(2)}$, a close contact occurs between Na5 and Na6 (2.2 Å) but since each atom is 50% occupied they presumably do not "see" each other. The Na7 position is a small peak which is adjacent to Na5 and has been refined to only 25% occupancy. Most of the electron density in the channel is modeled by these three positions but they are not well defined, and a large amount of error should be associated with these atoms.

The structure refined as $Na_{30.5}Ga_{53.6(2)}Ag_{6.4(2)}$ had similar problems with the atoms in the channel but all three peaks appear at different locations within the channel (Figure 1). Na5 appears to be fully occupied and moves closer to the center of the drum. This creates an unusually short contact (~2.8 Å) between symmetry equivalent Na5 atoms in $Na_{30.5}Ga_{53.6(2)}Ag_{6.4(2)}$. The lower limit between sodium atoms is typically 3.3 Å for these types of compounds. A "small" peak (~7 $e^-/Å^3$) is adjacent to the Na5 atom but since the Na5 position is fully occupied it is unreasonable to include this atom in the model. Strong coupling also occurs if this position is included in the refinement. The Na6 position in $Na_{30.5}Ga_{53.6(2)}Ag_{6.4(2)}$ is now at the origin of the unit cell but is 50% occupied. The distance between Na5 and Na6 is now more reasonable at 3.2 Å. Anisotropic refinement of these positions in both structures produces "cigar" shaped thermal ellipsoids with an aspect ratio of ~15:1 for Na5 and negative U_{11} and U_{22} thermal parameters. Na6 also produces a long ellipsoid down the channel with an aspect ratio of 1:300. Since the Fourier map does not show any elongation of the electron density in the channel and the thermal parameters do not couple with other parameters in the refinement, these poorly defined positions have been modeled with isotropic thermal parameters. Modeling the electron density in the channel is difficult and the reliability of the bond distances around these positions is questionable. Apparently, the lack of rigid coordination along the c-axis allows for disorder to occur. The amount of sodium in each compound has been refined to 30.5 atoms per unit cell but the true composition could be from 30 to 31 sodium atoms considering the extra electron density in the channels.

Considering the length of the unit cell along the channel (~9.3 Å) and the shortest distance usually observed between sodium atoms in related structures (~3.3 Å), it is reasonable that three sodium atoms would not be expected fit along the channel (3 x 3.3 = 9.9 Å). On the other hand, only two sodium atoms in the channel would leave open spaces between the atoms. In the actual structure, it is possible that the sodium atoms try to optimize the distance between themselves and end up having different positions in adjacent unit cells. The poor coordination with the framework atoms inside the channel would support this but then more elongated peaks of electron density would be expected in the Fourier map. The two to three atoms in the channel translate to a total of 30 to 31 sodium atoms in unit cell when the other sodium atoms are considered.

Since the amount of sodium and silver present in the structures are not well determined, energy dispersive spectroscopy (EDS) and inductively coupled plasma (ICP) techniques were performed. Both single crystals and bulk material were analyzed with the EDS technique while several crystals were visually selected from the reactions for ICP analysis. The air sensitive nature of these materials made it difficult to prepare flat, clean surfaces for proper EDS measurements. Another factor that inhibited our ability to accurately analyze these materials is the overlap of the energy peaks of sodium and gallium. Several crystals were analyzed using standard reference materials but a large range of compositions were observed even within the same sample. The silver content usually varied from ~3-9 atoms per unit cell but the photographs obtained from the EDS analysis showed some darker regions on the surface of the crystals that tended to have higher silver contents. These sites would be consistent with some Ag_3Ga binary present on the surface of the sample. The range

of sodium content varied even more but this is probably due to excess sodium on the surface of the sample. The ICP analysis had more precision and gave more reproducible results. Unfortunately, the stoichiometries were simply consistent with the loaded compositions because the Ag_3Ga binary could not be separated from the samples.

Related phases

The anionic framework of $Na_{30.5}Ga_{60-x}Ag_x$ is related to the recently reported $Na_8K_{23}In_{48}Cd_{12}$ structure.[14] Both compounds have the same space group and unit cell. In the latter compound, cadmium fully occupies the Ga5/Ag position. Even though cadmium and indium could not be distinguished very well by x-ray studies, a slight improvement in the R-factor was observed with cadmium in this position. The total cadmium content was also based on atomic absorption analysis of the crystal. The detection of silver on this position in the current compounds appears to confirm their result. The potassium-indium-(silver, gold, cadmium, or mercury)[15] systems also form this structure type but difficulties in determining the third element position or low yields made the investigations difficult. All of these phases suffer from the same cation disorder problems along the open channel in the structure. Again, this may be due to the fact that three potassium atoms cannot fit in one unit cell along the channel. Typical contacts between potassium atoms is ~3.8 Å and the length of the *c*-axis in the potassium–indium phases is ~10.4 Å (3 x 3.8 = 11.4). The mixed cations in $Na_8K_{23}In_{48}Cd_{12}$ appears to have solved the problem with two sodium and one potassium in the channel. One concern with the reported $Na_8K_{23}In_{48}Cd_{12}$ is a potassium atom located at the origin of the unit cell. Its closest contact (not including the sodium atom in the channel) is

4.11 Å to a sodium atom and ~4.16 Å to the nearest framework atom (Cd). This is longer than typical K–Na or K–Cd contacts so the cation would be expected to have a larger thermal parameter due to the thermal motion of the atom. It was slightly larger than the other potassium atoms (3.1 vs. 1.8) but not as big as would be expected. This position corresponds to the partially occupied Na6 position in $Na_{30.5}Ga_{60-x}Ag_x$ which has similarly long distances to the surrounding atoms.

Another reported phase, $Na_xMg_{5-x}Ga_9$ (x =2-3),[16] has the same unit cell and space group as the title compounds but the framework is missing one atom in the asymmetric unit. The waist atoms of the Ga_{18}-"drum" (Ga6) are not present so the remaining Ga5 atoms on the ends of the drum adjust to form a hexagonal prism with each atom exo-bonded to an icosahedron. This same structure type (in the same space group) has also been reported in the $Na_5Ga_{9-x}Sn_x$ (x = ~0.5) system[17] with tin mixing on some of the gallium sites. Both of these structural results suffer from residual peaks near the corresponding Ga5 atoms. The cations in $Na_5Ga_{9-x}Sn_x$ are well refined but the mixed cations in $Na_xMg_{5-x}Ga_9$ are not clearly defined.

Nonstoichiometry

Even though the mixing of gallium and silver on the same position may seem unreasonable, the Ag_3Ga binary which forms with the title compound also has mixed occupancy sites and a phase width (25–33 at. % Ga).[11] This suggests that the atomic orbitals of gallium and silver have similar energies and behave similarly in compounds. The phase diagram for the Cd–In system also contains a nonstoichiometric Cd_3In phase (Ag_3Ga structure type) but does not appear to have as large a phase width.

The anionic framework of both the silver-poorer and silver-richer samples are the same except for some small distortions. Most of the changes occur on the Ga_{18} drum where the silver mixes on the Ga5 position. As silver is added to the structure, the Ga5–Ga5 contacts increase from 2.986(2) Å to 3.081(1) Å around the ends of the drum. The larger size of silver should not be a factor because the distance is already longer than typical Ga-Ga (2.5–2.8 Å), Ga-Ag (2.6–2.8 Å), or Ag-Ag (2.7–2.8 Å) bond lengths[10] and overlap populations here do not change significantly with the change in electrons near the Fermi level. The amount of silver in the structure could also explain the shift of the Na5 position in the channel. Sodium–gallium bonds are ~0.1 Å shorter then sodium–silver bonds, so when the silver content is low, the sodium–M5 distance should be less. As the amount of silver is increased, this distance would be expected to lengthen. This could explain the large shift of the Na5 position between the two structures. In addition, the extra peaks of electron density in the channel may be explained as well by the random distribution of silver on the cluster between different unit cells although the sharp Guinier powder pattern lines do not support this. The $Na_8K_{23}In_{48}Cd_{12}$ compound did not exhibit any cation disorder along the channel but since the corresponding "Ga5" position is fully occupied by cadmium no disorder would be expected.

Electronic structure calculations

Electron counting of the Ga_3 and Ga_{12} clusters is straight forward. Each atom in the former is four-bonded and would have a formal charge of -1 so the total cluster charge would be Ga_3^{3-}. The icosahedron is a regular deltahedron and should follow Wade's rules. With 12 exo-bonds, it would be formulated as Ga_{12}^{2-}. With each unit cell having two Ga_3^{3-} and three

Ga_{12}^{2-} clusters, the formal charge on the single $(Ga,Ag)_{18}$ unit per cell would be 18– assuming that 30 cations are present in the structure. Wade's rules for an arachno-Ga_{18} cluster would require 42 skeletal electrons (2n+6), giving a formal charge of 12– for an all gallium cluster. Mixing silver into the framework reduces the electrons available by two electrons for every silver atom; silver is considered to have a filled d^{10} state so only one electron would be available for bonding versus three for gallium. If Wade's rules hold and the compound has a closed electronic shell, then the total number of silver atoms needed to reduce the electron count from 18 to 12 is three atoms per unit cell. Some exceptions to Wade's rules are known to occur for clusters with 16, 19, and 22 atoms[18] but calculations by Fowler[19] indicated a nearly spherical Ga_{20} deltahedron should follow Wade's rules.

A closer look at the drum reveals that the Ga6 waist atoms are closer together than the Ga5/Ag atoms in the end hexagons (2.875(3) vs. 3.081(1) Å in the silver-richer phase). So this cluster is concave and would not be expected to follow Wade's rules. In addition, the variable amount of silver in the structure suggests that the compound may not have a closed electronic shell although it is possible for both end members to be semiconducting. Conductivity measurements have not been performed because of the Ag_3Ga intermetallic impurity.

To establish the number of electrons required to stabilize this cluster, extended Hückel molecular orbital (EHMO) calculations were performed on an isolated Ga_{18} unit with dummy atoms terminating the exo-bonds on the Ga5 atoms. The dummy atoms are in the same position as the Ga3 atoms in the real structure. In order to model the cluster as accurately as possible, the dummy orbitals were assigned Slater type s orbital exponents and energies

equivalent to Ga 4p orbitals although Ga 4s energies produced similar results. The H_{ii} parameters used for Ga^{20} and Ag^{21} were -14.58 and -6.75 for Ga 4s and Ga 4p, respectively, and -10.55, -6.10, and -17.91, for Ag 5s, Ag 5p, and Ag 4d, respectively.

The optimal electron count for the Ga_{18} cluster is not clear. The gap between -6.9 and -5.9 eV, Figure 7, would be consistent with a cluster charge of 10- (2n + 4). A second gap occurs between -5.9 and -4.8 eV that would give a formal charge of 14- to the cluster (2n + 8). To achieve these charges, the total electron count in the unit cell would have to be 202 or 206 electrons, respectively. This corresponds to two or four silver atoms in the unit cell. The character of the molecular orbitals in this energy range is mainly nonbonding interactions, or a combination of weakly bonding and weakly antibonding. The overlap populations within the pure gallium cluster have been calculated for several electron counts but show little change as the electron count is varied. Since the optimum electron count for the cluster is difficult to determine, band calculations were performed on the full structure.

Modeling a system with mixed occupancy sites is not possible with the tight binding method so the calculations have been performed with silver occupying four of the 12 Ga5 positions in the unit cell being careful not to pick positions that were adjacent to each other. A total of 64 k-points were used in the calculation. The effect on the DOS of the small amount of silver that was added does not appear to be significant since the energies of the valance p electrons for both gallium and silver are similar (-6.75 vs. -6.10 eV, respectively). Calculations were also performed on the pure gallium structure and produced the same general results. The total density of states (DOS) shows two band gaps (Figure 8) at the same electron counts, 202 and 206, as expected from the EHMO calculation on the isolated cluster.

Figure 8 also shows the Ga5/Ag and Ga6 atoms contribution to the total DOS. This shows that the main interactions that occur near the Fermi level are located on the $(Ga,Ag)_{18}$ cluster. Since the $(Ga,Ag)_{18}$ cluster interacts with the Ga3 atoms on the icosahedra, the Ga3 atoms on the cluster are also affected by the change in electron count. Overlap populations between Ga3 and the atoms within the icosahedral cluster are not affected. In addition, the silver d-orbitals are low lying and do not affect the interactions near the Fermi level.

Overlap populations for the bonds within the cluster and the Ga3–Ga5 exo-bonds have been calculated for various electron counts (Table 5). Again, the optimum electron count is difficult to determine because the overlap populations do not change significantly with a change in electron count. Ga3–Ga5 has the largest overlap population, which is consistent with this being a 2-center–2-electron bond, while the bonds within the cluster are much weaker. The Ga5-Ga6 distances are the shortest within the 18-atom cluster and, as expected, have large overlap populations. A maximum overlap for these contacts occurs at 196 electrons but decreases slightly as more electrons are included in the unit cell. If the structure had two more electrons, 198, then bonding between Ga5 and Ga6 would decrease slightly but an increase in overlap would be gained in the Ga6–Ga6, Ga5–Ga5, and Ga3–Ga5 bonds. Up to 206 electrons (2n + 8) can be added to the unit cell without adversely affecting the structure. 208 electrons could also be possible but the bonding between the Ga5 atoms starts to decrease. Beyond 208 electrons, anti-bonding interactions between the cluster atoms begins to dominate so higher electron counts would not be expected. Electron counts below 198 reduce the overlap populations of Ga5–Ga5, Ga6–Ga6, and Ga3–Ga5 so lower electron counts would not be expected. The optimum electron count for this compound appears to be

in the range of 198–206 electrons but 208 electrons seems reasonable. This corresponds to a range in silver content from 6–2 atoms per unit cell if 30 sodium atoms are present. If the actual number of sodium atoms is 31 then 6.5–2.5 silver atoms would be expected. This agrees with the refined amounts of silver in the structures and the range of four silver atoms estimated from the loaded compositions. Similar conclusions were made from the calculations of $Na_8K_{23}In_{48}Cd_{12}$ but they only reported the one stoichiometry and did not check whether the phase was nonstoichiometric. They reported a range of 199-206 electrons based on the calculations. The lower limit of 199 electrons was determined from the total number of electrons available in the formula. Twice as much cadmium (vs silver) is needed to obtain the same electron count because each cadmium atom only reduces the electron count by one where as silver reduces it by two.

Conclusions

Many of the compounds in the alkali-metal–gallium systems tend to form structures which appear to have closed electronic shells, but since these materials are on the border between intermetallic and valence phases, some metallic character should not be surprising. The strongest bonding occurs in the lower energy molecular orbitals so a small change in the number of electrons near the Fermi level does not adversely affect the structure.

Several structures have been reported which contain late transition metals and gallium mixing on the same sites, e.g. $Na_{128}Au_{81}Ga_{275}$[22] and $Na_{35}Cd_{24}Ga_{56}$.[23] Electron counting indicates that they are usually close to being closed shell but, unfortunately, many of these compounds have not been completely characterized. Property measurements and simple

checks of phase width would be helpful in understanding some of these unique structures. One obstacle to overcome in the ternary systems is the competitive formation of stable binary phases. This was encountered in $Na_{30.5}Ga_{60-x}Ag_x$ and related structures. Some of these systems may just require more elaborate heating cycles but alternate reaction paths to these materials may be possible through intermediate binaries.

Acknowledgments

Molecular orbital calculations were performed on the Unix version of the band calculation program provided by Gordon Miller.

References

(1) This research was supported by the Office of the Basic Energy Sciences, Materials Sciences Division, U.S. Department of Energy. The Ames Laboratory is operated by Iowa State University under Contract No. W-7405-Eng.82.

(2) Belin, C.; Tillard-Charbonnel, M. *Prog. Solid St. Chem.* **1993**, *22*, 59.

(3) Frank-Cordier, U.; Cordier, G.; Schäfer, H. Z. Naturforsch. **1982**, *37B*, 119.

(4) Ling, R. G.; Belin, C. *Acta Crystallogr.*, **1982**, *38B*, 1101.

(5) *Chemistry, Structure and Bonding of Zintl Phases and Ions*; Kauzlarich, S., Ed.; VCH Publishers: New York, 1996.

(6) Wade, K. *Adv. Inorg. Chem. Radiochem.* **1976**, *18*, 1.

(7) Tillard-Charbonnel, M.; Chahine, A.; Belin, C. *Z. Krist.* **1993**, *208*, 372.

(8) Burdett, J. K.; Canadell, E. *Inorg. Chem.* **1991**, *30*, 1991.

(9) Teo, B. K. *Inorg. Chem.* **1985**, *24*, 4209.

(10) Stratton, R. P.; Kitchingman, W. J. *Acta. Cryst.* **1964**, *17*, 1471.

(11) "Binary Alloy Phase Diagrams," ASM International, Materials Park, Ohio, Vol 1, p. 37, 1990.

(12) Henning, R. W.; Corbett, J. D. Unreported research.

(13) Sheldrick, G. M. SHELXS-86, Universität Göttingen, Germany, 1986.

(14) Flot, D. M.; Tillard-Charbonnel, M. M.; Belin, C. *J. Am. Chem. Soc.* **1996**, *118*, 5229.

(15) Sevov, S. C., Ph. D. dissertation, Iowa State University, 1993.

(16) Nesper, R. *Angew. Chem. Int. Ed. Engl.* **1989**, *28*, 58.

(17) Vaughey, J.; Corbett, J. D. Unreported research.

(18) Brown, L. D.; Lipscomb, W. N. *Inorg. Chem.* **1977**, *16*, 2989.

(19) Fowler, P. W. *Polyhedron*, **1985**, *4*, 2051.

(20) Canadell, E.; Eisenstein, O.; Rubio, J. *Organometallics*, **1984**, *3*, 759.

(21) Clement, E.; Roetti, C. *At. Nucl. Data Tables*, **1974**, *14*, 177.

(22) Tillard-Charbonnel, M.; Belin, C.; Chouaibi, N. *Z. Krist.* **1993**, *206*, 310.

(23) Tillard-Charbonnel, M.; Belin, C. *Mat. Res. Bull.* **1992**, *27*, 1277.

Table 1: Data Collection and Refinement Parameters.

	$Na_{30.5}Ga_{57.4(2)}Ag_{2.6(2)}$	$Na_{30.5}Ga_{53.6(2)}Ag_{6.4(2)}$
Crystal size, mm	0.15 x 0.17 x 0.25	0.19 x 0.20 x 0.41
Space group, Z	P6/mmm (No. 191), 1	P6/mmm (No. 191), 1
Lattice parameters,[a] Å		
a	15.161(2)	15.192(1)
c	9.267(2)	9.299(2)
V, $Å^3$	1844.7(6)	1858.9(5)
d_{calc}, g/cm^3	4.486	4.579
Radiation; $2\theta_{max}$	Mo K_α; 60°	Mo K_α; 50°
Octants measured	+h, ±k, ±l	±h, +k, ±l
Scan method	2θ-ω	2θ-ω
Temperature, °C	23	23
Transmission range	0.3914-1.0000	0.3951-1.0000
μ, cm^{-1} (Mo K_α)	212.8	208.1
Number of reflections:		
measured	12746	6829
observed ($I \geq 3\sigma(I)$)	5721	4837
unique observed ($I \geq 3\sigma(I)$)	774	562
Number of variables	57	55
R_{avg}, ($I \geq 3\sigma(I)$), %	6.2	4.9
Residuals R; R_w,[b] %	3.4; 4.2	3.3; 4.3
Goodness of fit	1.59	3.66
Secondary Ext. Coef.	$1.2(2) \times 10^{-7}$	$3.1(4) \times 10^{-7}$
Largest peaks in final ΔF map, $e/Å^3$	+3.2 (1.9 Å from Na5, in the channel) -2.1	+7.1 (0.75 Å from Na5, in the channel) -2.0

[a]Guinier data with Si as an internal standard.
[b]$R = \Sigma||F_o|-|F_c||/\Sigma|F_o|$; $R_w = [\Sigma w(|F_o|-|F_c|)^2/\Sigma w(F_o)^2]^{1/2}$, $w = 1/\sigma^2$

Table 2: Positional parameters and B(eq) for $Na_{30.5}Ga_{57.4(2)}Ag_{2.6(2)}$ and $Na_{30.5}Ga_{53.6(2)}Ag_{6.4(2)}$.[a]

Atom	Wykoff	x	y	z	B(eq)	Occupancy
Ga1	6*m*	0.60575(8)	2x	1/2	1.23(8)	
		0.60515(8)	2x	1/2	1.2(1)	
Ga2	12*p*	0.1613(1)	0.4938(1)	0	1.02(4)	
		0.1620(1)	0.4947(1)	0	1.19(6)	
Ga3	12*n*	0.35508(9)	0	0.1493(1)	1.04(5)	
		0.3565(1)	0	0.1475(2)	1.15(8)	
Ga4	12*o*	0.55100(5)	2x	0.2533(1)	0.77(5)	
		0.55142(6)	2x	0.2528(2)	0.94(7)	
Ga5/Ag	12*n*	0.1969(1)	0	0.2697(2)	2.01(7)	78(1)/22(1)%
		0.2028(1)	0	0.2731(2)	1.97(8)	47(2)/53(2)%
Ga6	6*m*	0.1121(1)	0.2242	1/2	1.7(1)	
		0.1092(1)	0.2185	1/2	2.1(1)	
Na1	4*h*	1/3	2/3	-0.1999(9)	1.6(2)	
		1/3	2/3	-0.202(1)	1.7(3)	
Na2	12*o*	0.2109(2)	2x	0.3089(5)	1.7(2)	
		0.2104(2)	2x	0.3078(7)	2.1(3)	
Na3	6*l*	0.1354(3)	2x	0	2.1(5)	
		0.1356(3)	2x	0	2.3(6)	
Na4	6*k*	0.3742(6)	0	1/2	2.2(4)	
		0.3762(6)	0	1/2	2.4(5)	
Na5	2*e*	0	0	0.301(4)	3.3(6)	50%
		0	0	0.346(2)	1.1(2)	100%
Na6	1*a*	0	0	0.054(4)	6(1)	50%
		0	0	0	3(1)	50%
Na7[b]	2*e*	0	0	0.369(8)	3.3	25%

[a] Data for $Na_{30.5}Ga_{57.4(2)}Ag_{2.6(2)}$ is listed first for each position.

[b] Position is for $Na_{30.5}Ga_{57.4(2)}Ag_{2.6(2)}$.

Table 3: Anisotropic thermal parameters for $Na_{30.5}Ga_{57.4(2)}Ag_{2.6(2)}$ and $Na_{30.5}Ga_{53.6(2)}Ag_{6.4(2)}$.[a]

Atom	U11	U22	U33	U12	U13	U23
Ga1	0.0181(8)	0.013(1)	0.0140(8)	0.0064	0	0
	0.0200(8)	0.013(1)	0.009(1)	0.006	0	0
Ga2	0.0111(7)	0.0119(7)	0.0156(5)	0.0057(6)	0	0
	0.0140(8)	0.0156(8)	0.015(1)	0.0070(6)	0	0
Ga3	0.0134(6)	0.0117(7)	0.0141(5)	0.0058	0.0005(4)	0
	0.0156(6)	0.0139(7)	0.014(1)	0.007	0.0013(6)	0
Ga4	0.0092(5)	0.0079(7)	0.0111(5)	0.0040	-0.0003	-0.0007(5)
	0.0126(6)	0.0104(7)	0.0121(9)	0.0052	-0.0003	-0.0007(6)
Ga5/Ag	0.0271(7)	0.0232(8)	0.0248(8)	0.0116	0.0104(5)	0
	0.0278(6)	0.0221(7)	0.023(1)	0.011	0.0113(6)	0
Ga6	0.0269(9)	0.029(1)	0.0101(7)	0.0146	0	0
	0.026(1)	0.036(1)	0.019(1)	0.018	0	0
Na1	0.022(3)	0.022	0.017(4)	0.011	0	0
	0.021(3)	0.021	0.021(6)	0.011	0	0
Na2	0.020(2)	0.025(3)	0.021(2)	0.012	0.000	0.001(2)
	0.027(2)	0.029(3)	0.023(4)	0.015	0.002	0.004(3)
Na3	0.026(5)	0.016(8)	0.030(4)	0.008	0	0
	0.028(5)	0.021(7)	0.034(6)	0.011	0	0
Na4	0.031(4)	0.028(5)	0.021(4)	0.014	0	0
	0.038(4)	0.038(5)	0.014(5)	0.019	0	0
Na5	0.042(8)					
	0.014(3)					
Na6	0.07(1)					
	0.04(1)					
Na7[b]	0.042					

[a] Data for $Na_{30.5}Ga_{57.4(2)}Ag_{2.6(2)}$ is listed first for each position.
[b] Position is for $Na_{30.5}Ga_{57.4(2)}Ag_{2.6(2)}$.

Table 4: Bond Distances in $Na_{30.5}Ga_{60-x}Ag_x$ (d < 4.0 Å).

			x = 2.6(2)	x = 6.4(2)				x = 2.6(2)	x = 6.4(2)
Ga1	Ga4	2x	2.700(2)	2.700(2)	Na1	Ga4	3x	3.077(2)	3.072(2)
	Ga1	2x	2.772(4)	2.804(4)		Ga2	6x	3.205(5)	3.213(6)
	Na1	2x	3.208(8)	3.211(9)		Ga1	3x	3.208(8)	3.211(9)
	Na2	4x	3.303(5)	3.330(6)		Na2	6x	3.368(6)	3.391(6)
	Na4	2x	3.369(6)	3.353(5)		Na1		3.71(2)	3.75(2)
Ga2	Ga2		2.597(3)	2.596(3)	Na2	Ga6	2x	3.144(6)	3.198(6)
	Ga2		2.632(3)	2.620(3)		Ga4		3.171(3)	3.286(3)
	Ga3	2x	2.678(2)	2.679(2)		Ga3		3.191(3)	3.236(3)
	Ga4	2x	2.801(1)	2.802(2)		Ga2		3.278(5)	3.293(6)
	Na1	2x	3.205(5)	3.213(6)		Ga1	2x	3.303(5)	3.330(6)
	Na3		3.204(9)	3.215(8)		Ga5	2x	3.328(5)	3.263(5)
	Na2	2x	3.278(5)	3.293(6)		Na1		3.368(6)	3.391(6)
						Na4	2x	3.404(4)	3.416(4)
Ga3	Ga5		2.645(2)	2.611(2)		Na3		3.479(8)	3.469(8)
	Ga2	2x	2.678(3)	2.620(3)		Na2		3.55(1)	3.57(1)
	Ga4	2x	2.747(2)	2.745(2)					
	Ga3		2.767(3)	2.743(3)	Na3	Ga5	2x	3.068(3)	3.103(3)
	Na2	2x	3.191(3)	3.202(4)		Ga2		3.204(9)	3.215(8)
	Na3	2x	3.223(4)	3.236(3)		Ga3		3.223(4)	3.236(3)
	Na4		3.263(2)	3.291(2)		Na2		3.479(8)	3.469(8)
						Na3	2x	3.55(1)	3.568(9)
Ga4	Ga4		2.678(3)	2.701(3)		Na6		3.55(1)	3.569(8)
	Ga1		2.700(2)	2.700(2)					
	Ga3	2x	2.747(2)	2.745(2)	Na4	Ga4	2x	3.265(6)	3.270(6)
	Ga2	2x	2.801(1)	2.802(2)		Ga3		3.263(2)	3.291(2)
	Na1		3.077(2)	3.072(2)		Ga1		3.369(6)	3.353(5)
	Na2	2x	3.171(3)	3.286(3)		Ga5	2x	3.431(8)	3.365(8)
	Na4	2x	3.265(6)	3.270(6)		Ga6	2x	3.452(9)	3.520(9)
						Na2	4x	3.404(4)	3.416(4)
Ga5	Ga3		2.645(2)	2.611(2)					
	Ga6	2x	2.629(1)	2.621(1)	Na5	Na7		0.63(7)	
	Ga5	2x	2.986(2)	3.081(1)		Na5		3.69(7)	2.86(3)
	Na5		3.000(4)	3.155(3)		Ga5	6x	3.000(4)	3.155(3)
	Na3	2x	3.068(3)	3.103(3)		Ga6	6x	3.48(2)	3.207(7)
	Na7		3.12(2)			Na6		2.29(5)	3.22(1)
	Na2	2x	3.328(5)	3.263(5)					
	Na4		3.431(8)	3.365(8)	Na6	Na7		2.4(1)	
	Na6		3.60(2)	3.992(2)		Na5	2x	2.84(4)	3.22(1)
						Na3	6x	3.55(1)	3.569(8)
Ga6	Ga5	4x	2.629(1)	2.621(1)		Ga5		3.60(2)	3.992(2)
	Ga6	2x	2.944(3)	2.875(3)					
	Na2	2x	3.144(6)	3.198(6)	Na7	Na5		0.63(7)	
	Na7		3.18(3)			Na6		2.4(1)	
	Na5		3.48(2)	3.207(7)		Ga5	6x	3.12(2)	
	Na4		3.452(9)	3.520(9)		Ga6	6x	3.18(3)	

Table 5: Overlap populations on the $(Ga,Ag)_{18}$-drum as a function of electron count.

No. of Ag Atoms	Total electron count in the unit cell	Formal charge on cluster	Ga5–Ga5	Ga5–Ga6	Ga6–Ga6	Ga3–Ga5
7	196	-4	0.2165	0.3804	0.1985	0.7481
6	198	-6	0.2237	0.3658	0.2247	0.7575
4	202	-10	0.2212	0.3680	0.2170	0.7665
2	206	-14	0.2160	0.3681	0.2141	0.7799
1	208	-16	0.1922	0.3668	0.2140	0.7914

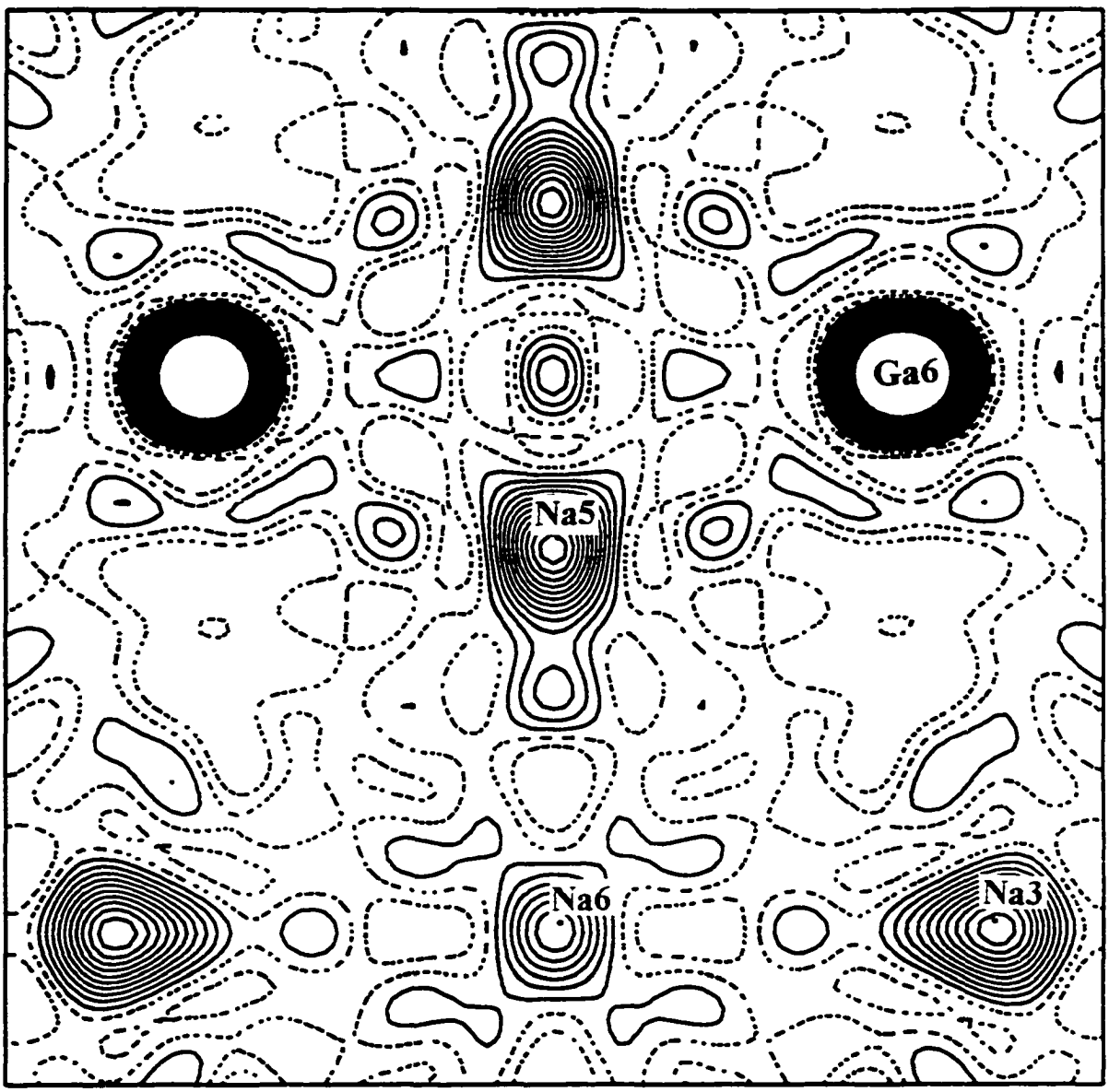

Figure 1. Fourier electron density map (F_{obs}) of the center of the $(Ga,Ag)_{18}$ drum in $Na_{30.5}Ga_{53.6(2)}Ag_{6.4(2)}$. View of [110] section with the *c*-axis vertical. Each contour line represents 1 electron.

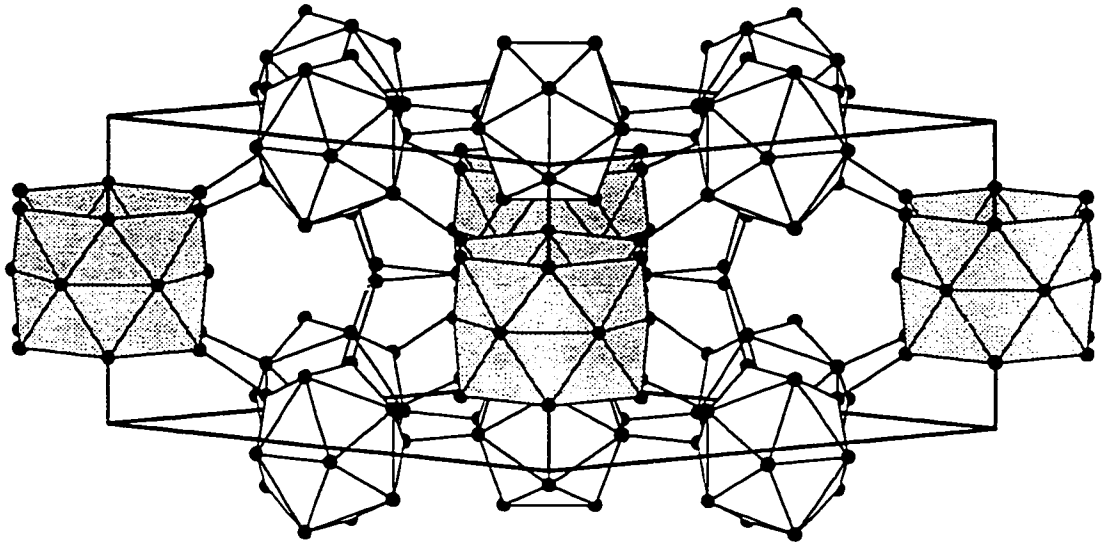

Figure 2. A projection down ~[110] of the unit cell of $Na_{30.5}Ga_{53.6(2)}Ag_{6.4(2)}$. Polyhedral representation of the clusters with bonding between clusters.

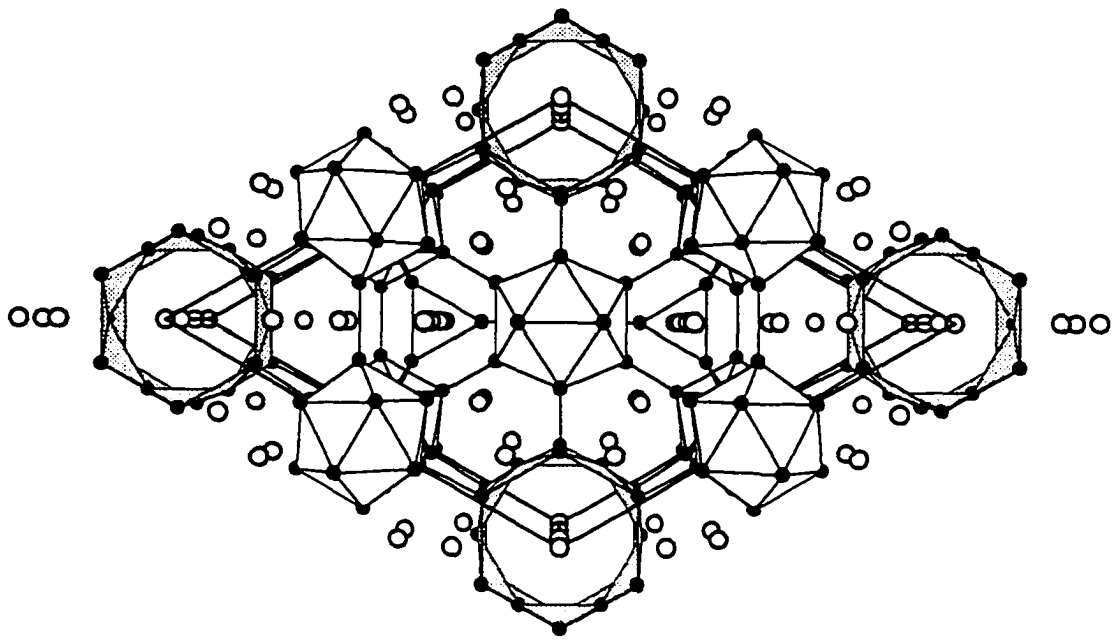

Figure 3. Perspective view down the c-axis of $Na_{30.5}Ga_{53.6(2)}Ag_{6.4(2)}$. Note open channels inside of the drums. Open circles represent sodium atoms.

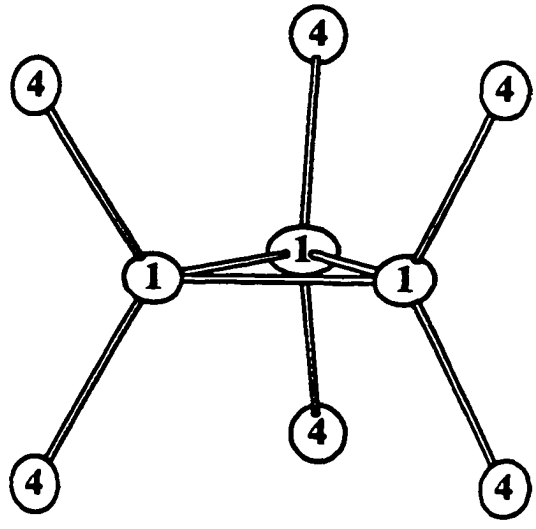

a

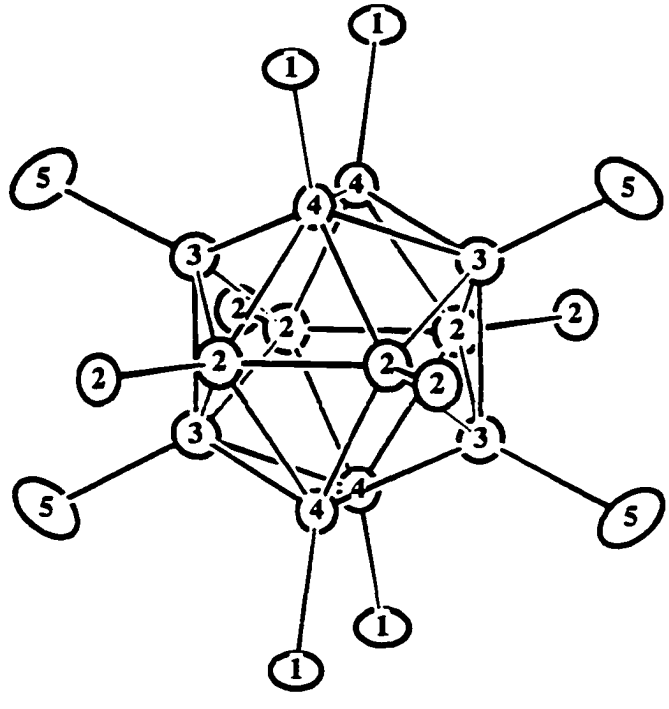

b

Figure 4. Triangular spacer (a) and regular 12-bonded icosahedron (b) in $Na_{30.5}Ga_{53.6(2)}Ag_{6.4(2)}$. Both clusters have the *c*-axis approximately vertical. The exo-bonds for each cluster are also shown. Thermal ellipsoids drawn at 90% probability.

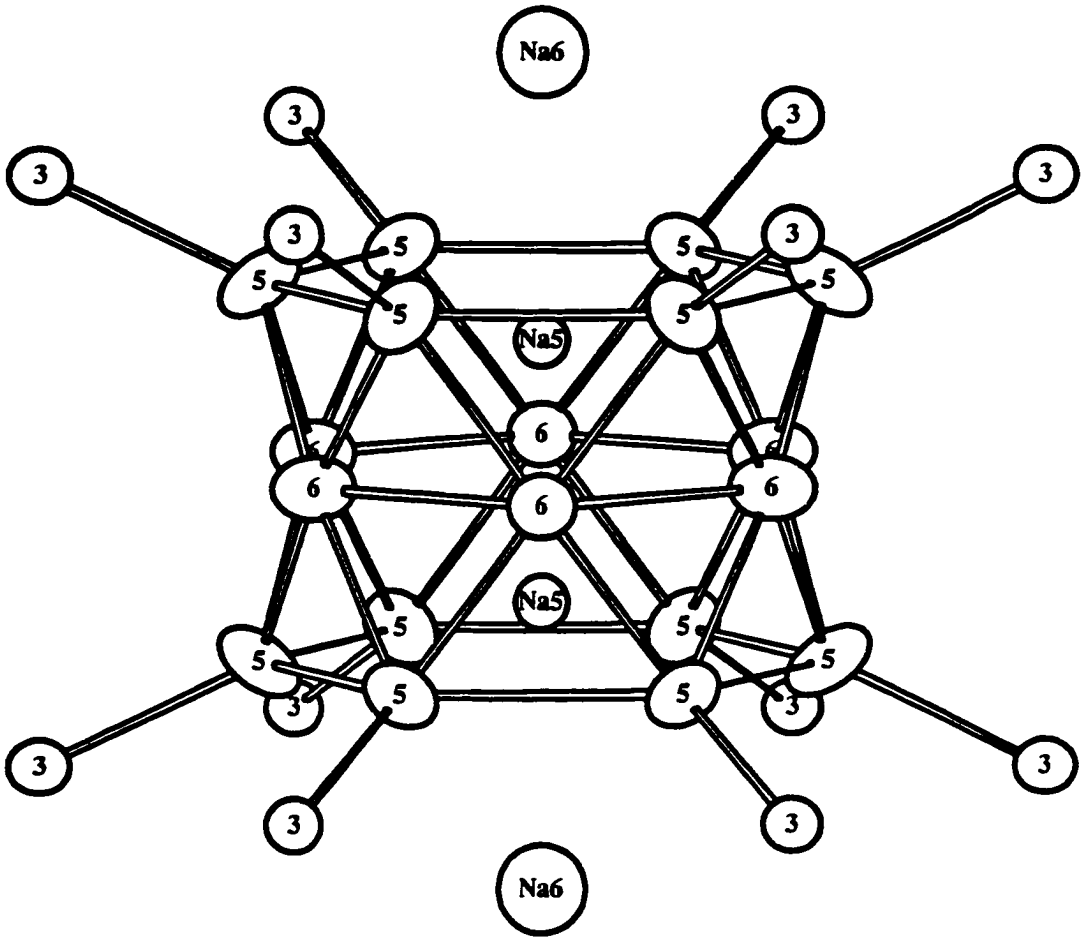

Figure 5. $(Ga5/Ag)_{18}$ "drum" in $Na_{30.5}Ga_{53.6(2)}Ag_{6.4(2)}$ with exo-bonds to adjacent icosahedra atoms included. Note Na5 atoms inside the drum. Thermal ellipsoids drawn at 90% probability.

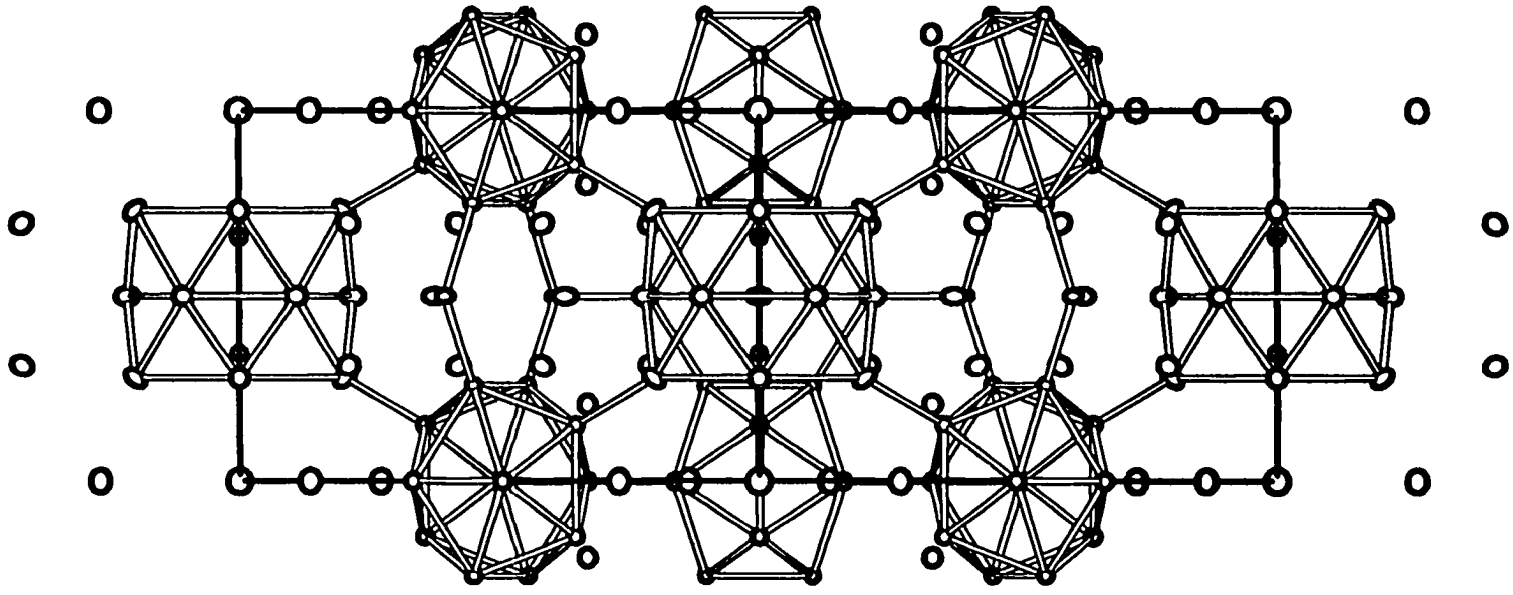

Figure 6. Sodium cations (open circles) fill the voids between the clusters. A projection down [110] of $Na_{30.5}Ga_{53.6(2)}Ag_{6.4(2)}$. Thermal ellipsoids are drawn at 50% probability.

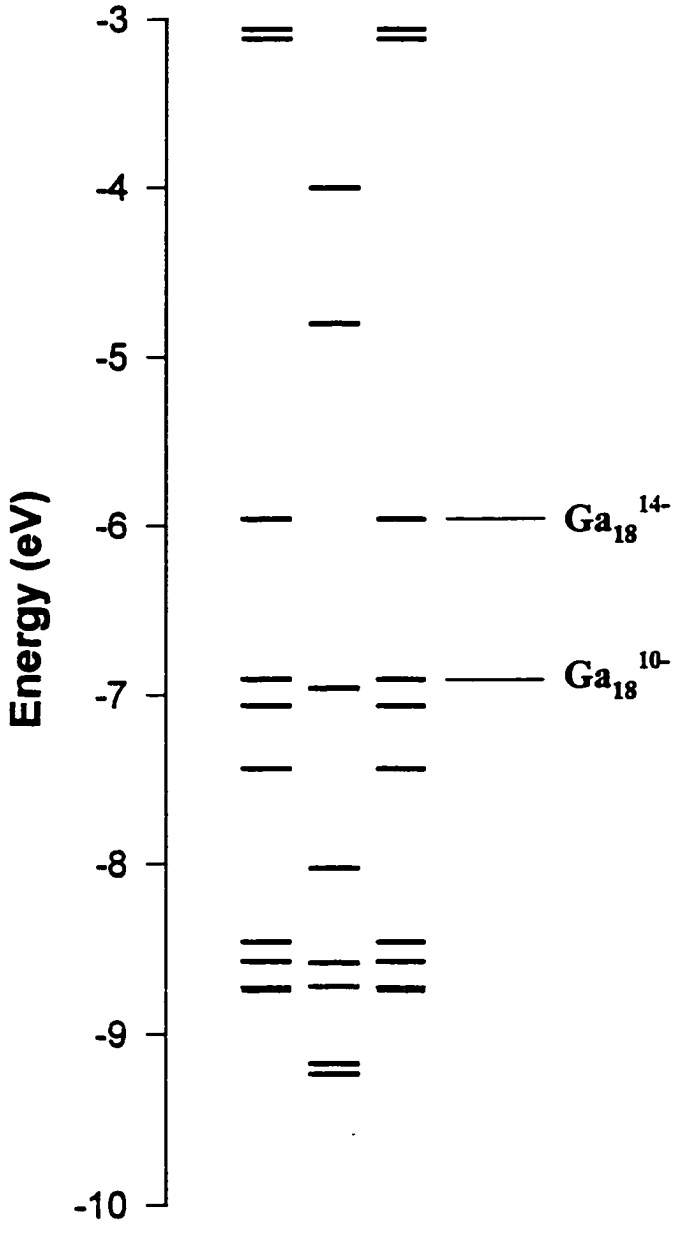

Figure 7. Molecular orbital diagram of an isolated Ga_{18} cluster of the observed geometry.

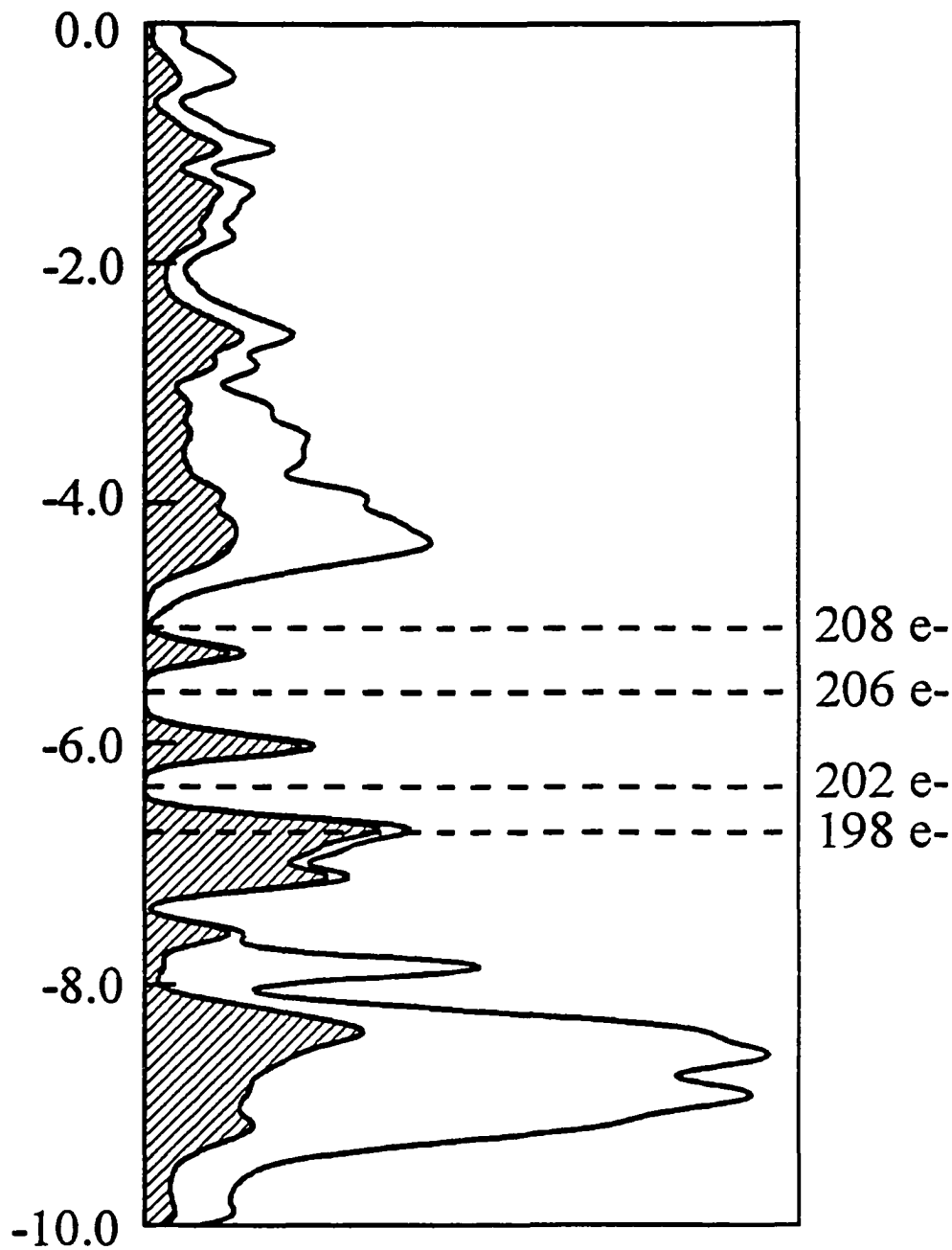

Figure 8. Total density of states plot (solid line) of $Na_{30.5}Ga_{60-x}Ag_x$ with four silver atoms (x = 4) mixed on the Ga5 positions. Shaded area represents the Ga5 and Ga6 atoms contribution to the total DOS.

FROM A ZINTL TO AN INTERMETALLIC PHASE. THE INTRODUCTION OF GOLD INTO THE $RbGa_3$ BINARY COMPOUND

A paper to be submitted to Solid State Chemistry

Robert W. Henning and John D. Corbett*

Department of Chemistry and Ames Laboratory—DOE,[1]

Iowa State University, Ames IA 50011

Abstract

Exploratory syntheses in the rubidium-gallium–late transition metal systems have revealed a family of nonstoichiometric compounds in $RbGa_{3-x}M_x$ (M = Cu, Ag, and Au). They are isostructural with the known binary AGa_3 compounds (A = K, Rb, and Cs) but with the transition elements substituting on the gallium positions. The $RbGa_3$ structure type is composed of Ga_8 dodecahedral clusters and 4-bonded gallium atoms. The rubidium-gallium-gold compounds form in high yield and have been studied in more detail. Up to two gold atoms per unit cell (x = 0.33 for $RbGa_{3-x}Au_x$) can be added to the structure, and this causes both one edge of the Ga_8 dodecahedral cluster to lengthen and a large shift of the lattice parameters via oxidation of a short Ga–Ga π bond. Extended Hückel calculations provide insight into the distortion of the dodecahedral cluster.

Introduction

The alkali-metal–group 13 binary systems are well known for forming stoichiometric compounds that have closed electronic shells.[2] They are routinely classified as Zintl phases[3] and are credited with filling the gap between intermetallic and valence (salt-like) compounds.[4] This may continue when a late transition element is introduced into the system. In $Na_{10}Ga_{10}Ni$,[5] isolated clusters form but network structures are more common, e.g. for $Na_{35}Cd_{24}Ga_{56}$[6] and $Na_{128}Au_{81}Ga_{275}$.[7] Many of the reported compounds form structures which have electron counts consistent with closed electronic shells, or nearly so, but, since these phases are on the border between intermetallic and valence compounds, the formation of metallic phases should not be unexpected. Several structures of compounds with unknown properties have been reported which contain disorder or are nonstoichiometric. The $RbGa_3$ binary was characterized previously by Belin and Ling[8] as a typical three-dimensional structure that is consistent with a closed shell compound, but this has not been verified.

When $RbGa_3$ is prepared in the presence of certain late transition metals, the third element is incorporated into the structure even though the resulting compounds are not closed-shell. This paper reports the nonstoichiometry of $RbGa_{3-x}Au_x$ and related compounds. The single crystal x-ray structures of two compounds with different amounts of gold will be discussed. Extend Hückel calculations on the original $RbGa_3$ binary and on the distorted structure have been performed in order to gain a better understanding of the electronic structures.

Experimental Section

The title compounds can be prepared by heating the elements above the melting point in the system (~600 °C) and slow cooling the samples to 500 °C or below. The reactivity of the starting materials and products required the use of nitrogen or helium-filled dry boxes. Tantalum tubing was used as an inert reaction container as previously reported.[9] $RbGa_{3-x}Au_x$ ($x = 0$~0.33) was obtained in ~85-90% yield but with $RbGa_7$[10] and $AuGa_2$[11] always present as byproducts. Excess gold (up to $x = 0.5$) had to be loaded because the formation of $AuGa_2$ altered the stoichiometry. A small amount of rubidium metal was always observed in one end of the tube. Since the boiling point of rubidium metal is at 686 °C, vaporization of some rubidium was believed to hinder the formation of a pure sample but reactions loaded with excess rubidium produced similar results. The melting point for $RbGa_3$ is reported as ~520 °C but this area of the phase diagram[12] has not been very well characterized. $AuGa_2$ melts at 491 °C[13] so if the actual melting point of $RbGa_3$ is below this temperature then $AuGa_2$ could form first on cooling. Annealing reactions loaded as $RbGa_{2.7}Ga_{0.3}$ for one month at various temperatures (400, 450, 500, and 520) coupled with the use of pressed pellets also failed to yield pure samples. Samples that were loaded with an excess of gold ($x \geq 0.5$) gave powder patterns which contained extra reflections that could not be identified. The extra lines increased in intensity as the gold content increased. Reactions loaded with less gold ($x < 0.5$) did not produce the extra lines in the powder patterns.

Reactions loaded as $RbGa_{2.64}M_{0.36}$ (M = Cu and Ag) and slowly cooled (3 °C/h) from 650 °C also produced lattice parameters (a = 6.2628(9), 6.314(3) Å and c = 15.232(3), 15.050(2) Å for Cu and Ag, respectively vs. a = 6.3221(4) Å and c = 15.007(2) Å for $RbGa_3$)

consistent with the substitution of the late transition metal into the structure but in both cases another intermetallic phase (Ag_3Ga (~50%) and an unidentified CuGa binary) formed in high yield. This reduced the yield of the desired phase and also altered the stoichiometry so that less transition metal was available for the $RbGa_3$ structure. The lattice parameters for the silver phase did not shift very much because of the large amount of Ag_3Ga that formed. Only a few reactions were loaded with copper and silver so it is difficult to determine how much of the transition metal could go into the structure. The $RbGa_{3-x}Au_x$ reactions were studied in more detail because of the higher reaction yields and the ability to distinguish gallium and gold in the single crystal x-ray structure refinement. Reactions loaded with zinc, cadmium, and mercury did not produce the expected lattice shifts due to the formation of the intermetallic binary compounds such as $RbCd_{13}$. Lattice parameter shifts for $KGa_{3-x}M_x$ were also identified in the potassium-gallium-(zinc and cadmium) systems but these phases were not investigated further because of the formation of K_2Ga_3.

The products of all reactions were brittle with a metallic luster. Reactions loaded with an excess of gold ($x \geq 0.4$) produced mixed phase powder patterns which were very sharp while reactions with less gold gave powder patterns with broader lines, consistent with a nonhomogeneous sample. Annealing the samples at 500 °C produced slightly sharper powder patterns but did not improve the yield of the desired phase.

Crystallites were selected from reactions loaded as $RbGa_{2.64}Au_{0.36}$ and $Rb_{1.2}Ga_{2.33}Au_{0.67}$ and sealed into 0.3 mm thin-walled capillary tubes. The product of the latter reaction contained Rb metal, $AuGa_2$ (~10%) and the unknown phase mentioned earlier. The crystals were checked for singularity by Laue photographs, and one crystal from each product was

used for a single crystal x-ray data collection. Both data sets were collected at room temperature on a Rigaku AFC6R four-circle diffractometer with Mo Kα radiation. Twenty-five reflections were obtained from a random search and used to index the crystals to body-centered tetragonal unit cells. The diffractometer lattice parameters for the gold-richer phase were within 3σ of those refined for an indexed Guinier powder pattern for this sample. The diffractometer lattice parameters for the other crystal were not in agreement with the Guinier powder pattern. The *a*-axis was nearly identical but the *c*-axis from the diffractometer was smaller by 0.075 Å (15.403(4) vs 15.478(6) Å). This may be due to a misaligned diffractometer or it is possible that a range of stoichiometries are present in this particular sample especially considering that the lines are a little broad in the powder pattern. The lattice parameters obtained from the powder pattern are more consistent with the lattice parameters of the other phases so they were used in the refinement. Two octants of data ($+h$, $+k$, $\pm l$) were collected up to 70° in 2θ for the crystal obtained from the first reaction and four octants ($+h$, $\pm k$, $\pm l$) up to 60° in 2θ for the second crystal. The body-centering condition was confirmed for both crystals by initially collecting the data for a primitive cell. Both data sets were corrected for absorption by three ψ-scans collected at different 2θ angles. The data sets were also corrected for Lorentz and polarization effects. Systematic absences and the N(Z) distribution suggested the noncentrosymmetric space group $I\bar{4}m2$ (no. 119). Application of direct methods[14] revealed two positions with separations appropriate for Rb-Rb contacts and three positions suitable for gallium. The refinement of the positional and isotropic thermal parameters for all five of these peaks revealed small, or even slightly negative, thermal ellipsoids for all three gallium positions in both compounds. The R-factor was ~9.5 % for

both compounds. Both gallium and gold were refined on all three gallium positions with the total occupancy of each set to 100%. The anisotropic thermal parameters of the gallium and gold atoms were set equal to each other and allowed to refine along with the occupancy. This lowered the R-factor to ~9.0 % for each data set. R_{avg} ($I \geq 3\sigma_I$) for the gold-richer sample was 13.0 % and 9.4% for the second crystal. The total gold content of the gallium sites in the crystal obtained from the gold-richer sample refined to x = 0.36(2) or ~2 atoms per unit cell. The refinement indicated that gold was present on all three gallium positions with 6.3(8), 16(1), and 20(1) % gold on Ga1, Ga2, and Ga3, respectively. Refinement of the other crystal indicated that less gold was present in the structure (x = 0.26(1)) with 3.8(5), 12.9(6), and 10.3(8) % gold on the respective sites. All refinements were performed on a VAX workstation using the TEXSAN[15] crystallographic package.

The positional parameters, isotropic thermal parameters, and refined occupancies for both structures are listed in Table 1. Anisotropic thermal parameters and data collection information are listed in Tables 2 and 3, respectively. Bond distances, lattice parameters and overlap populations are in Tables 4, 5, and 6, respectively.

Results and discussion

The $AGa_{3-x}M_x$ compounds are isotypic with the AGa_3 binaries except for the substitution of the late transition metal (M = Cu, Ag, Au) on the gallium positions. The main building blocks of the anionic framework are Ga_8 dodecahedra and tetrahedrally coordinated gallium atoms (Figure 1). The dodecahedra have D_{2v} symmetry and are formed by Ga1 and Ga2 atoms (Figure 2). The four Ga1 atoms around the waist of the cluster have five

neighbors within the cluster and one exo-bond to a Ga1 atom on an adjacent cluster. This exo-bonding between clusters forms layers of dodecahedra with four-fold symmetry along the *c*-axis. The Ga2 atoms have four bonds within the cluster and form an exo-bond to Ga3. Adjacent layers of dodecahedra are connected through the isolated Ga3 atoms. The tetrahedral coordination around the Ga3 atoms leads to orientation of the clusters of one layer in the depressions of the neighboring layers. This creates a body-centered tetragonal unit cell. The rubidium atoms have characteristic roles in the unit cell. Rb1 caps the Ga1–Ga2–Ga2 trigonal face on four different dodecahedra and Rb2 bridges a Ga2–Ga2 edge of one cluster and a Ga1–Ga2 edge of four others. The anisotropic thermal parameters are close to spherical for all atoms although the U11 axis of Ga(Au)2 is twice as long as U22. The larger thermal parameter is in the same direction as the bond lengthening and suggests that a small amount of disorder occurs on this mixed position.

The dodecahedral cluster is a regular deltahedron with triangular faces and has a skeletal electron count of 18 (2n + 2) which is consistent with Wade's rules.[16] This has been confirmed through EHMO calculations on the isolated cluster by Belin and Tillard-Charbonnel.[2] Bond distances within the cluster of the $RbGa_3$ binary are typical of a delocalized system with values in the range of 2.6–2.8 Å. The only exception is for the unique Ga2–Ga2 bond distance within the cluster which is 2.442(8) Å in the binary.[8] This is very short for a Ga–Ga contact especially considering that most 2-center–2-electron bonds for gallium are about 2.5-2.65 Å. Indexed Guinier powder patterns of the $RbGa_3$ binary (a = 6.3221(4) and c = 15.007(2) Å) were consistent with the literature values (a = 6.315(2) and c = 15.000(2) Å). A short bond distance also appears in the Ga_{15} spacer of $Na_{22}Ga_{39}$.[17]

Theoretical calculations by Burdett and Canadell indicate that the 2.435 Å distance is a double bond. MO calculations performed on the isolated Ga_8 cluster by Belin and Tillard-Charbonnel [2] indicate that some π-bonding is important between the Ga2 atoms. The high curvature of the cluster at the Ga2 position makes the tangential orbitals stick out above the surface of the cluster and form some π-interactions. So this bond could be classified as a double bond even though it is occurring in a delocalized bonded cluster. The effect of cation packing can force atoms closer together in some structures, but this short separation is also observed in the KGa_3[18] and $CsGa_3$[18] compounds so it is believed to be an intrinsic part of the electronic structure.

Distortion of the cluster

The shift in the lattice parameters is consistent with the amount of gold present in the reaction. Several reactions were loaded in which the Ga/Au content was varied (Table 5). As the loaded gold content increased from x = 0.0 to x = 0.5, the lattice parameters shift accordingly. Reactions loaded with greater amounts of gold did not change the lattice parameters but an unidentified phase appeared. A small amount (~5%) of the new phase appeared in the reaction with x = 0.5 but increased as more gold was added. The formation of the $AuGa_2$ binary altered the initial stoichiometry of the samples and made it difficult to quantify the amount of gold in the compounds. The amount of gold determined through the structure refinement (x = 0.26(1)) of the crystal obtained from the reaction loaded as $RbGa_{2.64}Au_{0.36}$ is consistent with amount of gold removed from the reaction through the formation of the $AuGa_2$ binary. The approximate yields for this reaction were 85%

$RbGa_{3-x}Au_x$, 10% $AuGa_2$, and 5% Rb. The maximum amount of gold that can be inserted into the structure is difficult to determine through the loaded reactions but it is close to two gold atoms per unit cell (x = .33). This is consistent with the amount of gold found in the crystal from the gold-richest sample (x = 0.36(1)).

As the amount of gold in the compound is increased, the structure changes significantly. The most noticeable change in atomic distances occurs for Ga(Au)2–Ga(Au)2 in the cluster. In the $RbGa_3$ binary, the Ga2–Ga2 distance is 2.442(8) Å but increases to 2.582(5) Å in $RbGa_{2.74(1)}Au_{0.26(1)}$ (6.5 % at. Au) and 2.632(6) Å in $RbGa_{2.64(2)}Au_{0.36(2)}$ (9.0 % at. Au). The other Ga(Au)–Ga(Au) distances in the rest of the structure do not change as significantly, ±0.04 Å or less, even though almost as much Au substitutes at Ga3 (up to 20%). The increase in the Ga2–Ga2 bond length affects the rest of the structure and is largely responsible for the large shift in the lattice parameters (-0.13 Å in *a*, +0.51 Å in *c*). As the Ga2–Ga2 contact increases, the Ga2–Ga3 exo-bond decreases slightly (≤ 0.03 Å), as expected, but the bond angles around Ga3 are affected more significantly. The Ga2–Ga3–Ga2 bond angle in $RbGa_3$ (between clusters within the same layer) is 100.0(2)° but as gold is added to the system, this angle decreases to 90.9(1)°. The Ga2–Ga3 bond distances do not change appreciably with increased gold content, rather the unit cell lengthens in the *c*-direction and decreases in the *a*-*b* plane. This also forces the clusters closer together with the Ga1–Ga1 contact between clusters decreasing appropriately.

Other bond distances within the cluster change in response to the Ga2–Ga2 lengthening but not as expected. Ga2 is coordinated to three Ga1 atoms in the cluster with two of them being symmetry equivalent. As the Ga2–Ga2 bond lengthens, the Ga2 atom

should move closer to one Ga1 atom and farther away from the other two but the opposite occurs with the single contact increasing by 0.034(6) Å from 2.609(5) to 2.643(3) Å and the other two contacts decreasing by 0.025(5) Å from 2.806(4) to 2.781(3) Å. A closer look at the cluster shows that the Ga1 atoms are shifted away from the basal plane in parallel with the contraction of the layer in the *a-b* plane. As the clusters move closer together, the Ga1–Ga1 exo-bonds between clusters do not absorb the full shift rather the clusters become distorted.

Gold positions in the structure

Since the Ga2–Ga2 bond length changes dramatically with an increase in gold content, gold substitution might be expected to occur only in this position versus the other gallium sites in the structure, but the single crystal x-ray refinements indicate that gold does not substitute exclusively on the Ga2 position. A majority of the gold appears on the Ga2 ($\leq$ 16(1)%) and Ga3 ($\leq$ 20(1)%) sites with a smaller amount on the Ga1 position ($\leq$ 6.3(8)%). The occupancies for both structure refinements are listed in Table 1. Gold has a larger metallic radius then gallium (1.34 vs. 1.25 Å)[19] so the bond distances might be expected to increase when gallium is replaced by gold. For comparison, the Au–Ga contacts in $AuGa_2$,[12] AuGa,[20] and Au_2Ga[21] are 2.63, 2.58, and 2.60 Å, respectively. Although the Ga2–Ga2 separation does increase to the same range, the Ga2–Ga3 bond actually shortens by 0.028(5) Å in $RbGa_{2.64(2)}Au_{0.36(2)}$. Thus a larger metallic radius of gold does not adequately explain the lengthening of the Ga2–Ga2 bond.

Electronic structure calculations

The application of Wade's rules to the dodecahedral cluster gives a skeletal electron count of 18 (2n + 2) and, with all eight vertices exo-bonded, the formal cluster charge should be 2–. The tetrahedrally coordinated Ga3 atom follows the octet rules and so is assigned a formal charge of 1–. Since the cluster and the Ga3 atom occur in the ratio of 1:1, the three rubidium atoms provide the required number of electrons to form a closed-shell compound, $(Rb^{+})_3Ga_8^{2-}(4b\text{-}Ga^{1-})$. To gain a better understanding of why the structure distorts with a change in electron count, extended Hückel calculations were carried out to analyze the electronic structure of the binary as well as the distorted structure of $RbGa_{2.64(2)}Au_{0.36(2)}$. The calculations were performed on the gallium framework of the full unit cell (Rb_6Ga_{18}, Z = 6) at 300 k-points. Since the tight binding method can not handle the mixing of gallium and gold on the same position, all positions were assigned to gallium for the ternary compound. The H_{ii} parameters used for Ga^{22} were -14.58 and -6.75 for Ga 4s and Ga 4p, respectively.

The total density of states (DOS) for the binary compound is shown is Figure 3 (solid line). The 18 gallium atoms contribute 54 total electrons and with the six electrons from the rubidium atoms, the total number of electrons available for bonding is 60 per cell. The Fermi level for 60 electrons occurs at -6.40 eV and falls in the band gap. This is characteristic for a compound with a closed electronic shell. The COOP curve for all Ga–Ga bonds in $RbGa_3$ is shown in Figure 4 (solid line). The right side of each plot represents bonding states while those on the left side reflect antibonding states. This shows that all bonding states are filled in $RbGa_3$ as expected for a Zintl phase.

The d-orbitals on gold are filled and are taken to be inert, so the number of valence electrons available for bonding is one per gold atom. Since gold is replacing gallium, each gold atom reduces the electron count by two and therefore reduces the total electron count in the structure. $RbGa_{2.64(2)}Au_{0.36(2)}$ has approximately two gold atoms per unit cell (Z = 6) which would reduce the total electron count of the cell to 56 electrons. The Fermi level for 56 electrons is then at -8.10 eV in the binary, in the middle of a large peak in the DOS. A closer look at the orbitals contributing to the DOS at the Fermi level indicate these are mainly Ga2 p orbitals (shaded area in Figure 3) but some Ga1 and Ga3 p states are present. The COOP curve for the Ga2–Ga2 bond is shown in Figure 4 (dashed line). As the electron count is decreased by adding gold to the system, bonding between the Ga2 atoms is weakened and the Ga2–Ga2 bonds lengthen. The experimental data indicates that approximately two gold atoms can be added per unit cell. From this information, it is not apparent why the limit is two gold atoms. The COOP curves for the $RbGa_3$ structure with $RbGa_{2.64(2)}Au_{0.36(2)}$ dimensions are shown in Figure 5. Again, bonding between the Ga2 atoms (dashed line in a) dominates near the Fermi level with a small contribution from the 2.643(3) Å Ga1–Ga2 bond within the cluster. Thus the distortion of the structure does not change the DOS or COOP curves significantly for the all-gallium model. The first four electrons that are removed from the cell are primarily involved in cluster bonding. Since each unit cell has two Ga_8 clusters, each cluster is effectively being oxidized by two electrons. The main interactions in the HOMO of the cluster are π-bonding between the Ga2 atoms. Removing two electrons effectively converts the "double" bond into a typical delocalized single bond. If more electrons could be removed from the structure, bonding between clusters would be affected. Figure 5b shows

the COOP curves for the Ga2–Ga3 bonds (dashed line) and the Ga1–Ga1 bonds (dotted line). Both of these bonds are formal 2-center–2-electron bonds which link the clusters and Ga3 atoms into a three-dimensional network. Optimum overlap is already achieved for both bonds with approximately 56 electrons in the unit cell. Further reduction in the number of electrons would not be expected.

The average overlap populations have been calculated for all Ga–Ga contacts in $RbGa_3$ and an all gallium structure with the lattice parameters of $RbGa_{2.64(2)}Au_{0.36(2)}$ (Table 6). The greatest reduction in bonding on oxidation occurs between the Ga2 atoms, as expected. The average overlap population changes from 0.814 to 0.499 as gold is added to the system. The reduction in bonding between one of the Ga1–Ga2 distances within the cluster is also observed. The other two Ga1–Ga2 atoms move closer together and have a slightly higher overlap population (0.339 vs. 0.389). The only other contact that changes significantly is between the exo-bonded Ga1 atoms where total overlap decreases from 0.753 to 0.674.

The calculations of the ternary compound were based on a pure gallium framework but the real structure contains gold atoms which would influence the bonding within the system. A better representation of the electronic structure might be obtained by substituting two of the gallium atoms by gold. Since the single crystal data indicated that the Ga2 and Ga3 positions contained more gold, one of each type was replaced by a gold atom being careful not to pick positions which would yield a Au–Au contact. The calculation for such a structure produced the same general results as the pure gallium framework with respect to the critical variations already discussed.

Conclusions

The reasons why gold can be incorporated into the structure are not well understood. A closer look at binary phase diagrams between gallium and the late transition metals indicates that several compounds have large phases widths. The structures for these compounds have both atoms mixing on the same sites so it should not be surprising to find it occurring in the ternary compounds, e.g. $Na_{35}Cd_{24}Ga_{56}$[6] and $Na_{128}Au_{81}Ga_{275}$.[7] The late transition elements do not routinely form deltahedral clusters but, under the right conditions, they can be prepared. A gold octahedron has been reported in the compound $[Au_6(PC_{21}H_{21})_6][C_{24}H_{20}B]_2$.[23]

Many of the compounds in the alkali-metal–gallium systems are reported to be stoichiometric but since these compounds are closely related to intermetallic phases careful analysis may reveal that more nonstoichiometry exists. This is especially true in the ternary systems with late transition metals where the substitution for gallium is very common. Compounds that contain unusual clusters or spacers may be more susceptible to this type of behavior. $Na_{30.5}Ga_{60-x}Ag_x$[24] contains an unusual hexacapped-hexagonal prism and has been found to be nonstoichiometric. Nonstoichiometry has also been noted in several compounds containing twinned icosahedra, e.g. $Li_9K_3Ga_{28.83}$[25] and $Na_{6.25}Rb_{0.6}Ga_{20.02}$.[26] Compounds containing regular deltahedra tend to form stoichiometric closed shell structures.

References

(1) This research was supported by the Office of the Basic Energy Sciences, Materials Sciences Division, U.S. Department of Energy. The Ames Laboratory is operated by Iowa State University under Contract No. W-7405-Eng.82.

(2) Belin, C.; Tillard-Charbonnel, M. *Prog. Solid State. Chem.* **1993**, *22*, 59.

(3) Corbett, J. D. *Structure and Bonding* **1997**, *87*, 157.

(4) *Chemistry, Structure and Bonding of Zintl Phases and Ions*; Kauzlarich, S., Ed.; VCH Publishers: New York, 1996.

(5) Henning, R. W.; Chapter 2, Ph. D. dissertation, Iowa State University, 1998.

(6) Tillard-Charbonnel, M.; Belin, C. *Mat. Res. Bull.* **1992**, *27*, 1277.

(7) Tillard-Charbonnel, M.; Belin, C. *Z. Krist.* **1993**, *206*, 310.

(8) Ling, R. G.; Belin, C. *Z. Anorg. Allg. Chem.* **1981**, *480*, 181.

(9) Henning, R.W.; Corbett, J.D. *Inorg. Chem.* **1997**, *36*, 6039.

(10) Belin, C. *Acta Cryst.* **1981**, *B37*, 2060.

(11) Warren Jr., W. W.; Shaw Jr., R. W.; Menth, A.; Disalvo, F. J.; Storm, A. R.; Wernick, J. H. *Phys. Rev. B*, **1973**, *7*, 1247.

(12) "Binary Alloy Phase Diagrams," ASM international, Vol 2, p. 1845, 1990.

(13) "Binary Alloy Phase Diagrams," ASM international, Vol 1, p. 369, 1990.

(14) Sheldrick, G. M. SHELXS-86, Universität Göttingen, Germany, 1986.

(15) TEXSAN, version 6.0, Molecular Structure Corp., The Woodlands, Texas, 1990.

(16) Wade, K. Adv. *Inorg. Chem. Radiochem.* **1976**, *18*, 1.

(17) Burdett, J. K.; Canadell, E. *J. Am. Chem. Soc.* **1990**, *112*, 7207.

(18) van Vucht, J. H. N. *J. Less-Common Met.* **1985**, *108*, 163.

(19) Pauling, L. *The Nature of the Chemicl Bond*; Cornell University Press, New York, 1960; p. 247.

(20) Cooke, C. J.; Hume-Rothery, W. *J. Less-Common Met.* **1966**, *10*, 42.

(21) Puselj, M.; Schubert, K. *J. Less-Common Met.* **1974**, *38*, 83.

(22) Canadell, E.; Eisenstein, O.; Rubio, J. *Organometallics*, **1984**, *3*, 759.

(23) Bellon, P.; Manassero, M.; Sansoni, M. *J. Chem. Soc., Dalton Trans.*, **1973**, *22*, 2423.

(24) Henning, R. W.; Corbett, J. D. To be submitted for publication.

(25) Belin, C. *J. Solid State Chem.* **1983**, *50*, 225.

(26) Charbonnel, M.; Belin, C. *J. Solid State Chem.* **1987**, *67*, 210.

Table 1: Positional parameters for $RbGa_{2.74(1)}Au_{0.26(1)}$ and $RbGa_{2.64(1)}Au_{0.36(1)}$.

Atom	Wykoff	x	y	z	B(eq)	Ga/Au, %
Rb1	2*a*	0	0	0	1.90(7)	
		0	0	0	1.3(1)	
Rb2	4*f*	0	1/2	0.3713(1)	1.8(1)	
		0	1/2	0.3711(2)	1.3(1)	
Ga1/Au1	8*i*	0.2074(3)	0	0.21995(8)	1.21(7)	96.2(5)/3.8(5)
		0.2085(4)	0	0.2196(1)	1.0(1)	93.7(8)/6.3(8)
Ga2/Au2	8*i*	0.2919(4)	0	0.38775(7)	2.05(7)	87.1(6)/12.9(6)
		0.2876(5)	0	0.3870(1)	1.6(1)	84(1)/16(1)
Ga3/Au3	2*b*	0	0	1/2	1.79(9)	89.7(8)/10.3(8)
		0	0	1/2	1.5(1)	80(1)/20(1)

[a]Data for $RbGa_{2.64(1)}Au_{0.36(1)}$ are listed second.

Table 2: Anisotropic thermal parameters for $RbGa_{2.74(1)}Au_{0.26(1)}$ and $RbGa_{2.64(1)}Au_{0.36(1)}$[a].

Atom	U11	U22	U33	U12	U13	U23
Rb1	0.030(2)	0.030	0.012(1)	0	0	0
	0.023(2)	0.023	0.005(2)	0	0	0
Rb2	0.019(1)	0.019(1)	0.028(1)	0	0	0
	0.012(2)	0.011(2)	0.027(2)	0	0	0
Ga1/Au1	0.0091(9)	0.017(1)	0.0197(6)	0	-0.0008(6)	0
	0.008(1)	0.013(1)	0.017(1)	0	-0.003(1)	0
Ga2/Au2	0.040(1)	0.0197(9)	0.0184(6)	0	0.0046(7)	0
	0.032(2)	0.015(1)	0.015(1)	0	0.006(1)	0
Ga3/Au3	0.023(2)	0.023	0.021(1)	0	0	0
	0.017(2)	0.017	0.022(3)	0	0	0

[a]Data for $RbGa_{2.64(1)}Au_{0.36(1)}$ are listed second.

Table 3: Data Collection and Refinement Parameters for $RbGa_{3-x}Au_x$.

	$RbGa_{2.74(1)}Au_{0.26(1)}$	$RbGa_{2.64(2)}Au_{0.36(2)}$
space group, Z	$I\bar{4}m2$ (No. 119), 6	$I\bar{4}m2$ (No. 119), 6
lattice params[a]		
a, Å	6.205(1)	6.195(1)
c, Å	15.478(6)	15.515(4)
V, Å^3	595.9(3)	595.6(2)
d_{calc}, g/cm^3	5.478	5.696
crystal dimensions, mm	0.10 x 0.18 x 0.21	0.14 x 0.16 x 0.19
diffractometer	Rigaku	Rigaku
radiation; $2\theta_{max}$	Mo K_α; 70°	Mo K_α; 60°
octants measured	+h, +k, ±l	+h, ±k, ±l
scan method	ω-2θ	ω-2θ
temp, °C	23	23
transmission range	0.202-1.000	0.642-1.000
μ, cm^{-1} (Mo K_α)	395.6	425.9
number of reflections:		
measured	1617	1890
observed ($I \geq 3\sigma_I$)	939	1160
unique observed ($I \geq 3\sigma_I$)	392	359
number of variables	25	25
R_{avg} ($I \geq 3\sigma_I$), %	9.4	13.0
residuals R, R_w,[b] %	3.9, 3.6	4.9, 4.7
goodness of fit	1.44	1.19
Largest peaks in final ΔF map, e/Å^3	+1.9 (0.5 Å from Rb2) -2.8	+3.9 (0.21 Å from Rb2) -3.1
Secondary Ext. Coef.	2.75(6) x 10^{-6}	0.7(1) x 10^{-6}

[a]Guinier data with Si as an internal standard, λ = 1.540562 Å, 23° C.
[b]$R = \Sigma||F_o|-|F_c||/\Sigma|F_o|$; $R_w = [\Sigma\omega(|F_o|-|F_c|)^2/\Sigma\omega(F_o)^2]^{1/2}$, $\omega = 1/\sigma^2$

Table 4: Selected Bond Distances in $RbGa_{3-x}Au_x$ reactions (d ≤ 4.0 Å).

			$RbGa_3$[a]	$RbGa_{2.74(1)}Au_{0.26(1)}$	$RbGa_{2.64(2)}Au_{0.36(2)}$
Ga1–	Ga1[b]		2.612(9)	2.574(4)	2.583(5)
	Ga2		2.609(5)	2.650(2)	2.643(3)
	Ga1	2x	2.741(6)	2.731(3)	2.722(4)
	Ga2	2x	2.806(4)	2.782(2)	2.781(3)
	Rb1		3.590(3)	3.640(2)	3.645(2)
	Rb2	2x	3.702(3)	3.644(2)	3.640(2)
Ga2–	Ga2		2.442(8)	2.583(5)	2.632(6)
	Ga3		2.528(4)	2.510(2)	2.500(3)
	Ga1		2.609(5)	2.650(1)	2.643(2)
	Ga1	2x	2.806(4)	2.782(2)	2.781(3)
	Rb2	2x	3.716(2)	3.602(1)	3.582(2)
	Rb1	2x	3.755(2)	3.783(1)	3.795(2)
	Rb2		3.749(5)	3.947(3)	3.977(3)
Ga3–	Ga2	4x	2.528(4)	2.510(2)	2.500(3)
	Rb2	4x	3.695(2)	3.687(1)	3.687(2)
Rb1–	Ga1	4x	3.590(3)	3.640(2)	3.645(2)
	Rb2	4x	3.695(2)	3.687(1)	3.687(2)
	Ga2	8x	3.755(2)	3.783(1)	3.795(2)
Rb2–	Ga2	4x	3.716(2)	3.602(1)	3.582(2)
	Ga1	4x	3.702(3)	3.644(2)	3.640(2)
	Ga3	2x	3.695(2)	3.687(1)	3.687(2)
	Rb1	2x	3.695(2)	3.687(1)	3.687(2)
	Rb2		3.660(9)	3.754(4)	3.759(2)
	Ga2		3.749(5)	3.947(3)	3.977(3)

[a] From reference 8.
[b] exo-bond.

Table 5: Lattice parameters[a] of some $RbGa_{3-x}Au_x$ Products.

Loaded Composition	*a* (Å)	*c* (Å)	V (Å^3)
$RbGa_3$	6.3221(4)	15.007(2)	599.82(8)
$RbGa_{2.9}Au_{0.1}$	6.283(7)	15.17(1)	598.9(6)
$RbGa_{2.8}Au_{0.2}$	6.254(2)	15.29(1)	598.2(6)
$RbGa_{2.7}Au_{0.3}$	6.261(4)	15.304(9)	599.9(6)
$RbGa_{2.64}Au_{0.36}$[b]	6.205(1)	15.478(6)	595.9(3)
$RbGa_{2.6}Au_{0.4}$	6.202(1)	15.485(6)	595.6(3)
$RbGa_{2.5}Au_{0.5}$	6.200(2)	15.513(7)	595.6(3)
$Rb_{1.2}Ga_{2.33}Au_{0.67}$[b]	6.195(1)	15.515(4)	595.6(2)

[a]Guinier data with Si as an internal standard, λ = 1.540562 Å, 23° C.
[b]Source of data crystals. $RbGa_{2.74(1)}Au_{0.26(1)}$ and $RbGa_{2.64(2)}Au_{0.36(2)}$, respectively.

Table 6: Distances (Å) and average overlap populations for all Ga–Ga contacts (d ≤ 3 Å) in $RbGa_3$ and $RbGa_{2.64(2)}Au_{0.36(2)}$ ($RbGa_3$ model).

	$RbGa_3$		$RbGa_{2.64(2)}Au_{0.36(2)}$	
	d	Overlap pop.	d	Overlap pop.
Ga2–Ga2	2.441	0.814	2.632	0.499
Ga2–Ga3	2.528	0.781	2.500	0.775
Ga1–Ga2	2.609	0.568	2.643	0.483
Ga1–Ga1	2.612	0.753	2.583	0.674
Ga1–Ga1	2.742	0.404	2.722	0.403
Ga1–Ga2	2.806	0.339	2.781	0.389

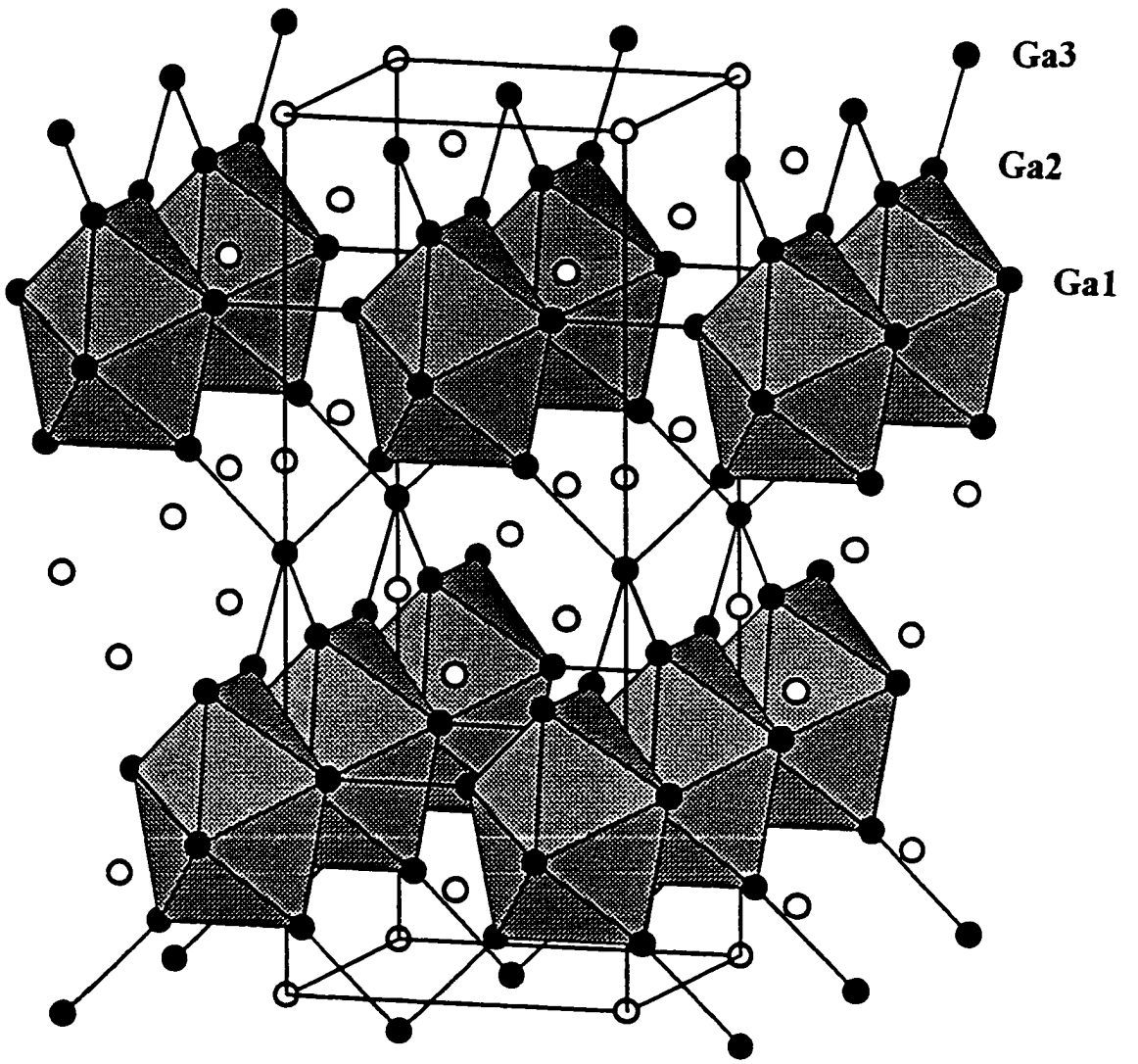

Figure 1. Unit cell of the tetragonal $RbGa_3$ and $RbGa_{3-x}Au_x$ structure *c*-axis vertical. Ga_8 dodecahedra (shaded clusters) form layers through exo-bond formation in the *a-b* plane. The layers are connected in along the *c*-axis through tetrahedrally coordinated Ga3 atoms. The open circles are rubidium atoms.

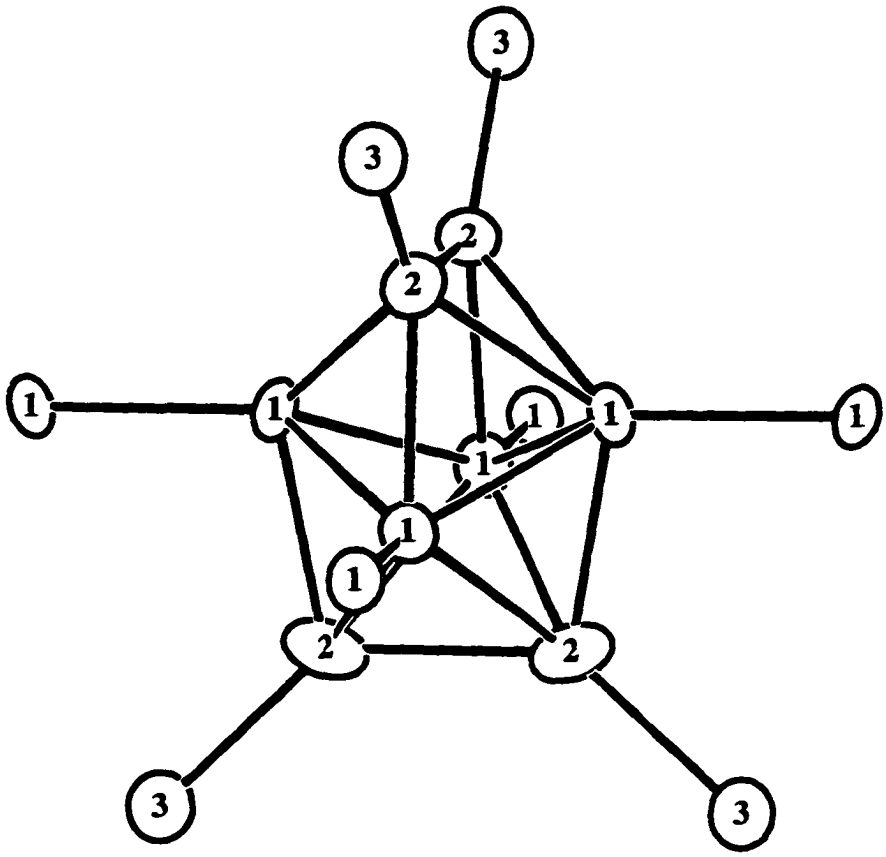

Figure 2. Ga_8^{2-} cluster with exo-bonds to adjacent gallium atoms (3) and clusters (1). Thermal ellipsoids drawn for the $RbGa_{2.64(1)}Au_{0.36(2)}$ (90%).

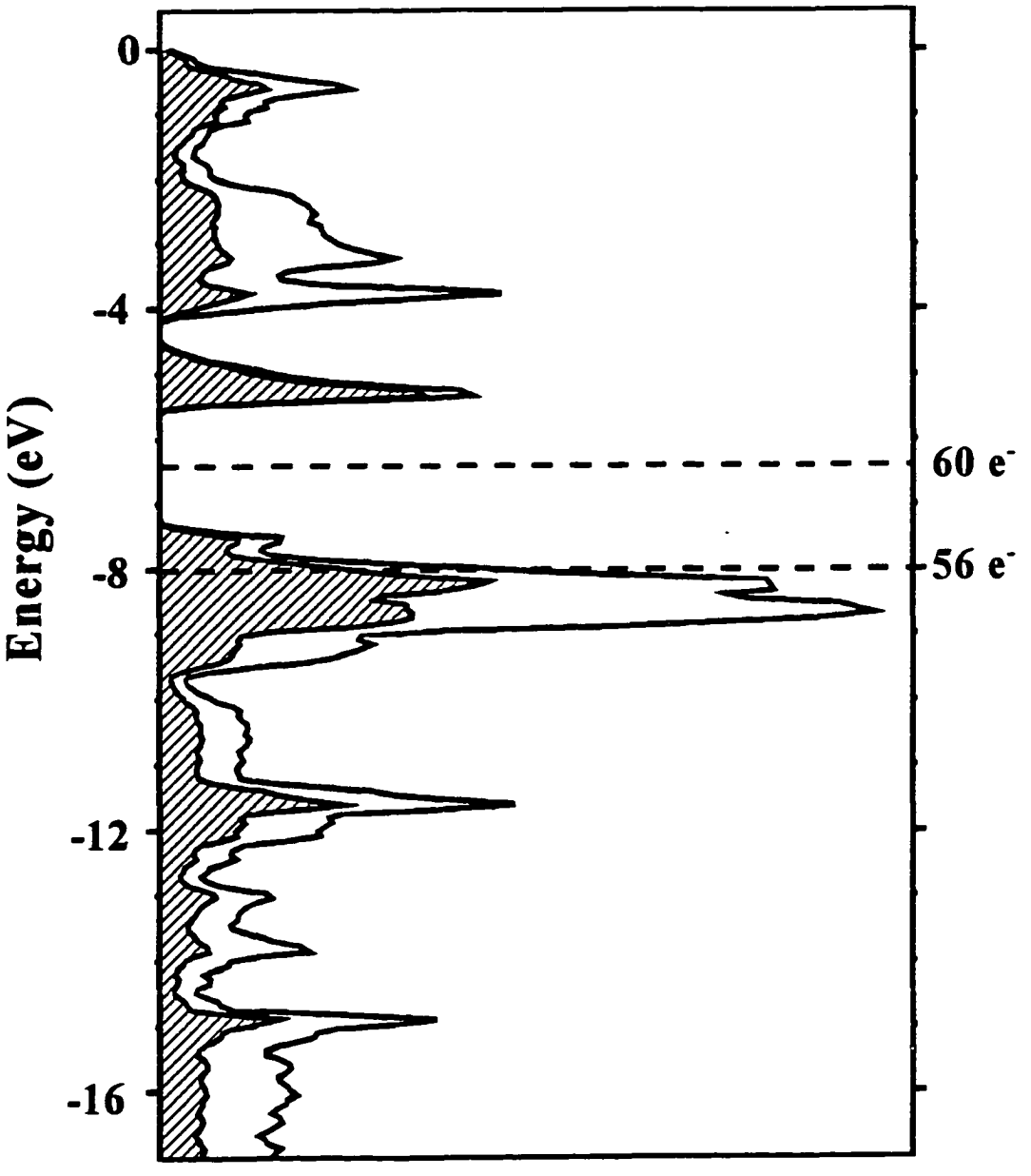

Figure 3. Ga2 contribution (shaded area) to the total DOS (solid line) for $RbGa_3$.

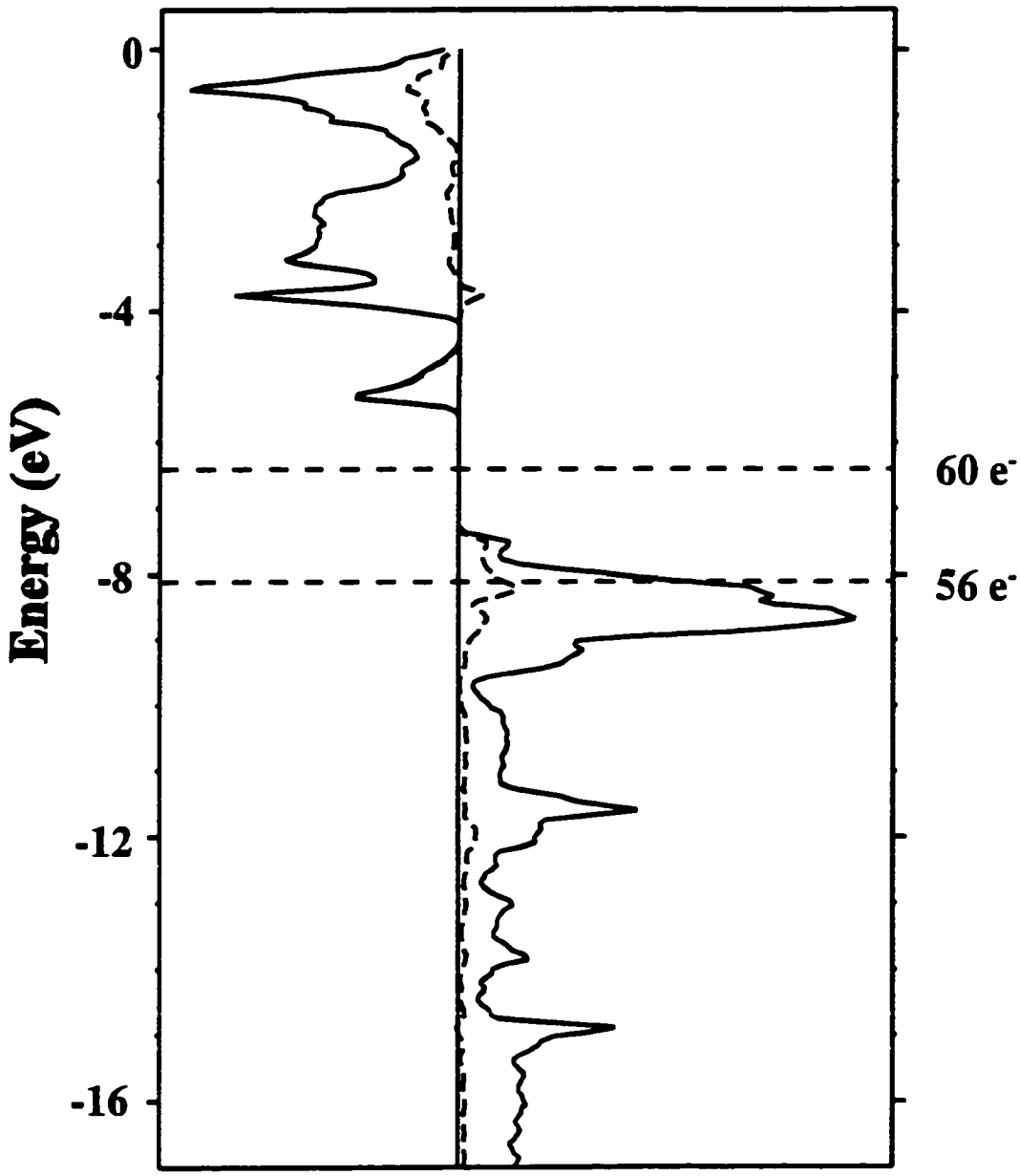

Figure 4. Ga2-Ga2 COOP curve (dashed line) and the total Ga–Ga COOP curve (solid line) for $RbGa_3$.

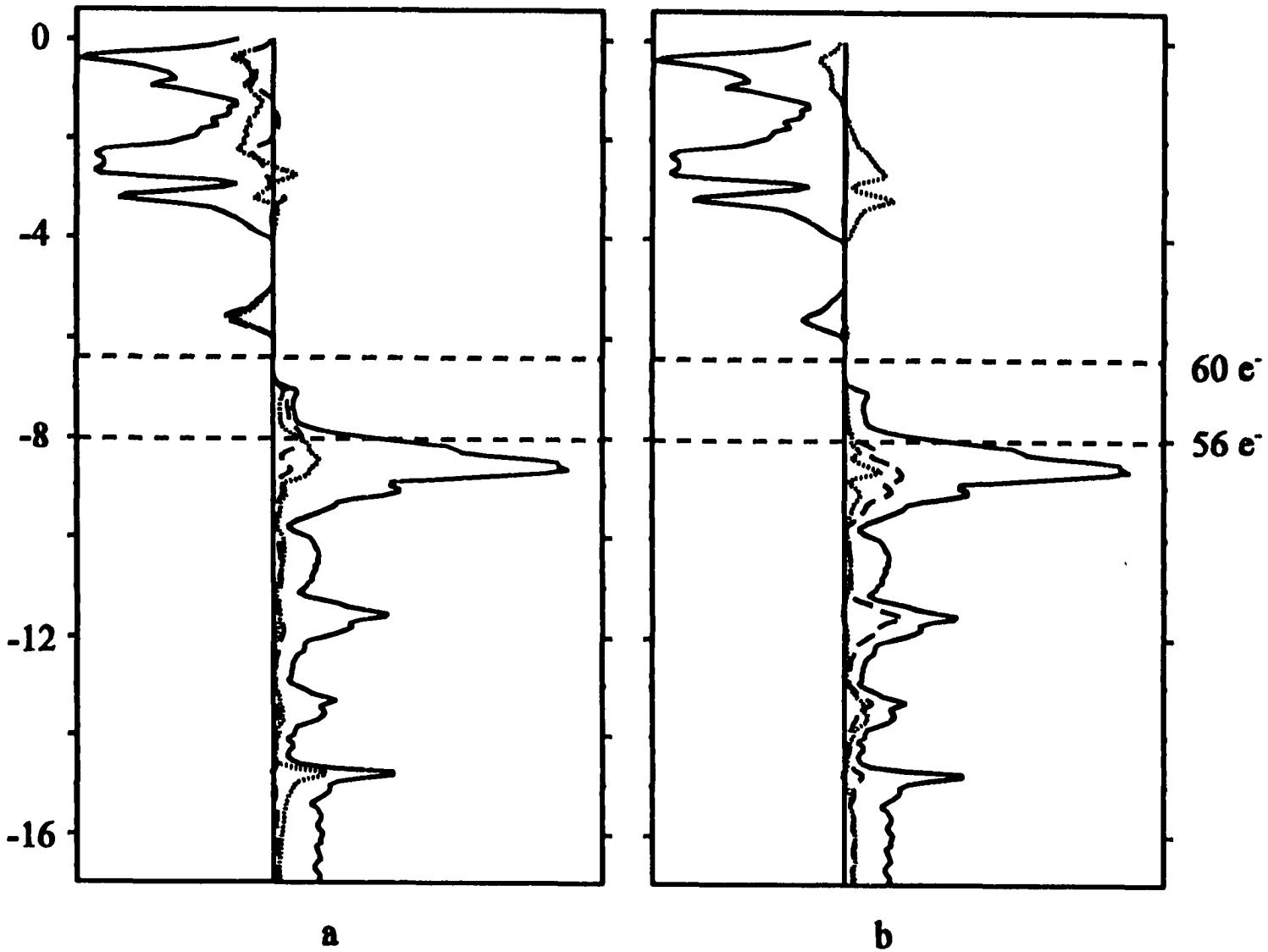

Figure 5. Ga2–Ga2 COOP (dashed line) and Ga1–Ga2 COOP (2.643(3) Å, dotted line) curves (a) and Ga2–Ga3 COOP (dashed line) and Ga1–Ga1 COOP (dotted line) curves (b) versus the total COOP curve (solid line) for $RbGa_{2.64(2)}Au_{0.36(2)}$ in each.

CONCLUSIONS

The alkali-metal–gallium systems display a large variety of structural chemistry ranging from isolated clusters to three-dimensional networks. Regular deltahedra are the most common type of cluster but several distorted clusters have been found as well. Nature balances atom size, cluster size, and electron count to form structures that not only fill space efficiently but usually form closed electronic shells at the same time. These compounds are frequently described as Zintl phases and provide a connection between intermetallic and valence structures.

One of the most significant aspects of this work was the discovery of isolated gallium clusters. Gallium typically forms exo-bonds to other clusters or to isolated atoms to alleviate the high formal charge on the cluster, but the high charge can be reduced if the cluster is distorted away from the regular deltahedral geometry. This was observed in Cs_8Ga_{11} and related phases which contain isolated penta-capped, trigonal prismatic gallium clusters. Another interesting aspect of the 8:11 compounds is the presence of a large hole and an extra electron. This combination allowed for the insertion of halogen atoms into the structure to form Zintl phases. A second type of isolated cluster was discovered in $Na_{10}Ga_{10}Ni$. Insertion of nickel into the center of the cluster stabilizes some of the gallium cluster orbitals. These two clusters are the only isolated clusters known in the alkali-metal–gallium systems.

Many of the phases reported in the literature have structures that appear to be closed shell electronically although in most cases this has not been confirmed experimentally. The binary systems (except Cs_8Ga_{11}) follow this trend, but when a late transition element is present in the structure the electron counting can become more difficult. The structures usually have

an electron count close to what is expected but in several cases it does not conform to a closed electronic shell. This should not be surprising since these materials have characteristics of both intermetallic and valence compounds. Some of these phases may exhibit nonstoichiometry, as in $Na_{30.5}Ga_{60-x}Ag_x$, although it is possible that one of the end members of the nonstoichiometric region is actually a Zintl phase. Nonstoichiometry has not always been checked when a new phase was discovered, but careful studies may reveal that this occurs more often than realized.

Attempted reactions, unresolved problems, and future work

Reports of new compounds in the alkali-metal–indium systems lead to the search for related structures with gallium. This led to the discovery of Cs_8Ga_{11} and $Na_{10}Ga_{10}Ni$ which are isostructural to K_8In_{11}[1] and $K_{10}In_{10}Ni$,[2] respectively. Attempts to prepare other compounds related to the indium structures were not as successful. $K_8In_{10}Zn$[3] can be obtained in high yield but reactions loaded as $Na_8Ga_{10}Zn$ or $K_8Ga_{10}Zn$ produced only the known binaries. Of particular interest was the attempt to prepare gallium analogs of the carbon-free fullerane compounds, $Na_{96}In_{97}Ni_2$ and $Na_{172}In_{197}Ni_2$.[4] The size of the cation is usually important in these systems so reactions with lithium, sodium, and potassium were tried. Again, only known compounds formed. Reactions with mixed cations also were unsuccessful. Mixed alkali-metal cations have proven very fruitful in the thallium system[5] but similar reactions with gallium only produce the known binaries.

$Na_{34}Ga_{105-x}Ag_x$ ($x \sim 14$, $R\bar{3}m$ (No. 166), $a = 16.424(1)$ and $c = 35.252(4)$ Å) forms in high yield (~90% with 10% Ag_3Ga) but good single crystals have been difficult to obtain.

This phase is isostructural to the previously reported $Na_{34}Ga_{93}Cu_{12}$[6] and $Na_{34}Ga_{81}Zn_{24}$.[7] The three-dimensional structure is composed of regular icosahedra, six coordinate gallium, and a cluster formed by the fusion of three icosahedra with silver substituting gallium at various positions. An unidentified phase also forms during the formation of the $RbGa_{3-x}Au_x$ compounds when excess gold ($x > 0.5$) is present, but this is probably just a new Ga–Au binary compound.

The alkali-metal–gallium systems have been explored in great detail through this project and others, so additional research was performed in the related indium systems. Even though many new compounds have been reported in indium system, several more phases have been identified by powder patterns but could not be sufficiently characterized. Attempts to find single crystals suitable for single crystal studies have been unsuccessful. Compounds believed to contain the $In_{10}Ni^{10-}$ cluster with a mixture of sodium and potassium cations exist as at least three new phases, none of which is isostructural with $K_{10}In_{10}Ni$. The Na–In–Pt system also has a new phase with an approximate composition of $Na_{10}In_{10}Pt$, but single crystals have not been obtained. A compound with approximate composition of $Rb_9In_{17}Au_5$ has been identified and single crystals have been obtained, but the structure refinement is not complete.

A large amount of research is still possible in the alkali-metal–indium systems but the problem of growing suitable crystals may be difficult to overcome for some of these phases. The next step for the gallium and indium systems may be to proceed to quaternary compounds but this will add complexity to the already difficult problem of characterizing these materials. Several of the binary compounds appear to be quite stable and the formation of these phases

would have to be suppressed some how. The K–Ga system, for example, forms K_2Ga_3 quite readily and every K–Ga–X reaction that has been loaded in this system produces at least a small amount of K_2Ga_3.

This work has not only expanded the range of known Zintl phases but has also contributed to our understanding of the structure/property relationships in the alkali-metal–gallium systems. The gap between intermetallic and valence compounds is slowly being bridged. The alkali-metal–group 13 compounds demonstrate a wide variety of structural chemistry, and continued exploration of this area of the periodic table will probably expand this range even further.

References

(1) Sevov, S. C.; Corbett, J. D. *Inorg. Chem.* **1991**, *30*, 4875.

(2) Sevov, S. C.; Corbett, J. D. *J. Am. Chem. Soc.* **1993**, *115*, 9089.

(3) Sevov, S. C.; Corbett, J. D. *Inorg. Chem.* **1993**, *32*, 1059.

(4) a. Sevov, S. C.; Corbett, J. D. *Science* **1993**, *262*, 880. b. Sevov, S. C.; Corbett, J. D. *Solid State Chem.* **1996**, *123*, 344.

(5) a. Dong, Z. C.; Corbett, J. D. *J. Am. Chem. Soc.* **1994**, *116*, 3429. b. Dong, Z. C.; Corbett, J. D. *J. Am. Chem. Soc.* **1995**, *117*, 6447. c. Dong, Z. C.; Corbett, J. D. *Inorg. Chem.* **1996**, *35*, 3107.

(6) Tillard-Charbonnel, M.; Chouaibi, N.; Belin, C. *J. Solid State. Chem.* **1992**, *100*, 220.

(7) Tillard-Charbonnel, M.; Chouaibi, N.; Belin, C. C. R. Acad. Sci. Paris, Série II, **1992**, *315*, 661.

APPENDIX

A NEW BINARY COMPOUND IN THE POTASSIUM–INDIUM SYSTEM. A PARTIAL SOLUTION.

Robert W. Henning and John D. Corbett*

Introduction

The phase diagram for the binary potassium–indium system has been investigated previously by thermal analysis, and two phases were shown to be present. These were later identified as KIn_4[1] and $K_{22.33}In_{39.67}$.[2] Both of these compounds contain extended network structures which is common for this system. The former is isostructural to $BaAl_4$[3] and the latter is related to $Na_{22}Ga_{39}$.[4] In 1991, Sevov and Corbett found K_8In_{11}[5] which contains a unique isolated cluster, In_{11}^{7-}, but the most recent compound to be reported in the binary system is $K_{17}In_{41}$.[6,7] This compound has a large cubic unit cell composed of indium icosahedra and indium-centered In_{16} deltahedra.

Further exploration of the potassium–indium binary system has led to the discovery of a new compound with the approximate stoichiometry of KIn. This composition is based on loaded stoichiometries and yields because the complete crystal structure has not been solved. The compound has been prepared directly from the elements and the partial structure determined by single crystal x-ray diffraction (*Imma* (No. 74), a = 17.445(8), b = 17.444(4), and c = 24.658(6) Å). The three-dimensional structure contains well defined indium

icosahedra that form exo-bonds to adjacent icosahedra. The potassium atoms coordinate the surface of the clusters at typical bond distances. Although the basic framework appears to be well defined, a large peak of electron density appears in the Fourier electron density map which is not reasonable for either potassium or indium. A second unusual characteristic of this structure is that it has a large hole (radius ~6.6 Å) which is uncommon for these materials. The alkali-metal–group 13 compounds typically form efficiently packed structures.

The characterization of this compound is not complete. In particular, the space group assignment is probably incorrect, but the proper symmetry could not be determined. This appendix describes what is known about the synthesis, characterization, and the crystallographic problems of "KIn" for future reference of others seeking to finish the structural characterization.

Experimental Section

All materials were handled in a nitrogen-filled dry box due to the air sensitive nature of the starting materials and products. A 1:1 ratio of elemental potassium (99.95%, Alfa) and indium (99.99%, Cerac) were sealed into welded tantalum tubing which was used as the reaction vessel. The tantalum was then sealed into an evacuated fused silica jacket to protect it from oxidation during the reaction cycle. The samples were heated to 600 °C for 1 hour and quenched in water. Annealing at 150 °C for 1 month or more produced the highest yields (~100%) according to Guinier powder patterns with no excess potassium in the sample. Products that were pure "KIn" according to Guinier powder patterns always occurred as dark grey powders. If other binaries (KIn_4, $K_{17}In_{41}$, $K_{22.33}In_{39.67}$, or K_8In_{11}) were present in the

powder pattern then the sample contained shiny, brittle particles. Greater amounts of potassium also generated the desired phase but the excess potassium was visible in the samples. Reactions loaded with lower potassium content generated the other binary phases depending on the loaded stoichiometry. Even though the well refined atoms give a composition of $K_{17}In_{24}$ (41.5% K, discussed later), reactions loaded near this stoichiometry formed $K_{22.33}In_{39.67}$ (36.0% K) and K_8In_{11} (42.1% K). Reactions loaded as K_8In_{11} produced mainly the 8:11 phase but "KIn" did form in ~10% yield. The phase can only be prepared in high yield from reactions loaded with greater amounts of potassium such as KIn (50% K). Annealing the sample at temperatures greater than 150 °C yielded mainly the other well established compounds but slow cooling from the melt produced some (20%) of the new product. Rough melting point determinations indicated that the sample melted (or decomposed) between 150 and 200 °C.

Single crystal x-ray data collections have been performed on several crystals from different reactions, but all of them generated the same structural problems. The highest quality crystals came from reactions loaded with an excess of potassium (K_2In) and annealed at 150 °C for three months so these will be discussed more thoroughly. Crystallites were sealed into 0.3 mm thin-walled capillary tubes and checked for singularity by Laue photographs. A crystal suitable for single crystal x-ray analysis was selected for data collection on a Enraf-Nonius CAD4 four-circle diffractometer with the aid of Mo Kα radiation. Twenty-five reflections were collected at random over a range of 2θ and centered. Omega-theta scans of each reflection indicated the peaks were well defined with no sign of splitting. All 25 reflections could be indexed to three different unit cells; F-cubic (a = 24.63

Å, V = 14,946 Å^3), I-orthorhombic (a = 17.42 Å, c = 24.63 Å, V = 7474 Å^3), and C-monoclinic (a = 30.10 Å, b = 17.42 Å, c = 17.42 Å, β = 125.25°, V = 7476 Å^3). The standard deviations for the lattice parameters were within the expected range. Axial photographs taken on the diffractometer for each of the possible settings did not indicate problems with any of the cell choices. Indexing only the weaker reflections also suggested these three unit cells. Weissenburg photographs of the hk0, hk1, and hk2 layers were taken previously and suggested that the orthorhombic setting was correct. Mirror planes, an a-glide along c, and the body-centering condition were also confirmed. Since no violations of the orthorhombic symmetry could be detected, and the cubic symmetry could not be confirmed from the film data, the orthorhombic setting was chosen for the data collection. Two octants of data ($-h$, k, $\pm l$) were collected at room temperature up to 55° in 2θ. The I-centering condition was confirmed by collecting on the primitive cell for the first 1500 reflections. The remainder of the data collection had the I-centering condition imposed. Absorption corrections were applied with the aid of six ψ-scans which were collected at different 2θ angles. The data were also corrected for Lorentz and polarization effects.

Systematic absences and the N(Z) distribution strongly suggested the centrosymmetric space group *Imma* (no. 74) but the acentric space group *Ima*2 (no. 46) was also possible. *Imma* was chosen for the initial refinement but the acentric space group and other lower symmetry settings (with the same unit cell) also gave the same difficulties (discussed later) observed in the higher symmetry setting. The starting model, obtained through direct methods,[8] produced eight peaks which had contacts consistent with In–In bond distances and seven appropriate for potassium atoms. These peaks were inserted into the starting model and

the positional and isotropic thermal parameters were refined to convergence (R_F = 14.5 %). A Fourier difference electron density calculation produced two large peaks (~40 $e^-/Å^3$) whereas the rest of the map was relatively flat (~5 $e^-/Å^3$). The size and location of the extra peaks did not correspond to typical indium or potassium positions. Each peak was located near an inversion center so a symmetry equivalent position was ~2.5 Å away. This is too close for In–In (~3.0 Å), In–K (~3.5 Å), or K–K (~4.0 Å) contacts. All other atoms surrounding these positions were potassium ~4.0 Å away. Averaging the data (R_{avg} ($I \geq 3\sigma_I$) = 3.3 %) reduced the R_F to 14.1 % but did not change the Fourier map. Anisotropic refinement of all positions improved the R_f (14.0%) only marginally. The same extra peaks appeared in a Fourier difference density map. Refinement in other space groups (*Im*2*a*, *Iba*2, , *Ibam*, *Ibca*, *I*222, $I2_12_12_1$, $P2_12_12_1$, *C*2/*m*, *Cm*, *C*2, *P*2/*m*, *Pm*, *P*2, *P*1) produced the same problem. Since the approximate stoichiometry is KIn and the refined composition of the well defined atoms is $K_{17}In_{24}$, the extra peaks (labeled K8 and K9) were treated as fully occupied potassium atoms even though the contact between them was too short to be reasonable. This reduced the R_F to 7.3% and gave a final composition of $K_{21}In_{24}$ (46.7% K). After placing the extra peaks (K8 and K9) into the refinement, the largest positive and negative peaks in the difference map were 7.0 $e^-/Å^3$ (0.52 Å from K9) and -2.5 $e^-/Å^{-3}$. All structure refinements were carried out with the TEXSAN package on a VAX station.[9]

Since the crystal structure for this compound has been difficult to solve, several data sets have been collected on different crystals and for each of the three unit cells. A data set was even collected for the C-monclinic setting but the refinement produced the same effective structure with similar *R*-factors, thermal parameters, and extra peaks as the higher symmetry

cells. Attempts to determine the appropriate symmetry through indexed Guinier powder patterns could not distinguish between the different unit cells. The standard deviations obtained from the least squares refinements for all three settings indicated that all of them were reasonable and no violations were observed.

It is possible that the crystals could be twinned so several models were attempted with the use of the Shelx93 package. Inversion twinning was suspected since the extra peaks (K8 and K9) and their symmetry equivalent positions are related by an inversion center, but all refinements failed to resolve the structural problem. Reflection and rotation twinning models also failed. If the crystal is twinned then this could be confirmed by investigations with a transmission electron microscope.

The data collection parameters, atomic positions, and anisotropic thermal data are listed in Tables 1, 2, and 3, respectively. Bond distance data are listed in Table 4.

Results and Discussion

Even though the structure could not be completely characterized, the basic framework is well defined and is believed to be substantially correct. The predominate structural feature of "KIn" is indium icosahedra linked through intercluster bonds to form a three-dimensional network (Figure 1 and 2). The clusters have the same arrangement as Cu in the $MgCu_2$ structure type but the corresponding Mg position is an open void with a radius of ~4.1 Å to the extra peaks (4x) and ~6.6 Å to the potassium atoms (24x). Two types of icosahedral clusters occur in a 1:1 ratio but both have 2/m symmetry. Each cluster has six exo-bonds to adjacent icosahedra with the remaining vertices on the cluster pointing towards the void

(Figure 3). Bonding between the clusters occurs through the In1–In1, In2–In3, and In4–In4 bonds (d = 3.082(7)–3.086(7) Å). In5, In6, In7, and In8 do not form exo-bonds to adjacent clusters. The In–In contacts within the cluster range from 3.004(5)–3.233(3) Å. The potassium atoms coordinate the triangular faces of the cluster with distances between 3.543(7)–3.83(1) Å. The thermal parameters for the first three potassium atoms are normal (~2) because they coordinate the triangular faces on either three or four clusters. The other potassium atoms coordinate only two clusters with one side open to the void, and these atoms have larger thermal parameters. All contacts between the atoms (except the extra peaks K8 and K9) are at distances that are typical for these systems.

Two large peaks (labeled K8 and K9) appear in the electron density map and are difficult to interpret. Both are located near the inversion centers (0, 0, 0.5 and 0.25, 0.25, 0.25) and have symmetry equivalent positions ~2.5 Å away (Figure 4). They are surrounded by six potassium atoms at ~4.1 Å with all of these potassium atoms on one side of the peak. A plot of the F_{obs} electron density map (Figure 5) shows a large peak at the K8 position. The 0, 0, 0.5 position is at the center of the map with the c-axis vertical and the b-axis horizontal. The symmetry equivalent peak (~2.5 Å away) is also present along with two potassium cations. The position labeled K9 has the same problems as K8. Electron density maps of this same position but in lower symmetry unit cells produce similar results. This position refines to 71% of an indium atom and could be modeled as an indium with 50% occupancy. This would take care of the short contact but the coordination environment is still not reasonable. Also, more potassium would be expected in the structure considering the loaded stoichiometry. Without the extra peaks in the refinement, the stoichiometry is $K_{17}In_{24}$ but if

the extra peaks were treated as potassium, the stoichiometry would be $K_{21}In_{24}$ (46.7% K). This is still unreasonable because of the short contact but is more consistent with the loaded composition. Reactions loaded at this composition and annealed for three months at 150 °C generated mainly K_8In_{11} (80%) but "KIn" did form in ~20% yield. This indicates that even more potassium is in the structure.

The coordination around this position is very unusual and indicates that something is wrong with the current structural solution. The symmetry of the indium positions and the potassium atoms are probably correct but the electron density in the hole can not be modeled. Refinements in other space groups were attempted but produced the same symmetry equivalent peaks as in the orthorhombic setting. Film data did not reveal any "extra" reflections that would suggest an alternate setting. The reflections associated with the unresolved electron density in the hole and the correct cell are probably very weak. The use of an area detector may be useful in determining the correct symmetry of the system.

The alkali-metal–triel compounds usually form structures that fill space very efficiently so this open framework is unusual. The A_8Tr_{11} compounds (A = K, Rb, and Cs; Tr = Ga,[10] In,[5] Tl[11], Chap. 1) also have a hole in the structure but this is comparably small (~3.5 Å). Since the loaded compositions suggest that more potassium is expected in the structure, the "voids" probably contain the extra alkali metal. It is not clear where the extra potassium would reside within this void considering that almost all contacts would be with other potassium atoms and that the hole is quite large. Although most of the missing structure is probably potassium, a small amount of indium may be present in the "voids" as well.

Related structures

The well defined atoms in "KIn" are closely related to the $K_{17}In_{41}$ and $Na_{17}Ga_{29}In_{12}$[12] structures. $K_{17}In_{41}$ has a large cubic unit cell (*Fd3m*, 24.241(5) Å vs. 24.618(6) Å for "KIn") but with the same icosahedral framework as "KIn". Even though "KIn" has been refined in an orthorhombic setting, it can be refined with a face-centered cubic setting with approximately the same cell parameters (24.658(6) Å) as $K_{17}In_{41}$. This was first evident in the unit cell choices proposed at the beginning of the data collection. Both compounds have the same icosahedral framework and potassium atom coordination around the cluster. The main difference is that the voids in "KIn" are filled with indium-centered, tetracapped truncated indium tetrahedra in $K_{17}In_{41}$ (Figure 6). These can also be described at indium-centered In_{16} icosioctahedron. This accounts for the additional 17 indium atoms in the formula unit for $K_{17}In_{41}$. $Na_{17}Ga_{29}In_{12}$ has the same symmetry as $K_{17}In_{41}$ but the icosahedra and part of the truncated tetrahedra has been replaced by gallium. An additional similarity exists between the extra peaks of electron density in "KIn" and the indium atom capping the hexagonal faces of the tetrahedral unit in $K_{17}In_{41}$. They are roughly in the same position except that in $K_{17}In_{41}$ the symmetry equivalent peaks are 3.7 Å apart. Since $K_{17}In_{41}$ and "KIn" have such similar structures, it might be possible that they are the same and that one of the refinements is incorrect but both of these compounds have been identified in Guinier powder patterns (Figure 7).

Conclusions

Although the characterization of "KIn" is not complete, some of the basic indium framework is believed to be correct. In addition, the potassium atoms coordinating the surface of the clusters also appear to be right. The difficulty in modeling the atoms within the voids lies in the inability to determine the proper symmetry of the crystal. The use of an area detector may help resolve some weak peaks that are present or it may also reveal some split peaks that were not evident in the film work. The possibility that the compound always forms twinned crystals has been investigated but a suitable twinning model could not be attained.

References

(1) Bruzzone, G. *Acta. Cryst.* **1969**, *25B*, 1206.

(2) Cordier, G.; Müller, V. *Z. Krist.* **1992**, *198*, 302.

(3) Andress, R. M.; Albertini, E. *Z. Metallk.* **1935**, *27*, 126.

(4) Ling, R. G.; Belin, C. *Acta Cryst.* **1982**, *B38*, 1101.

(5) Sevov, S. C.; Corbett, J. D. *Inorg. Chem.* **1991**, *30*, 4875.

(6) Cordier, G.; Müller, V. *Z. Krist.* **1993**, *205*, 353.

(7) Cordier, G.; Müller, V. *Z. Naturforsch.* **1994**, *49b*, 721.

(8) Sheldrick, G. M. SHELXS-86, Universität Göttingen, Germany, 1986.

(9) TEXSAN, version 6.0, Molecular Structure Corp., The Woodlands, Texas, 1990.

(10) Henning, R. W.; Corbett, J. D. *Inorg. Chem.* **1997**, *36*, 6039.

(11) Dong, Z. C.; Corbett, J. D. *J. Cluster Science*, **1995**, *6*, 187.

(12) Cordier, G.; Müller, V. *Z. Krist.* **1993**, *205*, 133.

Table 1: Data Collection and Refinement Parameters for "KIn"

Crystal size, mm	0.13 x 0.16 x 0.20
Space group, Z	*Imma* (No. 74), 4
Lattice parameters,[a]	
a, Å	17.445(8)
b, Å	17.444(4)
c, Å	24.658(6)
V, Å^3	7504(3)
d_{calc}, g/cm^3	3.027
Radiation; $2\theta_{max}$	Mo K_α; 55°
Scan method	ω
Temperature, °C	23
Transmission range	0.8188-1.0000
μ, cm^{-1} (Mo Kα)	80.577
Number of reflections:	
measured	9793
observed ($I \geq 3\sigma(I)$)	4971
unique observed ($I \geq 3\sigma(I)$)	2681
Number of variables	26
$R_{avg.}$ ($I \geq 3\sigma(I)$), %	3.6
Residuals *R*; R_w,[b] %	7.3; 11.4
Goodness of fit	3.425

[a]Guinier data with Si as an internal standard, λ = 1.540 562 Å, 23° C.

[b]$R = \Sigma||F_o|-|F_c||/\Sigma|F_o|$; $R_w = [\Sigma\omega(|F_o|-|F_c|)^2/\Sigma\omega(F_o)^2]^{1/2}$, $\omega = 1/\sigma_F^2$

Table 2: Positional and isotropic thermal parameters for "KIn"

Atoms	Wykoff	x	y	z	B
In1	8*i*	0.0883(2)	3/4	0.2579(1)	1.4(1)
In2	16*j*	0.1771(1)	0.6613(1)	0.16909(9)	1.3(1)
In3	16*j*	0.0886(1)	0.5729(1)	0.08066(9)	1.4(1)
In4	8*h*	0	0.6616(2)	-0.0079	1.4(1)
In5	8*h*	0	0.4246(2)	0.1134(1)	1.5(1)
In6	16*j*	0.1742(1)	0.5990(1)	0.2875(1)	1.4(1)
In7	8*i*	0.1746(2)	3/4	0.3635(1)	1.5(1)
In8	16*j*	0.1511(1)	0.4243(1)	0.0376(1)	1.5(1)
K1	8*h*	0	0.5659(8)	0.2174(5)	2.7(5)
K2	4*e*	0	3/4	0.1242(6)	1.5(6)
K3	8*i*	0.1853(7)	3/4	0.0323(5)	2.6(5)
K4	16*j*	0.1816(6)	0.4438(6)	0.1876(4)	3.9(5)
K5	8*h*	0	0.8735(9)	0.3691(6)	3.6(6)
K6	16*j*	0.3062(5)	0.5682(6)	0.0627(4)	3.7(4)
K7	8*i*	-0.124(1)	3/4	-0.1192(6)	4.0(7)
K8[a]	8*h*	0	0.0585(5)	0.4714(4)	0.7(1)
K9[a]	8*i*	0.3089(6)	1/4	0.2210(4)	0.7(1)

[a]Short contact between symmetry equivalent peaks for each position.

Table 3: Anisotropic thermal parameters for "KIn"

Atom	U11	U22	U33	U12	U13	U23
In1	0.015(2)	0.021(2)	0.017(2)	0	-0.001(1)	0
In2	0.014(1)	0.019(1)	0.018(1)	0.001(1)	-0.003(1)	-0.000(1)
In3	0.017(1)	0.017(1)	0.019(1)	0.000(1)	-0.001(1)	-0.002(1)
In4	0.022(2)	0.016(2)	0.017(2)	0	0	-0.001(1)
In5	0.018(2)	0.021(2)	0.018(2)	0	0	0.001
In6	0.017(1)	0.019(1)	0.019(1)	-0.001(1)	0.000(1)	0.000(1)
In7	0.019(2)	0.019(2)	0.019(1)	0	0.000(1)	0
In8	0.018(1)	0.019(1)	0.019(1)	0.002(1)	0.000(1)	0.001(1)
K1	0.019(6)	0.051(8)	0.032(6)	0	0	-0.009(6)
K2	0.021(8)	0.022(8)	0.014(7)	0	0	0
K3	0.039(7)	0.024(6)	0.036(7)	0	-0.008(6)	0
K4	0.065(7)	0.037(5)	0.047(6)	-0.007(5)	-0.024(5)	-0.004(4)
K5	0.030(7)	0.06(1)	0.050(8)	0	0	-0.009(7)
K6	0.035(5)	0.059(6)	0.046(5)	-0.003(5)	0.000(4)	-0.016(5)
K7	0.06(1)	0.038(8)	0.053(9)	0	-0.014(8)	0
K8[a]	0.009(2)					
K9[a]	0.009(2)					

[a]Short contact between symmetry equivalent peaks for each position.

Table 4: Bond Distances in "KIn" (d < 4.2 Å)

In1–	In7		3.009(5)	In6–	In2		3.010(3)	K4–	In6		3.66(1)
	In1		3.082(7)		In1		3.117(3)		In5		3.67(1)
	In2	2x	3.096(4)		In2		3.117(3)		In8		3.75(1)
	In6	2x	3.117(3)		In6		3.229(5)		In2		3.82(1)
	K2		3.64(1)		In7		3.233(3)		In3		3.83(1)
	K1	2x	3.70(1)		K1		3.543(7)		K1		3.89(1)
	K5	2x	3.81(1)		K4		3.66(1)		K4		3.89(2)
					K5		3.676(9)		K7		3.92(1)
In2–	In6		3.010(3)		K4		3.75(1)		K9	2x	4.07(1)
	In3		3.085(3)		K6		3.75(1)		K9	2x	4.13(1)
	In2		3.094(5)								
	In1		3.096(4)	In7–	In1		3.009(5)	K5–	In6	2x	3.676(9)
	In6		3.117(3)		In2	2x	3.120(4)		In7	2x	3.733(9)
	In7		3.120(4)		In6	2x	3.233(3)		In1	2x	3.81(1)
	K2		3.628(5)		K3		3.55(1)		K1		3.89(1)
	K1		3.706(8)		K5	2x	3.733(9)		K6	2x	3.91(1)
	K3		3.71(1)		K6	2x	3.67(1)		K8	2x	4.10(2)
	K4		3.82(1)						K8	2x	4.11(2)
	K6		3.82(1)	In8–	In3		3.006(3)				
					In3		3.114(3)	K6–	In7		3.67(1)
In3–	In8		3.006(3)		In4		3.118(3)		In8		3.67(1)
	In2		3.085(3)		In8		3.228(5)		In8		3.74(1)
	In4		3.090(4)		In5		3.230(3)		In2		3.82(1)
	In3		3.091(5)		K3		3.545(7)		In3		3.82(1)
	In8		3.114(3)		K6		3.67(1)		K3		3.88(1)
	In5		3.119(4)		K7		3.670(9)		K6		3.90(2)
	K2		3.618(5)		K6		3.74(1)		K5		3.91(1)
	K1		3.71(1)		K4		3.75(1)		K8	2x	4.06(1)
	K3		3.716(8)						K8	2x	4.13(3)
	K6		3.82(1)	K1–	In6	2x	3.543(7)				
	K4		3.83(1)		In5		3.56(1)	K7–	In8	2x	3.670(9)
					In1	2x	3.70(1)		In5	2x	3.74(1)
In4–	In5		3.004(5)		In2	2x	3.706(8)		In4	2x	3.81(1)
	In4		3.086(7)		In3	2x	3.71(1)		K3		3.88(2)
	In3	2x	3.090(4)		K4	2x	3.89(1)		K4	2x	3.92(1)
	In8	2x	3.118(3)		K5		3.89(2)		K9		4.10(2)
	K2		3.60(1)		K2		3.95(2)		K9		4.12(2)
	K3	2x	3.72(1)								
	K7	2x	3.81(1)	K2–	In4	2x	3.60(1)	K8–	K8		2.48(2)
					In3	4x	3.618(5)		K6	2x	4.06(1)
In5–	In4		3.004(5)		In2	4x	3.628(5)		K5		4.10(2)
	In3	2x	3.119(4)		In1	2x	3.64(1)		K5		4.11(2)
	In8	2x	3.230(3)		K1	2x	3.95(2)		K6	2x	4.13(1)
	K1		3.56(1)		K3	2x	3.95(2)				
	K4	2x	3.67(1)					K9–	K9		2.50(2)
	K7	2x	3.74(1)	K3–	In8	2x	3.545(7)		K4	2x	4.07(1)
					In7		3.55(1)		K7		4.10(2)
					In4	2x	3.60(1)		K7		4.12(2)
					In2	2x	3.71(1)		K4	2x	4.13(1)
					In3	2x	3.716(8)				
					K6	2x	3.88(1)				
					K7		3.88(2)				
					K2		3.95(2)				

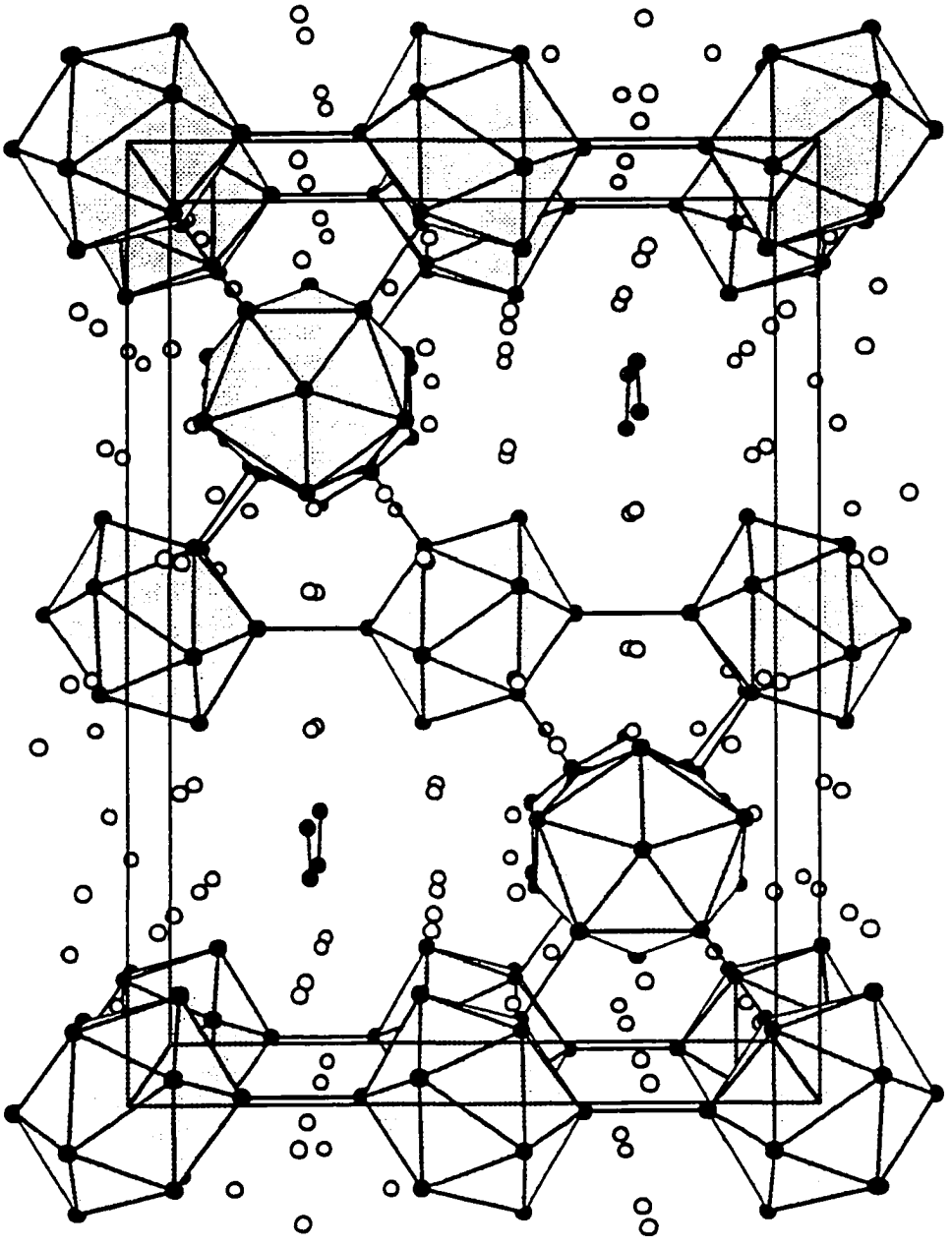

Figure 1. View down [100] of "KIn" with *c*-axis vertical. Shaded polyhedra are In_{12} clusters and open circles are potassium atoms. Black dimers represent the K8 and K9 peaks of extra electron density.

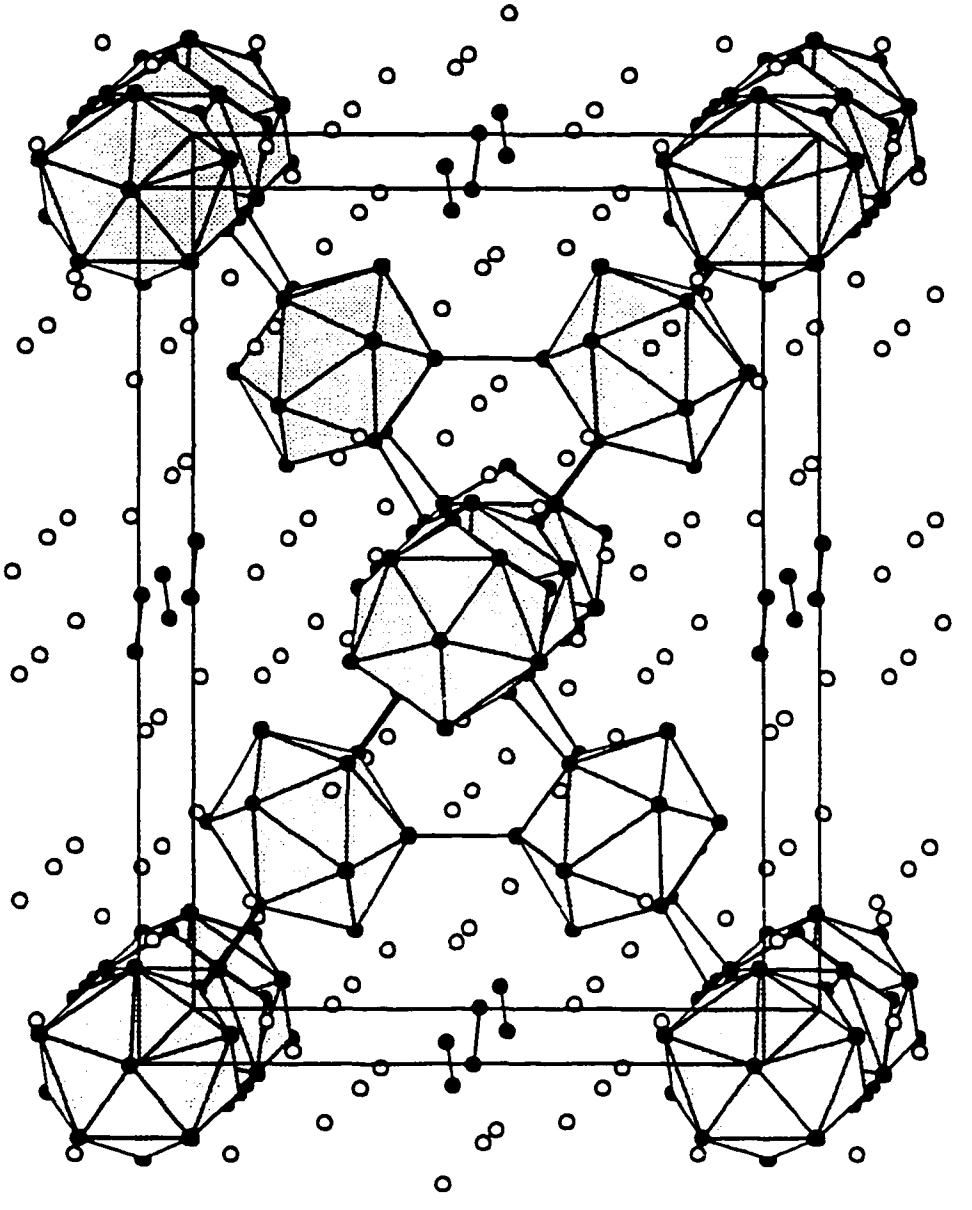

Figure 2. View down [010] of "KIn" with *c*-axis vertical. Shaded polyhedra are In_{12} clusters and open circles are potassium atoms. Black dimers represent the K8 and K9 peaks of extra electron density.

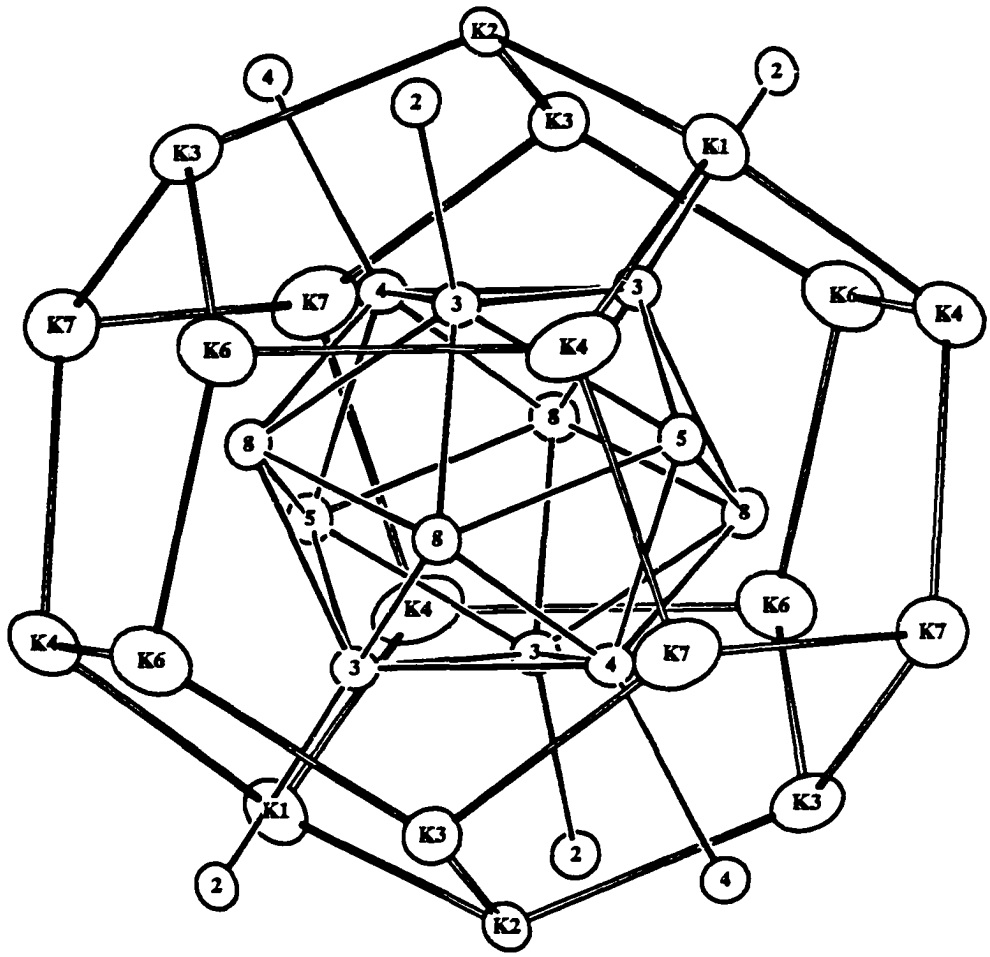

Figure 3. One of the In_{12} icosahedra with the six exo-bonds to adjacent clusters. Potassium atoms coordinate the triangular faces of the cluster and form a pentagonal dodecahedron. Thermal ellipsoids drawn at 75% probability.

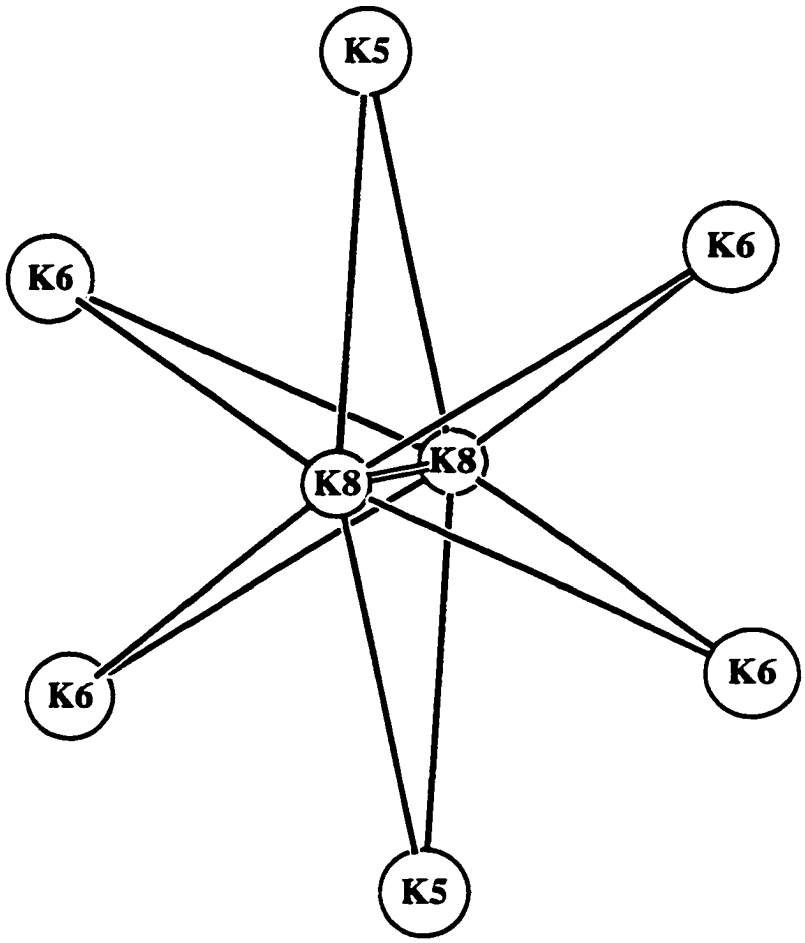

Figure 4. Extra peak of electron density (labeled K8) in "KIn" refinement. K8–K8 distance (~2.5 Å) is unreasonable for either a potassium or indium atom and the coordination environment is also unusual. All six potassium atoms are on one side of the peak and the open void is on the other side. The distance between the potassium atoms and the extra peak is ~4.1 Å.

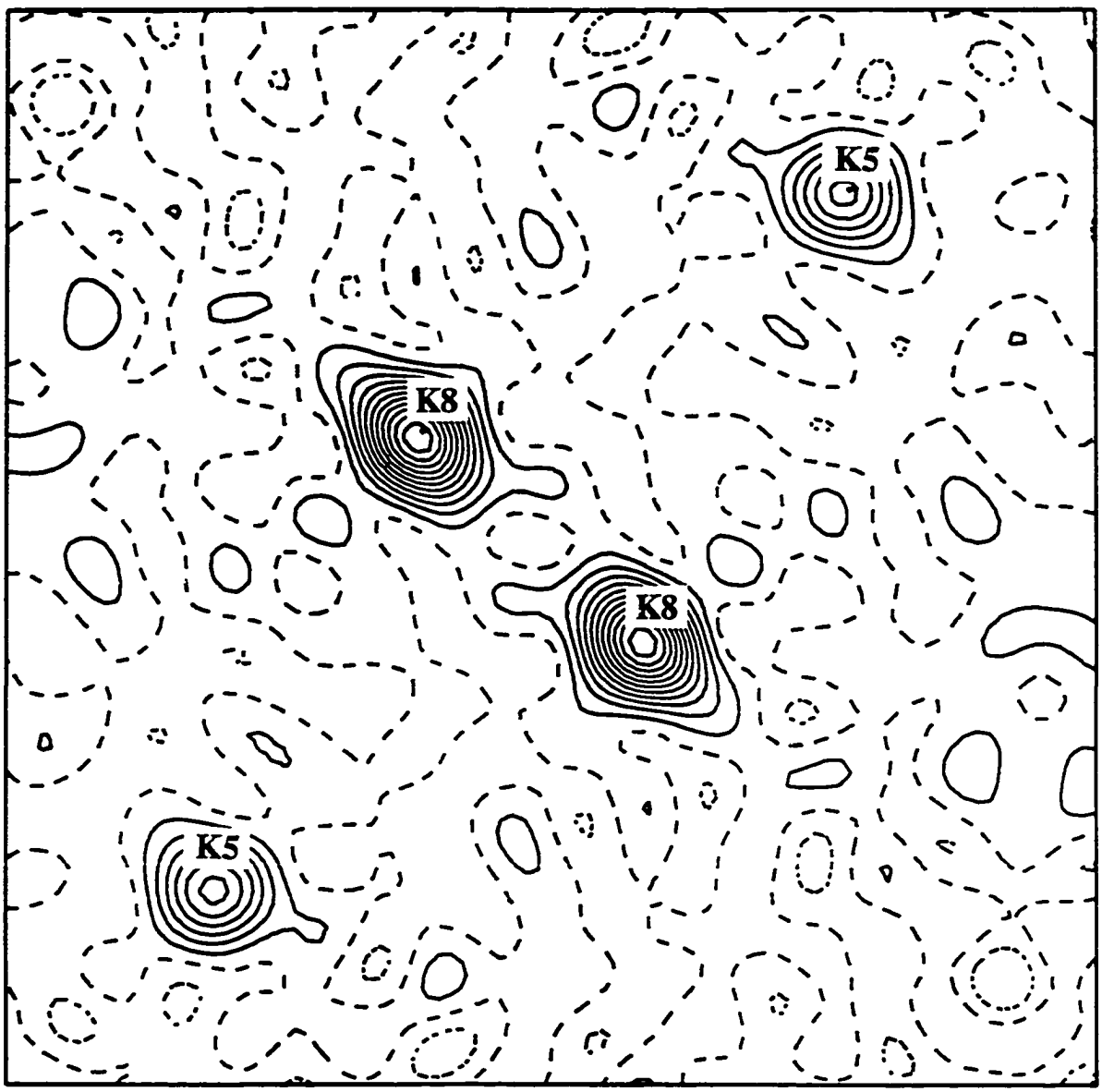

Figure 5. Electron density plot ($F_{obs.}$) of the K8 position in "KIn". The c-axis is vertical and the b-axis is horizontal. Each contour line represents 3 electrons.

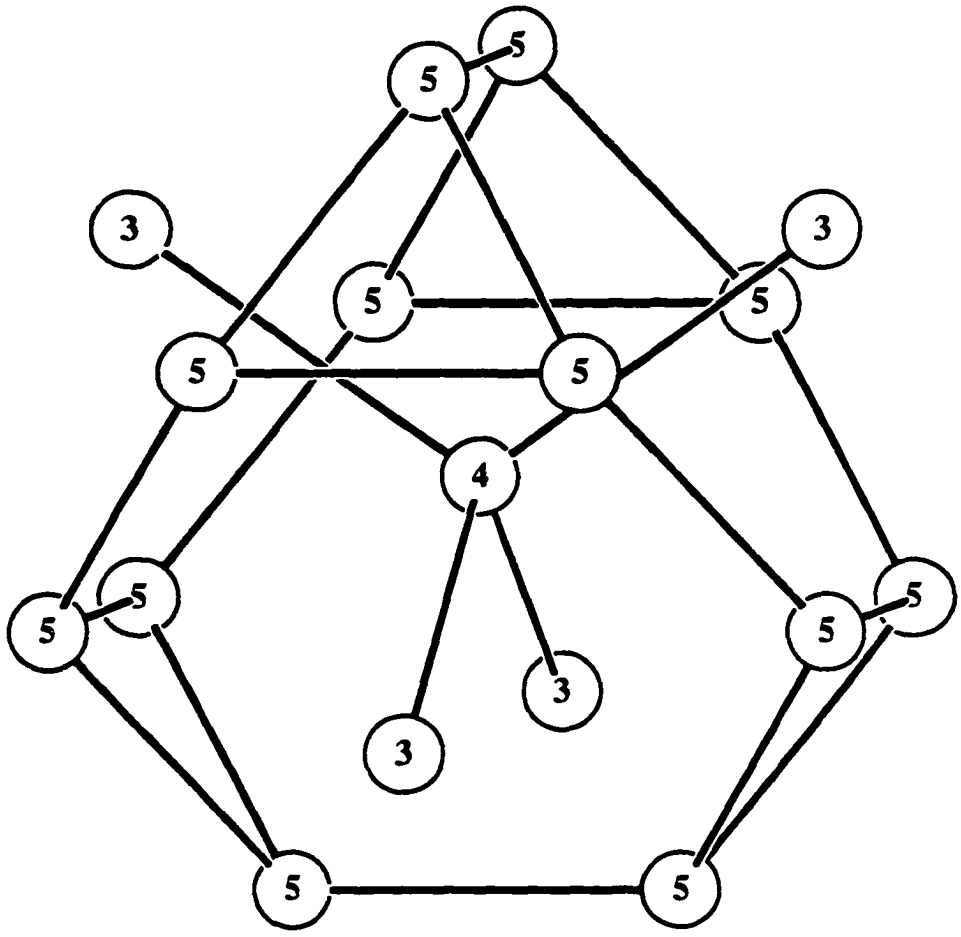

Figure 6. Truncated tetrahedron (In5) in $K_{17}In_{41}$. In4 centers the clusters and In3 caps each of the hexagonal faces.

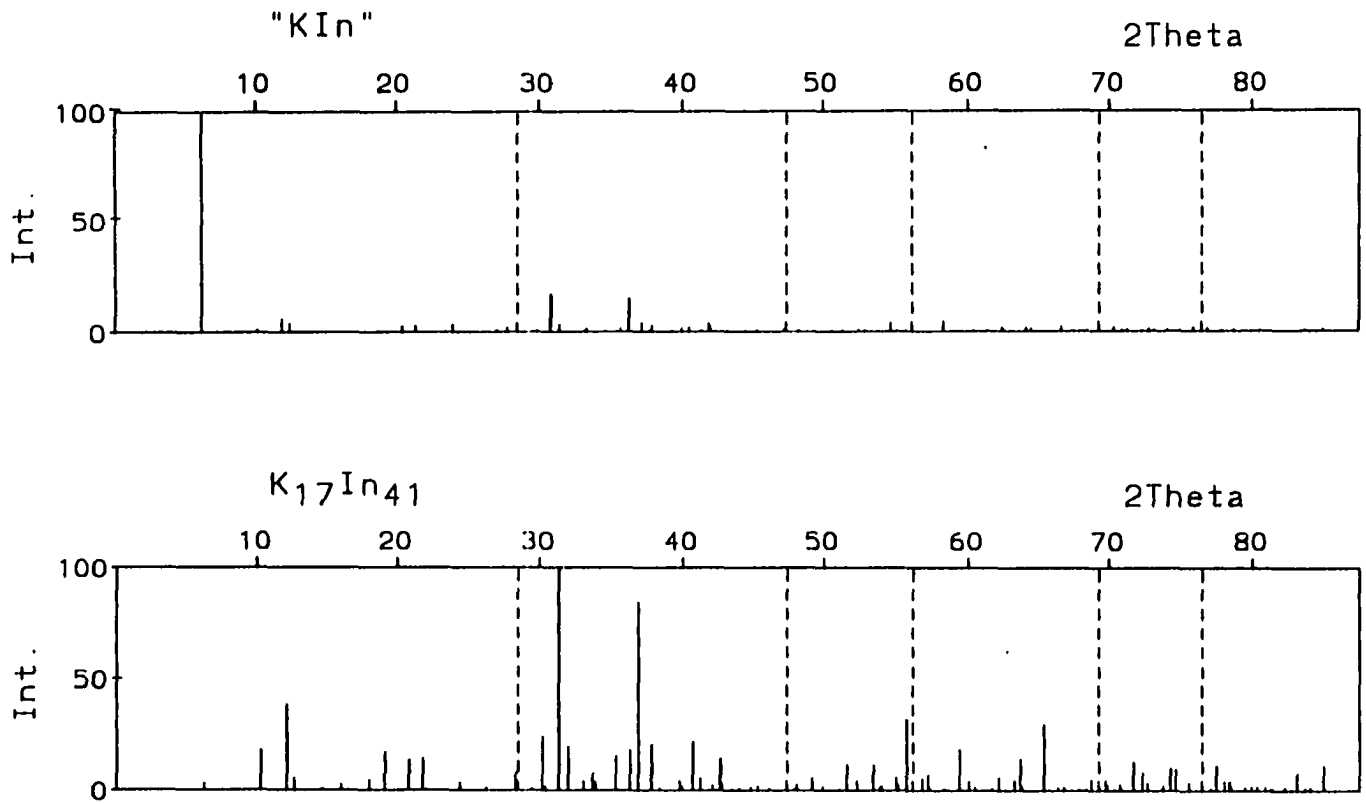

Figure 7. Calculated Guinier powder patterns of "KIn" and $K_{17}In_{41}$.

ACKNOWLEDGMENTS

I could not have finished this work without the help of several people who have guided me throughout the course of this research. I would like to thank Dr. John D. Corbett for his support and understanding and for allowing me to pursue new areas of solid state chemistry. His hard work and pursuit of knowledge is an example for me to follow. Dr. Gordon Miller provided some of the extended Hückel programs that were used but I will remember him more for our conversations about chemistry and life in general. I would also like to thank the rest of the inorganic faculty members at Iowa State. Their guidance during my classes and helpful suggestions about my research will be remembered for a life time.

Other people that helped me include Jerome E. Ostenson with magnetic susceptibility measurements, Warren Straszheim with EDS experiments, and Lenny Thomas with advice on the diffractometers.

I am also grateful for the support from Shirley Standley and all past and present group members of Dr. Corbett's and Dr. Franzen's groups. Our discussions about chemistry and life were very beneficial.

The support of my parents, family, and friends has given me the strength that I needed to continue my education. This is especially true of the one person who has continuously stood by my side and provided the support and understanding when I needed it most, my wife Heather. She encourages me to push myself to become the best person I can. Thank you.

IMAGE EVALUATION
TEST TARGET (QA-3)

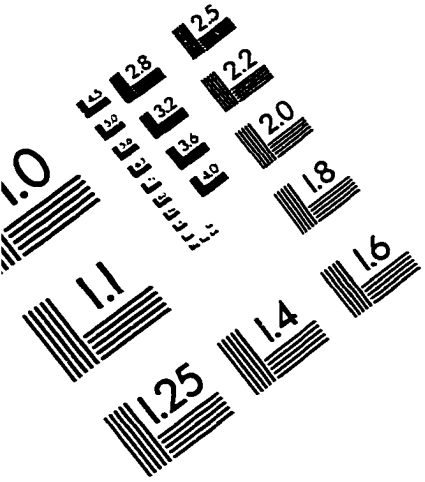

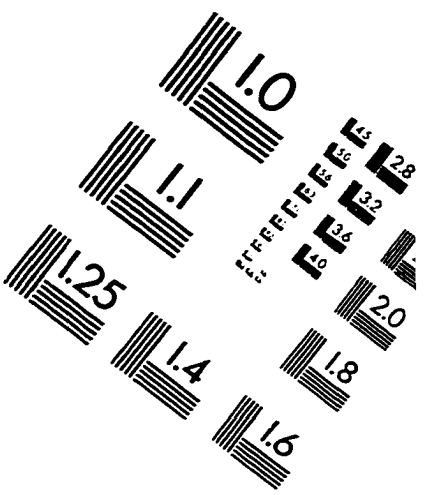

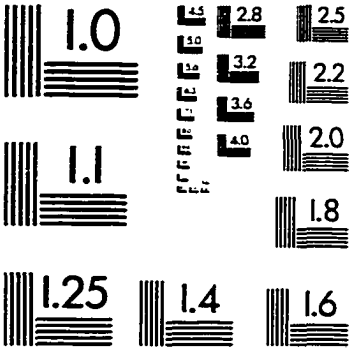

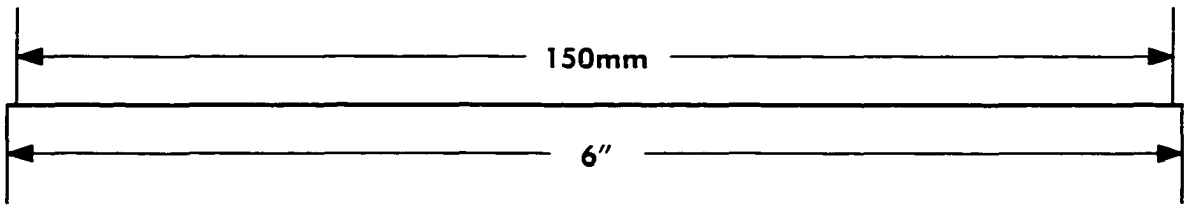

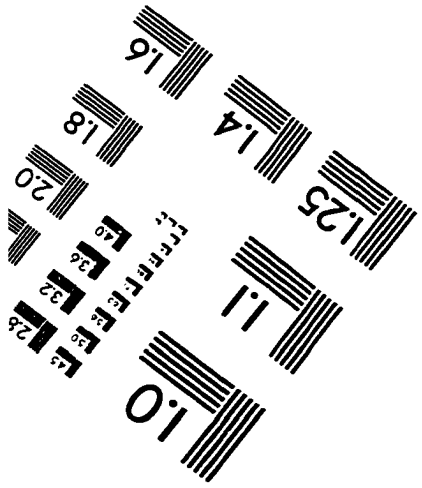

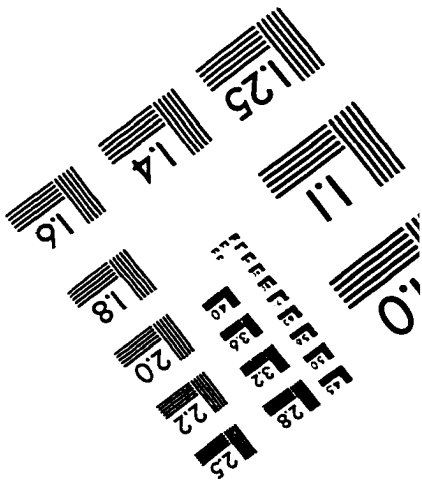

APPLIED IMAGE, Inc
1653 East Main Street
Rochester, NY 14609 USA
Phone: 716/482-0300
Fax: 716/288-5989